

**CHARACTERISTICS OF POLYACRYLONITRILE  
PAN-BASED POLYMER ELECTROLYTES FOR  
BATTERY APPLICATIONS**

**CHONG WOON GIE**

**DISSERTATION SUBMITTED IN FULFILLMENT OF  
THE REQUIREMENTS FOR THE DEGREE OF  
MASTER OF SCIENCE**

**DEPARTMENT OF PHYSICS  
FACULTY OF SCIENCE  
UNIVERSITY OF MALAYA  
KUALA LUMPUR**

**2013**

# UNIVERSITI MALAYA

## ORIGINAL LITERARY WORK DECLARATION

Name of Candidate: **CHONG WOON GIE** I/C/Passport No: **881215-05-5248**  
Registration/Matric No.: **SGR110077**  
Name of Degree: **MASTER OF SCIENCE**

Title of Project Paper/Research Report/Dissertation/Thesis ("this Work"):

**"CHARACTERISTICS OF POLYACRYLONITRILE PAN-BASED POLYMER ELECTROLYTES FOR BATTERY APPLICATIONS"**

Field of Study: **ADVANCED MATERIAL**

I do solemnly and sincerely declare that:

- (1) I am the sole author/writer of this Work,
- (2) This Work is original,
- (3) Any use of any work in which copyright exists was done by way of fair dealing and for permitted purposes and any excerpt or extract from, or reference to or reproduction of any copyright work has been disclosed expressly and sufficiently and the title of the Work and its authorship have been acknowledged in this Work,
- (4) I do not have any actual knowledge nor do I ought reasonably to know that the making of this work constitutes an infringement of any copyright work,
- (5) I hereby assign all and every rights in the copyright to this Work to the University of Malaya ("UM"), who henceforth shall be owner of the copyright in this Work and that any reproduction or use in any form or by any means whatsoever is prohibited without the written consent of UM having been first had and obtained,
- (6) I am fully aware that if in the course of making this Work I have infringed any copyright whether intentionally or otherwise, I may be subject to legal action or any other action as may be determined by UM.

(Candidate Signature)

Date:

Subscribed and solemnly declared before,

Witness's Signature

Date:

Name: **ASSOC. PROF. DR ZURINA OSMAN**

Designation

## ABSTRACT

In the present study, three systems of polyacrylonitrile (PAN)-based polymer electrolytes samples were prepared. The first system is plasticized-PAN films containing different ratio of ethylene carbonate (EC) and dimethyl phthalate (DMP). The second system is salted-PAN films (PAN-LiBF<sub>4</sub>) and the third system is plasticized PAN films containing varying amounts of lithium tetrafluoroborate (PAN-EC-DMP-LiBF<sub>4</sub>). Pure PAN film was prepared as a reference. The room temperature conductivity for the highest conducting sample in the PAN-EC-DMP system, PAN-LiBF<sub>4</sub> system and PAN-EC-DMP-LiBF<sub>4</sub> system are  $1.11 \times 10^{-6} \text{ S cm}^{-1}$ ,  $1.83 \times 10^{-3} \text{ S cm}^{-1}$  and  $1.08 \times 10^{-2} \text{ S cm}^{-1}$ , respectively. The conductivity of the PAN-based polymer electrolyte has been found to be salt concentration dependent which is attributed to the increase in the number of mobile ions within the polymer matrix. The temperature dependence of conductivity for the films in PAN-LiBF<sub>4</sub> system and PAN-EC-DMP-LiBF<sub>4</sub> system from ambient temperature to 353 K obeys Arrhenius rule. The activation energies,  $E_a$  for these films were calculated to be in the range between 0.38 eV and 0.22 eV. The interactions of Li<sup>+</sup> ions with nitrile groups of PAN in PAN-LiBF<sub>4</sub> system and PAN-EC-DMP-LiBF<sub>4</sub> system have been confirmed by Fourier Transform Infrared spectroscopy (FTIR). Differential Scanning Calorimetry (DSC) results have shown that both unplasticized and plasticized polymer electrolyte films were found to be thermally stable up to 200 °C. X-ray diffraction (XRD) results and glass transitions temperature studies have revealed that the crystalline region of PAN was effectively decreased upon addition of salt and plasticizers. The ionic and cationic transference numbers were evaluated by DC and combined DC and AC polarization methods to determine the charge carrier species within the polymer electrolyte films. The lithium ion conduction in the polymer electrolyte films is confirmed from Cyclic Voltammetry (CV) and transport number measurements. Linear sweep voltammetry (LSV) was employed to

estimate the decomposition potential of the polymer electrolytes. The films were found to be electrochemically stable up to 4.4 V. A Li/LiCoO<sub>2</sub> cell with the most electrochemically stable polymer electrolyte film has been fabricated and tested.

## ABSTRAK

Dalam kajian ini, tiga sistem sampel elektrolit polimer berasaskan poliakrilonitril (PAN) telah disediakan. Sistem yang pertama ialah filem polimer PAN yang mengandungi agen pemplastik etilena karbonat (EC) dan dimetil phthalate (DMP). Sistem kedua ialah filem PAN yang didopkan dengan litium tetrafluoroborate (PAN-LiBF<sub>4</sub>) dan yang ketiga ialah filem PAN yang mengandungi kedua-dua agen pemplastik dan garam yang berlainan kepekatan (PAN-EC-DMP-LiBF<sub>4</sub>). Filem PAN tulen disediakan sebagai sampel rujukan. Kekonduksian elektrik yang paling tinggi pada suhu bilik bagi sistem-sistem PAN-EC-DMP, PAN-LiBF<sub>4</sub> dan PAN-EC-DMP-LiBF<sub>4</sub> ialah masing-masing  $1.11 \times 10^{-6} \text{ S cm}^{-1}$ ,  $1.83 \times 10^{-3} \text{ S cm}^{-1}$  and  $1.08 \times 10^{-2} \text{ S cm}^{-1}$ . Nilai kekonduksian elektrolit polimer pepejal didapati bergantung kepada kepekatan garam disebabkan peningkatan bilangan ion-ion bebas dalam matriks polimer. Kekonduksian elektrik dari suhu bilik ke 353 K bagi filem-filem dari sistem PAN-LiBF<sub>4</sub> dan sistem PAN-EC-DMP-LiBF<sub>4</sub> mematuhi hukum Arrhenius. Tenaga pengaktifan,  $E_a$  bagi filem-filem ini ialah di antara 0.38 eV dan 0.22 eV. Interaksi ion Li<sup>+</sup> dengan kumpulan nitril PAN dalam sistem PAN-LiBF<sub>4</sub> dan PAN-EC-DMP-LiBF<sub>4</sub> telah ditentukan melalui spektroskopi infra-merah. Kedua-dua sistem yang didopkan dengan garam dan sistem yang diplastikkan mempunyai kestabilan terma setinggi 200 °C. Keputusan pembelauan sinar-X (XRD) dan kajian suhu peralihan kaca menunjukkan rantau kehabluran PAN berkurang dengan penambahan garam dan agen pemplastik. Nombor pengangkutan ion dan kation dinilai dengan kaedah polarisasi arus terus dan polarisasi gabungan arus terus dan arus ulang-alik untuk menentukan spesies pembawa cas dalam filem elektrolit polimer. Konduksi ion litium dalam filem elektrolit polimer disahkan dengan voltammetri berkitar (CV) dan pengukuran nombor pengangkutan. Voltammetri sapuan linear (LSV) digunakan untuk menganggar keupayaan penguraian elektrolit polimer. Filem-filem didapati mempunyai kestabilan elektrokimia sehingga 4.4 V. Sel Li/LiCoO<sub>2</sub>

dengan filem elektrolit polimer mempunyai kestabilan elektrokimia yang paling tinggi telah difabrikasi dan diuji.

## **Acknowledgement**

I would like to express the deepest appreciation to my supervisor, Assoc. Prof. Dr. Zurina Osman, for her continuous guidance and support of my Master study and research. Her enthusiasm and immense knowledge in materials science has improved my research skills and prepared me for future challenge.

Besides my supervisor, I would like to thank my lab seniors and labmates, Lisani Othman, Khairul Bahiyah Md. Isa, Nurul Husna Zainol and Siti Mariam Samin for their encouragement, insightful suggestion and comments during my study.

I would also like to convey thanks to University of Malaya for fellowship awarded and for providing the financial support and laboratory facilities.

I am deeply grateful to my parents and my family for their love, moral support and encouragement for making this thesis a success. Last but certainly not least, appreciation is expressed to all the individuals who have directly and indirectly assisted me and led to the completion of my study.

## CONTENTS

CONTENTS	PAGE
Declaration	ii
Abstract	iii
Abstrak	v
Acknowledgements	vii
Contents	viii
List of Figures	xiii
List of Tables	xvii
List of Published and Presented Papers	xx

## CHAPTER 1 : INTRODUCTION

1.1	Background	1
1.2	Objectives of the Present Work	2
1.3	Organization of the Dissertation	3

## CHAPTER 2 : LITERATURE REVIEW

2.1	Introduction	5
2.2	Classification of polymer electrolytes	
2.2.1	<i>Solid Polymer Electrolytes</i>	6
2.2.2	<i>Gel Polymer Electrolytes</i>	7
2.3	Complexation of polymer-salt	8
2.4	Polyacrylonitrile (PAN)	10
2.4.1	<i>PAN as polymer electrolyte</i>	11
2.5	Lithium Tetrafluoroborate (LiBF <sub>4</sub> )	11
2.6	Plasticization	13



2.7	Polymer electrolytes in applications	14
2.7.1	<i>Battery</i>	14
2.7.2	<i>Charge/discharge mechanism</i>	16
2.7.3	<i>Cathodes</i>	17
2.7.4	<i>Anodes</i>	18

## CHAPTER 3 : EXPERIMENTAL TECHNIQUES

3.1	Sample preparation	
3.1.1	<i>Preparation of plasticized PAN-EC-DMP system</i>	20
3.1.2	<i>Preparation of PAN-LiBF<sub>4</sub> system</i>	21
3.1.3	<i>Preparation of PAN-EC-DMP-LiBF<sub>4</sub> system</i>	21
3.2	Measurement of Ionic Conductivity	
3.2.1	<i>Electrochemical Impedance Spectroscopy (EIS)</i>	21
3.2.2	<i>Conductivity-Temperature Behaviour</i>	23
3.3	Ion transport number measurements	25
3.3.1	<i>D.C. polarization technique for the evaluation of total ionic transport number</i>	26
3.3.2	<i>Combined A.C./D.C. techniques for the evaluation of cationic transport number</i>	26
3.4	Morphology and Structural Studies	
3.4.1	<i>Field Emission Scanning Electron Microscopy (FESEM)</i>	27
3.4.2	<i>X-Ray Diffraction (XRD)</i>	28
3.5	Fourier Transform Infrared Spectroscopy (FTIR)	30
3.6	Thermal Analysis	
3.6.1	<i>Thermogravimetric Analysis (TGA)</i>	33
3.6.2	<i>Differential Scanning Calorimetry (DSC)</i>	35
3.7	Potential Sweep Voltammetry	

3.7.1	<i>Linear Sweep Voltammetry (LSV)</i>	37
3.7.2	<i>Cyclic Voltammetry (CV)</i>	38
3.8	Lithium Polymer Cell Fabrication	39

## CHAPTER 4 : RESULTS AND DISCUSSIONS

### 4.1 Electrical Studies

4.1.1	Impedance Spectroscopy (IS) Analysis	40
4.1.2	Room temperature electrical conductivity studies	
4.1.2.1	<i>PAN plasticized with varying amounts of EC and DMP</i>	40
4.1.2.2	<i>PAN-LiBF<sub>4</sub> system</i>	43
4.1.2.3	<i>PAN-EC-DMP-LiBF<sub>4</sub> system</i>	48
4.1.3	Elevated temperature electrical conductivity studies	
4.1.3.1	<i>PAN-LiBF<sub>4</sub> System</i>	53
4.1.3.2	<i>PAN-EC-DMP-LiBF<sub>4</sub> system</i>	55
4.1.4	Transport Number	
4.1.4.1	<i>Ionic Transport Number</i>	57
4.1.4.2	<i>Cationic Transport Number</i>	59

### Structural Studies

### 4.2 X-ray Diffraction (XRD) Studies

4.2.1	X-ray Diffraction Analysis	62
4.2.2	PAN-LiBF <sub>4</sub> system	64
4.2.3	PAN-EC-DMP-LiBF <sub>4</sub> system	64

### 4.3 Fourier Transform Infrared (FTIR) studies

4.3.1	Introduction	67
4.3.2	Infrared spectra of pure substances	
4.3.2.1	<i>Pure Polyacrylonitrile (PAN)</i>	68

4.3.2.2	<i>Ethylene carbonate (EC)</i>	69
4.3.2.3	<i>Dimethyl Phthalate (DMP)</i>	70
4.3.2.4	<i>Lithium Tetrafluoroborate (LiBF<sub>4</sub>)</i>	72
4.3.3	Interaction between PAN and Plasticizers	74
4.3.4	Interaction between PAN and LiBF <sub>4</sub> salt	78
4.3.5	Interaction between PAN-EC-DMP and LiBF <sub>4</sub> salt	81
<b>4.4</b>	<b>Field Emission Scanning Electron Microscopy (FESEM) Analysis</b>	
4.4.1	Introduction	87
4.4.2	Pure PAN film	87
4.4.3	PAN-EC-DMP film	88
4.4.4	PAN-LiBF <sub>4</sub> system	89
4.4.5	PAN-EC-DMP-LiBF <sub>4</sub> system	90
<b>4.5</b>	<b>Thermal Studies</b>	
4.5.1	Introduction	93
4.5.2	Pure PAN	93
4.5.3	PAN-EC-DMP system	94
4.5.4	PAN-LiBF <sub>4</sub> System	96
4.5.5	PAN-EC-PC-LiBF <sub>4</sub> System	99
<b>4.6</b>	<b>Electrochemical Studies</b>	
4.6.1	Introduction	102
4.6.2	Linear Sweep Voltammetry (LSV)	
4.6.2.1	<i>PAN-LiBF<sub>4</sub> System</i>	102
4.6.2.2	<i>PAN-EC-DMP-LiBF<sub>4</sub> System</i>	104
4.6.3	Cyclic Voltammetry	
4.6.3.1	<i>PAN-LiBF<sub>4</sub> System</i>	105
4.6.3.2	<i>PAN-EC-DMP-LiBF<sub>4</sub> System</i>	106

<b>4.7</b>	<b>Cell Performance</b>	110
<b>CHAPTER 5 : DISCUSSION, CONCLUSION AND SUGGESTIONS</b>		113
<b>FOR FUTURE WORK</b>		
<b>REFERENCES</b>		117
<b>APPENDIX</b>		127

## LIST OF FIGURES

<b>Figure</b>	<b>Descriptive</b>	<b>Page</b>
Figure 2.1	Chemical structure of PAN	10
Figure 2.2	Chemical structure of LiBF <sub>4</sub>	12
Figure 2.3	Chemical structures of (a) EC (b) DMP	14
Figure 2.4	Lithium Polymer Battery	15
Figure 2.5	Schematic illustration of charge and discharge process for secondary battery	16
Figure 3.1	Cole-Cole plot	23
Figure 3.2	Schematic diagram of FESEM experiment	28
Figure 3.3	Principle of X-ray Diffraction	30
Figure 3.4	Schematic illustration of Bragg condition and Bragg's law.	30
Figure 3.5	Schematic Diagram of FTIR	32
Figure 3.6	Block Diagram of a Thermobalance	33
Figure 3.7	TG Curve	34
Figure 3.8	Differential scanning calorimeter sample and reference holder	36
Figure 3.9	DSC Thermogram	36
Figure 4.1	The complex impedance plot for pure PAN film.	42
Figure 4.2	The complex impedance plot for PAN-EC-DMP film.	42
Figure 4.3	Variation of conductivity with different ratio of EC and DMP in the PAN-EC-DMP system.	43
Figure 4.4	Impedance plot for PAN film containing 5 wt% of LiBF <sub>4</sub>	46
Figure 4.5	Impedance plot for PAN film containing 50 wt.% of LiBF <sub>4</sub> .	46
Figure 4.6	Variation of conductivity with different amounts of salt in PAN-LiBF <sub>4</sub> system	47
Figure 4.7	Dielectric constant versus frequency for films in PAN-LiBF <sub>4</sub> system	47

Figure 4.8	Dielectric loss versus frequency for films in PAN-LiBF <sub>4</sub> system	48
Figure 4.9	Impedance plot for PAN-EC-DMP film containing 5 wt.% of LiBF <sub>4</sub> .	50
Figure 4.10	Impedance plot for PAN-EC-DMP film containing 40 wt.% of LiBF <sub>4</sub> .	51
Figure 4.11	Variation of conductivity with different amounts of salt in PAN-EC-DMP-LiBF <sub>4</sub> system	51
Figure 4.12	Dielectric constant versus frequency for films in PAN-EC-DMP-LiBF <sub>4</sub> system	52
Figure 4.13	Dielectric loss versus frequency for films in PAN-EC-DMP-LiBF <sub>4</sub> system	52
Figure 4.14	Temperature dependence of ionic conductivity of PAN-LiBF <sub>4</sub> system.	54
Figure 4.15	Temperature dependence of ionic conductivity of PAN-EC-DMP-LiBF <sub>4</sub> system.	56
Figure 4.16	Normalized current versus time plots for films in PAN-LiBF <sub>4</sub> system.	58
Figure 4.17	Normalized current versus time plots for films in PAN-EC-DMP-LiBF <sub>4</sub> system.	59
Figure 4.18	A.C. complex impedance plot before and after D.C. polarization of a typical symmetric Li  SPE  Li cell.	61
Figure 4.19	Polarization current plot as a function of time for the highest conducting film in PAN-EC-DMP-LiBF <sub>4</sub> system with Li  SPE  Li cell.	61
Figure 4.20	X-ray diffractogram of pure PAN	62
Figure 4.21	X-ray diffractogram of EC	63
Figure 4.22	X-ray diffractogram of LiBF <sub>4</sub>	63
Figure 4.23	X-ray diffractogram of the films in the PAN-LiBF <sub>4</sub> system	66
Figure 4.23(a)	Variation of peak intensity at 17 ° with concentration of LiBF <sub>4</sub> salt.	66

Figure 4.24	X-ray diffractogram of the films in PAN-EC-DMP-LiBF <sub>4</sub> system	67
Figure 4.25	FTIR spectra of pure PAN film in the region from 1000 to 3500 cm <sup>-1</sup>	69
Figure 4.26	FTIR spectra of ethylene carbonate in the region from 650 to 3000 cm <sup>-1</sup>	71
Figure 4.27	FTIR spectra of dimethyl phthalate in the region from 700 to 3500 cm <sup>-1</sup>	72
Figure 4.28	FTIR spectra of lithium tetrafluoroborate in the region from 650 to 2400 cm <sup>-1</sup>	73
Figure 4.29	Infrared spectra of PAN film with plasticized with different ratios of EC and DMP in the region 650 to 1000 cm <sup>-1</sup> .	74
Figure 4.30	Infrared spectra of PAN film with plasticized with different ratios of EC and DMP in the region 1000 to 1600 cm <sup>-1</sup> .	75
Figure 4.31	Infrared spectra of PAN film with plasticized with different ratios of EC and DMP in the region 1600 to 2000 cm <sup>-1</sup> .	77
Figure 4.32	Infrared spectra of PAN film with plasticized with different ratios of EC and DMP in the region 2200 to 2300 cm <sup>-1</sup> .	77
Figure 4.33	Infrared spectra of PAN film doped with varying amount of LiBF <sub>4</sub> in the region 900 to 1800 cm <sup>-1</sup> .	79
Figure 4.34	Infrared spectra of PAN film doped with varying amount of LiBF <sub>4</sub> in the region 2200 to 2300 cm <sup>-1</sup> .	80
Figure 4.35	Infrared spectra of the $\nu_1$ mode of BF <sub>4</sub> <sup>-</sup> correspond to (i) free ions (ii) ion pairs for films at different concentrations of LiBF <sub>4</sub> in PAN-LiBF <sub>4</sub> system	80
Figure 4.36	Infrared spectra of PAN-EC-DMP film doped with varying amount of LiBF <sub>4</sub> in the region 900 to 1900 cm <sup>-1</sup> .	83
Figure 4.37	Infrared spectra of PAN-EC-DMP film doped with varying amount of LiBF <sub>4</sub> in the region 2200 to 2300 cm <sup>-1</sup> .	84
Figure 4.38	Infrared spectra of the $\nu_1$ mode of BF <sub>4</sub> <sup>-</sup> for films containing different concentrations of LiBF <sub>4</sub> in PAN-EC-DMP-LiBF <sub>4</sub> system.	84
Figure 4.39	Infrared spectra of the (i) unbonded (ii) bonded nitrile band	85

	of films at different concentrations of $\text{LiBF}_4$ in PAN-EC-DMP- $\text{LiBF}_4$ system	
Figure 4.40	Micrograph of pure PAN film	87
Figure 4.41	Micrograph of PAN-EC-DMP film	88
Figure 4.42	(a) Micrograph of PAN film containing 10 wt.% of $\text{LiBF}_4$	89
	(b) Micrograph of PAN film containing 40 wt.% of $\text{LiBF}_4$	90
	(c) Micrograph of PAN film containing 50 wt.% of $\text{LiBF}_4$	90
Figure 4.43	(a) Micrograph of PAN-EC-DMP film containing 10 wt.% of $\text{LiBF}_4$	91
	(b) Micrograph of PAN-EC-DMP film containing 30 wt.% of $\text{LiBF}_4$	92
	(c) Micrograph of PAN-EC-DMP film containing 40 wt.% of $\text{LiBF}_4$	92
Figure 4.44	(a) DSC and (b) TG thermograms of pure PAN film.	94
Figure 4.45	(a) DSC and (b) TG thermograms of PAN-EC-DMP film.	96
Figure 4.46	DSC curve for films in PAN- $\text{LiBF}_4$ system.	98
Figure 4.47	TGA thermogram for films in PAN- $\text{LiBF}_4$ system.	99
Figure 4.48	DSC thermogram for films in PAN-EC-DMP- $\text{LiBF}_4$ system.	100
Figure 4.49	TGA thermogram for films in PAN-EC-DMP- $\text{LiBF}_4$ system.	101
Figure 4.50	Linear sweep voltammograms of the cell prepared with the PAN films containing (a) 20 wt.% (b) 30 wt.% (c) 40 wt.% (d) 50 wt.% in PAN- $\text{LiBF}_4$ system.	103
Figure 4.51	Linear sweep voltammograms of the cell prepared with the PAN films containing (a) 10 wt.% (b) 20 wt.% (c) 30 wt.% (d) 40 wt.% PAN-EC-DMP- $\text{LiBF}_4$ system.	104
Figure 4.52	Cyclic voltammogram of cell-I: SS SPE SS with 40 wt.% of $\text{LiBF}_4$ salt at scan rate of $5 \text{ mV s}^{-1}$ .	107
Figure 4.53	Cyclic voltammogram of cell-II: Li SPE Li with 40 wt.%	108



	of LiBF <sub>4</sub> salt at scan rate of 5 mV s <sup>-1</sup> .	
Figure 4.54	Cyclic voltammogram of cell-III: SS SPE SS with 30 wt.% of LiBF <sub>4</sub> salt at scan rate of 5 mV s <sup>-1</sup> .	108
Figure 4.55	Cyclic voltammogram of cell-IV: Li SPE Li with 30 wt.% of LiBF <sub>4</sub> salt at scan rate of 5 mV s <sup>-1</sup> .	109
Figure 4.56	Variation of voltage of a Li / SPE / LiCoO <sub>2</sub> cell during discharge with a current of 30 μA.	111
Figure 4.57	Discharge capacities of Li / SPE / LiCoO <sub>2</sub> cell as a function of cycle number.	111

## LIST OF TABLES

<b>Table</b>	<b>Descriptive</b>	<b>Page</b>
Table 2.1	Comparison of Typical Cathode Materials	18
Table 3.1	Compositions of PAN, EC and DMP in PAN-EC-DMP system	21
Table 4.1	Average bulk resistances and conductivity values of plasticized PAN films with different ratio of EC and DMP	41
Table 4.2	Compositions, bulk resistance, $R_b$ and conductivity of films in the PAN-LiBF <sub>4</sub> system.	45
Table 4.3	Compositions, bulk resistance, $R_b$ and conductivity of films in the PAN-EC-DMP-LiBF <sub>4</sub> system.	50
Table 4.4	Activation energies for films in PAN-LiBF <sub>4</sub> system.	54
Table 4.5	Activation energies for films in PAN-EC-DMP-LiBF <sub>4</sub> system	56
Table 4.6	Ionic Transport Number for PAN-LiBF <sub>4</sub> and PAN-EC-DMP-LiBF <sub>4</sub> systems.	58
Table 4.7	The vibrational modes and wavenumbers of pure PAN film.	68
Table 4.8	The vibrational modes and wavenumbers exhibited by ethylene carbonate.	70
Table 4.9	The vibrational modes and wavenumbers of dimethyl phthalate.	71
Table 4.10	The vibrational modes and wavenumbers of lithium tetrafluoroborate.	73
Table 4.11	Band-Fitting Results in the Tetrafluoroborate Anion $\nu_1(A1)$ Manifold FTIR Spectra of LiBF <sub>4</sub> in PAN-LiBF <sub>4</sub> system.	81
Table 4.12	The position and integrated area of paired tetrafluoroborate ions formed in films of different LiBF <sub>4</sub> content in PAN-EC-DMP-LiBF <sub>4</sub> system.	85
Table 4.13	Band-Fitting Results of the $C \equiv N$ absorbance for PAN	86

in PAN-EC-DMP-LiBF<sub>4</sub> system.

Table 4.14	Glass transition temperature and endotherm peak temperature of heat treated PAN films in PAN-LiBF <sub>4</sub> system.	98
Table 4.15	Glass transition temperature and endotherm peak temperature of heat treated PAN films in PAN-EC-DMP-LiBF <sub>4</sub> system.	101

## LIST OF PUBLISHED AND PRESENTED PAPERS

1. **W. G. Chong**, Z. Osman, L. Othman and K. B. Md Isa, “Ionic Conductivity and Dielectric Properties of Plasticized Polyacrylonitrile Based Solid Polymer Electrolyte Films” , Advanced Materials Research Vol 626 (2013) 211-214.
2. **W. G. Chong** and Z. Osman, “Studies of Ionic Conductivity and Electrical Properties of PAN-Lithium Tetrafluoroborate Polymer Electrolytes”, presented at International Conference of Young Researchers on Advanced Materials (ICYRAM), 1- 6 July 2012, Biopolis, Singapore.
3. F. Sonsudin, Z. Osman, **W.G. Chong**, K.B. Md Isa, L. Othman, N.H. Zainol, S.M. Samin and I. Supaat, “AC Impedance and Dielectric Behavior Studies of Polyacrylonitrile Based Ion Conducting Polymer Electrolytes”, presented at 9<sup>th</sup> International Symposium on Electrochemical Impedance Spectroscopy (EIS 2013), 16-21 June 2013, Okinawa, Japan.
4. N. H. Zainol, S.M. Samin, L. Othman, K.B. Md Isa, **W.G. Chong** and Z. Osman, “Magnesium Ion-Based Gel Polymer Electrolytes: Ionic Conduction and Infrared Spectroscopy Studies”, International Journal of Electrochemical Sciences, (2013), 3602-3614.
5. L. Othman, K.B. Md Isa, N.H. Zainol, S.M. Samin, **W.G. Chong**, Z. Osman and R. Yahya, “Effects of Lithium Salt Concentration on Morphological and Spectroscopic Properties in PMMA Based Gel Polymer Electrolytes” presented at 7<sup>th</sup> International Conference on Materials for Advanced Technologies, 30 June-5 July 2013, Singapore.
6. K.B. Md Isa, L. Othman, N. H. Zainol, S.M. Samin, **W. G. Chong**, Z. Osman, “ Lithium Ion Conducting and Ion-Polymer Interactions in PvdF-HFP Based Gel Polymer Electrolytes”, presented at 7<sup>th</sup> International Conference on Materials for Advanced Technologies, 30 June-5 July 2013, Singapore.

# **CHAPTER 1**

## **INTRODUCTION**

## 1.1 Background

Solid polymer electrolyte (SPE) based on PEO was first discovered by Wright and co-workers who have brought out the technological significance to the development of the energy resources (Fenton, Parker & Wright, 1973; Wright, 1975; Lee & Wright, 1978). Polymer electrolyte offers advantages that are light weight, good flexibility, leak proof, wide electrochemical window and good cyclic stability (MacCallum & Vincent, 1987, 1989; Matsuda, Morita & Tsutsumi, 1993; Scrosati, 1993; Wakihara & Yamamoto, 1998). Therefore, an intense research and development on the study of physical, chemical and electrochemical properties of polymer electrolyte was induced in order to develop an optimized material as a substitute to conventional liquid electrolyte.

Many approaches were done in order to develop a polymer electrolyte with good ionic conductivity lead to the evolution of polymer electrolyte from a simple SPE to different forms such as plasticized polymer electrolyte, polymer blends, composites, gel and ionic liquids contained electrolyte. Certainly, the most important parameters are the types of polymer, the amount and the types of doping material and the preparation method which will dramatically change the properties of the polymer electrolyte.

Polyacrylonitrile (PAN) based polymer electrolyte has been widely applied to secondary rechargeable battery due to its mechanical stability. There are reported high conductivity values of PAN-based polymer electrolytes ranging from  $10^{-3}$  to  $10^{-2}$  S cm<sup>-1</sup> at room temperature which is close to the value of commercial liquid electrolyte (Tsutsumi & Kitagawa, 2006; Amaral, Dalmolin & Canobre, 2007). In addition, dendrite growth in charging process of lithium batteries can be inhibited by PAN (Yuan, Chen, Yang, Li & Wang, 2005). Incorporation of plasticizers was found to be useful in reducing the crystalline region of the polymer and hence improve the ionic conduction. Ethylene carbonate which is favourable solvent due to its high dielectric constant is commonly used as organic solvent. It was reported that the presence of EC aids the

formation of effective protective film (SEI) on a graphitic anode (Abouimrane, Belharouak & Amine, 2009). The advantages of binary solvent was discovered by Pistoia, Rossi and Scrosati and Pistoia (1970) that a good combination of solvents not only improve the ion dissociation, the mixture balancing their unique characteristics and at the same time improve the interfacial properties. Rajendran, Mahendran and Kannan (2002) have made phthalate a possible plasticizer candidate in polymer electrolyte. Phthalates, a well-known plasticizer was used to increase the flexibility, transparency, durability, and longevity of plastic is rarely studied.

In this work, the preparation of SPE comprised of PAN, a new combination of carbonates and phthalates and lithium tetrafluoroborate salt,  $\text{LiBF}_4$  will be reported. The amount of salt and plasticizers are manipulated and the effect of plasticization will be justified in the aspect of electrical, structural, thermal, and electrochemical properties.

## 1.2 Objectives of the Present Work

The main goal of this work is to conduct a comparative study of unplasticized and plasticized polymer electrolyte systems based on polyacrylonitrile (PAN) for battery applications. Thus, the specific objectives of this study are:

- 1) To study the effect of different ratio of EC and DMP on the structural, thermal, electrical and electrochemical properties of PAN film.
- 2) To investigate the influence of different concentrations of  $\text{LiBF}_4$  on the properties of unplasticized and plasticized PAN films.
- 3) To determine the current carrier species using DC polarization method or known as Wagner's method. The cationic transport number will be calculated by using the combination of AC and DC methods.

- 
- 4) To fabricate the lithium battery with the most electrochemically stable SPE film that carries the high conductivity as an electrolyte. The charge-discharge performance of the battery will be investigated.

### 1.3 Organizations of the Dissertation

This dissertation reports the study of the properties of PAN-based polymer electrolytes. The report is arranged into five chapters. The first chapter presents the background of the research and the objectives of the research interest.

Chapter two displays a review of the previous work about polymer electrolytes including basic definition the materials used. Brief explanation of the characterization method, comparison of the types of polymer electrolyte available and the working principle of the polymer electrolyte will be elaborated. The potential applications of the doped polymer films will be discussed.

Chapter three lists the materials used in this project. Three different systems of PAN-based polymer electrolyte were prepared by solution casting methods. They are unsalted PAN films with varying amount of plasticizers while the second system is unplasticized PAN films doped with varying amount of lithium tetrafluoroborate ( $\text{LiBF}_4$ ). The last system is plasticized PAN films doped with varying amount of  $\text{LiBF}_4$ . The characterizations are done by using various techniques include Electrochemical Impedance spectroscopy (EIS), transport number measurements, Fourier Transform Infrared Spectroscopy (FTIR), X-Ray Diffraction (XRD), Field Emission Scanning Electron Microscopy (FESEM), Differential Scanning Calorimetry (DSC), Thermogravimetric Analysis (TGA), Linear Sweep Voltammetry (LSV) and Cyclic Voltammetry (CV). The theoretical aspects of the characterization methods will be discussed.



---

Chapter four combines the results obtained from the experiment together with the discussion on the findings. A comparison of the structural, electrical, thermal and electrochemical properties for both systems will be presented in this chapter. The ionic conductivity, transport number and dielectric properties of solid polymer electrolyte films will be studied. The polymer-salt complex formation and the morphological properties of the SPE films will be investigated using Fourier Transform Infrared spectroscopy, X-ray Diffraction studies and FESEM. The electrochemical properties SPE films will be determined using Linear Sweep Voltammetry. The most electrochemically stable samples from PAN-LiBF<sub>4</sub> and PAN-EC-DMP-LiBF<sub>4</sub> systems will be tested again by using CV to confirm the stability limit of the SPE films. The practicability of the SPE films for battery applications will be analysed through the cycling profile. Finally, chapter five concludes the research work with some suggestions for future work.

# **CHAPTER 2**

## **LITERATURE REVIEW**

## 2.1 Introduction

The ionic conductivity of poly(ethylene oxide), PEO with alkali metal salts was discovered by Wright and co-workers were then followed by the visionary suggestion of Armand for the use of PEO as a solid electrolyte system for the transport of ions (Fenton et al., 1973; Wright, 1975; Lee & Wright, 1978). Since then, the area of polymer electrolytes has attracted considerable interest. Ionic conduction is generally associated with liquids, either solvents with high dielectric constants or molten salts. However, solids that can function as electrolytes also known as solid electrolytes with typical conductivity value ranging from  $10^{-6}$  to  $10^{-1} \text{ S cm}^{-1}$  are interesting due to their wide ranging applications such as gas sensors (Chowdari, Chandra & Singh, 1992; Nicholson, Whittingham, Farrington & Smeltzer, 1992), electrochemical display devices (Bange & Gambke, 1990; Visco et. al, 1993), power sources (Gabano, 1983), fuel cells (Rickert, 1978), solid state high energy density batteries (Bonino, Ottaviani, Scrosati & Pistoia, 1988) and so on.

All solid state rechargeable lithium batteries operating at room temperature are highly desirable because of several advantages such as high energy density (150 Wh/g), high voltage (4.0 V/ cell) and longer charge retention characteristics (Aono, Imanaka, Adachi, 1994). Polymers that work as solid electrolytes are a subclass by themselves and are known as polymer electrolytes (Ratner & Shriver, 1988; Gray, 1991). Besides the advantage of flexibility, polymers can also be casted into films of desired thickness. Therefore, the resistance of the electrolyte can be easily monitored and also reduces the volume and the weight, which in turn lead to the increase in the energy stored per unit weight and volume.

In view of the attractive features, there has been considerable focus in recent years on the development of both inorganic and organic polymers as electrolytes for ion transport.

---

The research interests are focused on

- (i) understanding the interactions involved in the formation of polymer electrolyte phases and the detailed mechanism of ion transport,
- (ii) the synthesis of new polymer electrolytes with optimized electrical, chemical and mechanical properties; and
- (iii) the study of the behaviour of these materials when incorporated with other components of an electrochemical cell.

## **2.2 Classification of polymer electrolytes**

In order to improve the performance of polymer electrolyte, a wide variety of polymer structures have been formed such as networks, blends, graft-copolymers, etc. Generally, polymer electrolytes exist in liquid, solid and gel form.

### **2.2.1 Solid Polymer Electrolytes**

In overcoming the limitations of the conventional liquid electrolytes, an alternative method was derived by using polymers as a medium to hold on the conducting free ions within the matrix formed. Solid polymer electrolytes (SPE) offer good mechanical strength and high chemical, thermal and dimensional stability, no leakage, easy processing, low self-discharge and high energy density. Most of the early work carried out on SPE concentrates on PEO. Since then, the ionic conductivities of poly(methyl methacrylate) (PMMA), poly(vinyl alcohol) PVA, poly(propylene oxide) (PPO) and poly(ethylene imine) (PEI) and different types of polymer were studied.

Various modifications were made on SPE in order to increase the ionic conductivity and mechanical stability lead to the emergence of plasticized polymer electrolyte and composite polymer electrolyte. Plasticized polymer electrolytes are prepared by adding liquid plasticizers into dry SPEs in such a way that a compromise

between solid polymer and liquid electrolyte exists (Agrawal & Pandey, 2008). However, the magnitude of the room temperature conductivity gets substantially enhanced on the expense of the mechanical stability (Croce & Scrosati, 1993). Therefore, the dispersion of a small fraction of micro/ nanosize inorganic or organic filler particles into the conventional SPEs formed a new class of polymer electrolyte that is composite polymer electrolyte (Agrawal & Pandey, 2008). As a consequence, a compromise between ionic conductivity and mechanical stability of SPEs can be achieved and interfacial activity is enhanced concurrently.

‘Polymer-in-Salt’ electrolytes are another subclass of polymer electrolyte. The ionic conductivity is realised as a result of doping metal salts in the host polymer which contains suitable donor sites. Generally, high conductivities are observed only at low Li/O ratios. Increase in salt concentration leads to a rapid increase in the crystallinity of the materials and/or an increase in the glass transition temperatures (Ratner & Shriver, 1988; Gray, 1991). Both of these effects are detrimental to ionic conductivities and hence suppress charge carrier concentrations. In an alternative approach adopted by Angell and co-workers (1993) instead of doping the metal salts into a polymer, small amounts of polymer are combined with salt mixtures. Thus, when a mixture of LiI, LiOAc and LiClO<sub>4</sub> in mole percentages of 50, 30 and 20 are doped with a small amount of polypropylene oxide, a “polymer (in salt) electrolyte” is obtained with an ambient temperature conductivity of  $\sim 10^{-4} \text{ S cm}^{-1}$ . These materials have glass transition temperatures low enough to remain rubbery at room temperature while preserving good lithium ion conductivities and a high electrochemical stability.

### 2.2.2 Gel Polymer Electrolytes

Gel polymer electrolytes are dimensionally stable electrolytes consisting of a mixture of organic plasticizers along with structurally stable polymers such as

polyacrylonitrile (PAN) or polyvinyl sulfone (PVS) or poly vinyl pyrrolidine (PVP) or poly vinyl chloride (PVC) and several lithium salts have been tested and found to have excellent ionic conductivities at ambient temperature (Watanabe, Kanba, Nagaoka & Shinohara, 1983; Abraham & Alamgir, 1990). In these gel type electrolytes, the primary role of the polymers is to immobilize the lithium salt solvates of the organic plasticizer liquids. Gel polymer electrolyte carries the same advantages exhibited by solid polymer electrolyte in the mean while offering better ionic conductivity values. Watanabe and co-workers (1983) prepared for the first time solid electrolytes comprising PC and  $\text{LiClO}_4$  in PAN and reported a maximum conductivity of  $2 \times 10^{-4} \text{ S cm}^{-1}$ . Abraham and Alamgir (1990, 1994) prepared  $\text{Li}^+$  conductive polymer electrolytes with extremely high ambient temperature conductivities of  $4 \times 10^{-3} \text{ S cm}^{-1}$ . These electrolytes are composed of Li salts such as  $\text{LiClO}_4$  dissolved in organic solvents EC and PC and immobilized in a polymer network of PAN, poly(tetra ethylene glycol diacrylate) (PEGDA) or poly(vinyl pyrrolidone) PVP.

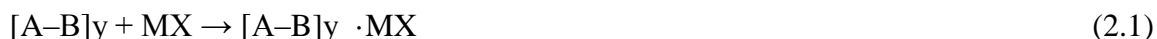
### 2.3 Complexation of polymer-salt

The candidate of the host polymer should generally possess a minimum of these three essential characteristics (Vincent, 1987):

- (i) atoms or groups, usually in the main chain, with sufficient electron donor power to form coordinate bonds with cations,
- (ii) a suitable distance between such coordinating centers to permit the formation of multiple intrapolymer-ion bonds, and
- (iii) low barriers to rotation for atoms in the main chain so as to ensure high flexibility and hence facilitate segmental motion.

The preparation of a polymer salt complex is achieved by the dissolution of the two materials in a common solvent such as acetonitrile, dimethylformamide (DMF) or

tetrahydrofuran (THF) followed by a slow removal of the solvent in vacuum. The reaction that occurs in the formation of a polymer-metal salt complex can be written as



where  $[A-B]_y$  is a polymer chain and  $MX$  is an alkali metal salt or a transition metal halide. Divalent metal salts have also been used (Ratner & Shriver, 1988).

Polymer-metal salt complex formation takes place readily, provided the polymer matrix effectively solvates the ions and overcomes the lattice energy of the ionic salt. Three essential criteria for this process have been identified (MacCallum & Vincent, 1987):

- (i) Electron pair donicity (DN)
- (ii) Acceptor number (AN) and
- (iii) an entropy term.

The polymer which should function as a host in the polymer electrolyte should possess an electron rich coordinating sites such as oxygen, sulphur or nitrogen either in the backbone or in a group attached in the form of a side chain to the polymer. Similarly, the AN term describes the solvation of the anion, the Lewis base. The third term (entropy) has been related to the spatial disposition of the solvating unit and it has been shown that ethylene oxy ( $CH_2CH_2O$ ) containing polymers such as PEO have the most favourable spatial orientation of the solvating units.

In addition to the above factors polymer with low cohesive energy and a high flexibility is more favourable in solvation the ions. The former is characterized by lack of intermolecular interactions such as hydrogen bonding while the latter feature is indicated by a low glass transition temperature ( $T_g$ ). Thus although polymers like polyamides contain oxygen and nitrogen atoms as donor sites in their backbone, these polymers are quite unsuitable as polymer hosts in polymer electrolytes because of the presence of extensive intermolecular hydrogen bonding. Metal complexation with these polymers would lead to the disruption of this energetically favourable situation. The

second factor which is the high torsional flexibility of the polymer is indicated by a low  $T_g$  and is crucial for ion transport. Thus large segmental motions of the polymer (either the backbone or the side chain) which is possible above its  $T_g$  can lead to fast ion movement. In view of the above requirements, the polymers that have been studied as polymer electrolytes are oxygen-, nitrogen-, or sulphur-containing materials. The heteroatoms are either part of the backbone of the polymer or are present in the side chain attachments (Bellon-Maurel, 1998).

## 2.4 Polyacrylonitrile (PAN)

Polyacrylonitrile (PAN), a synthetic resin prepared by the polymerization of acrylonitrile. A member of the important family of acrylic resins, it is a hard, rigid thermoplastic material that is resistant to most solvents and chemicals, slow to burn and of low permeability to gases. Most polyacrylonitrile is produced as acrylic and modacrylic fibre, a common substitute for wool in clothing and home furnishings. Figure 2.1 shows the chemical structure of monomer of PAN. PAN has none of the hazardous properties of the monomer. Owing to the formation of strong chemical bonds between the nitrile (CN) groups, the polymer molecules resist most organic solvents and having high melting point of  $317\text{ }^{\circ}\text{C}$  and do not melt without decomposing ("Polyacrylonitrile", 2013). The semicrystalline polymer has glass transition temperature of  $85\text{ }^{\circ}\text{C}$  and molecular weight of repeat unit is  $53.06\text{ g/mol}$ .

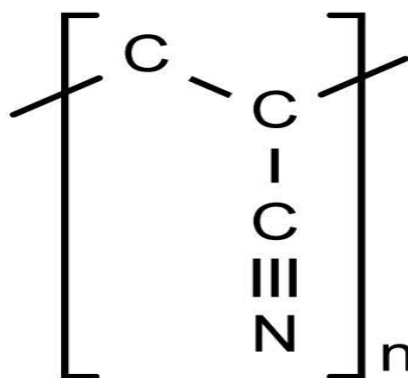


**Figure 2.1:** Chemical structure of PAN (Helmenstine, n.d.)



### 2.4.1 PAN as polymer electrolyte

Owing to the strong mechanical property PAN, PAN-based polymer electrolytes have been extensively studied. Various methods were done on increasing the conductivity values of PAN by incorporation of fillers, blending and more. Tsutsumi and Kitagawa (2006) synthesized a new type polymer electrolyte films based on PAN and cyanoethylated poly(vinyl alcohol) (CN-PVA) which achieved high conductivity value as  $14.6 \times 10^{-3} \text{ S cm}^{-1}$ . The interaction of  $\text{Li}^+$  and nitrile groups of PAN in the matrix were confirmed by FTIR analysis. Despite improving the conductivity values, the mechanism of the ion transport has become a great research interest. The local cation coordination motifs and ion dynamics in electrolyte system PAN: $\text{LiBF}_4$ :DMSO covering the range from salt-in-polymer to the polymer-in-salt regime was studied by Voight et al. (2012) employing advanced solid state NMR techniques, XRD and DSC. The electrochemical properties of PAN based polymer electrolyte and the discharge characteristics of an  $\text{Li}/\text{LiCoO}_2$  cell were investigated by Kim et al. (1997). The result shows that the electrolyte displayed high electrochemical stability up to 4.3 V (versus  $\text{Li}^+/\text{Li}$ ) and good cycling performance. Lithium polymer primary cell with fire-retardant PAN-based gel electrolyte was prepared by Akashi et al. (2002) presented a good volumetric energy density again confirmed the practicability of PAN-based polymer electrolyte.

### 2.5 Lithium Tetrafluoroborate ( $\text{LiBF}_4$ )

Lithium ions form many different compounds easily due to its reactivity. However, when selecting the suitable salt as the electrolyte solute for rechargeable batteries, the lithium salt should have high solubility and mobility in the non-aqueous media. Both cations and anions should remain inert toward the cell components. Besides inert to electrolyte solvents and stable against oxidative decomposition at the

cathode, the anion should be nontoxic and remain stable against thermally induced reactions with electrolyte solvents and other cell components. Most of the lithium salts that are qualified for the minimal solubility standard are based on complex anions that are composed of simple anion core stabilized by Lewis acid agent (Xu, 2004). The common salts used for  $\text{Li}^+$  conductive polymer electrolytes, such as lithium triflate ( $\text{LiCF}_3\text{SO}_3$ ), lithium tetrafluoroborate ( $\text{LiBF}_4$ ) and lithium perchlorate ( $\text{LiClO}_4$ ) have large anions and low lattice energies. Figure 2.2 represents the chemical structure of  $\text{LiBF}_4$ . The researchers who initiated the study of  $\text{LiBF}_4$  as compared with other salt,  $\text{LiBF}_4$  is less toxicity than  $\text{LiAsF}_6$  and higher safety than  $\text{LiClO}_4$  (Takata, Morita & Matsuda, 1985). However, its moderate ion conductivity has been a major obstacle to its application.  $\text{BF}_4^-$  has the highest mobility but its dissociation constant is significantly smaller than those of  $\text{LiAsF}_6$  and  $\text{LiPF}_6$ . Electrochemically, the  $\text{BF}_4^-$  anion was found to be stable against the oxidation on a glassy carbon (GC) surface up to 3.6 V vs a standard colomel electrode (SCE), which translate into ~5.0 V vs lithium (Ue, Takeda, Takehara & Mori, 1997; Ue, Murakami, Nakamura & Mori, 2002)

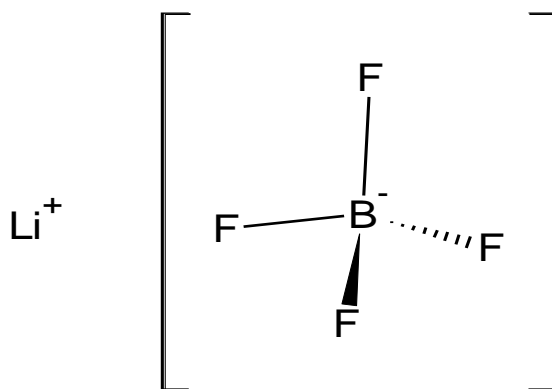


**Figure 2.2:** Chemical structure of  $\text{LiBF}_4$  (“Lithium tetrafluoroborate”, 2013)

## 2.6 Plasticization

The ionic conduction takes place in the amorphous region of the polymer matrix. However, solid polymer films are usually highly crystalline at room temperature, resulting in a low conductivity. Increasing the amorphous nature of the polymer at ambient temperature can be achieved by the addition of plasticizing agents (Wang, Huang, Xue, Huang & Chen, 1999). The expectations should be met upon addition of plasticizers are

- (i) The decrease of glass transition temperature,  $T_g$
- (ii) Enhanced dissolution of dopant salt
- (iii) Additional coordinating sites for ions migration

Figure 2.3 shows the chemical structures of ethylene carbonate (EC) and dimethyl phthalate (DMP). Ethylene carbonate is an indispensable electrolytes solvent which was used in the conventional liquid electrolyte with the combination of different carbonates solvent (Abouimrane et al., 2009). The combination should give balanced benefits of both solvents such as high dielectric constant, low viscosity, chemical resistant to the cell components, low melting point and high boiling point, nontoxic and economical. Phthalates are esters of phthalic acid and are mainly used as plasticizers of plastics to increase the flexibility, transparency, durability, and longevity. Benedict et al. (1998) and Rajendran et al. (2002) have reported (PEO)<sub>8</sub>-LiAsF<sub>6</sub> composite and PMMA-PEO hybrid polymer electrolyte doped with different phthalates proved that DMP can effectively improve ionic conduction.

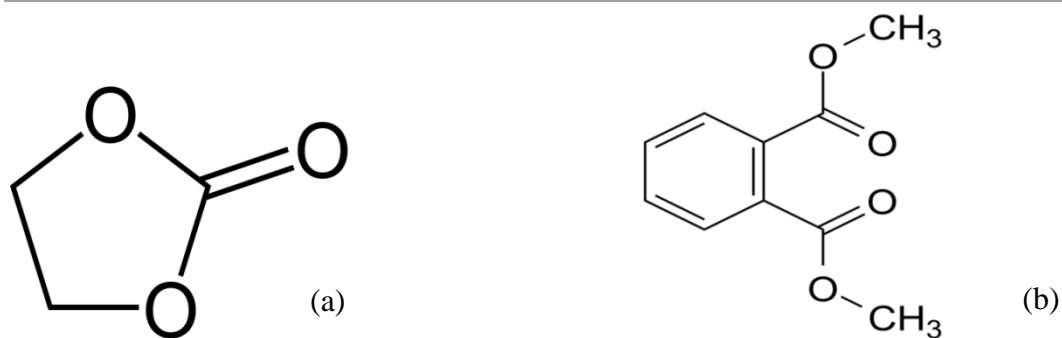


**Figure 2.3:** Chemical structures of (a) EC (“Ethylene Carbonate”, n.d.) and (b) DMP (“Dimethyl phthalate”, 2012)

## 2.7 Polymer electrolytes in applications

To date, polymer electrolytes has developed into wide range of applications which are secondary batteries, fuel cells, sensors, actuators, supercapacitors, electrochromic devices and dye-sensitized solar cells. Generally, the roles of the polymer electrolytes in these applications are (Di Noto, Lavina, Giffin, Negro & Scrosati, 2011).

- (i) Separating two electrodes
- (ii) Providing good electronic insulation
- (iii) Allowing a fast and selective transport of the desired ions

### 2.7.1 Battery

A battery, is an electrochemical cell, is a device that produces electricity from a chemical reaction. A battery consists of two or more cells connected in series or parallel, but the term is generally used for a single cell. A cell consists of a negative electrode, an electrolyte, a separator, and a positive electrode. The electrolyte may be aqueous (composed of water) or nonaqueous (not composed of water), in liquid, paste, or solid form. When the cell is connected to an external load, the negative electrode supplies a current of electrons that flow through the load and are accepted by the positive electrode. A primary battery is one that can convert its chemicals into electricity only once and

then must be discarded. A secondary battery has electrodes that can be reconstituted by passing electricity back through it; also called a storage or rechargeable battery, it can be reused many times (Bellis, n.d.). In general, the parameters of desirable battery properties studies are focused on energy content per unit volume and weight, discharge and charge characteristics at different rates and temperature, internal resistance, capacity, efficiency, charge retention, life and mechanical stability. Figure 2.4 represents a diagram of lithium polymer battery.

The Li-Polymer battery is found to be advantageous due to its flexibility allowed manufacturing are not bound by standard cell formats. With high volume, any reasonable size can be produced economically. Its light weight gelled electrolytes enable simplified packaging by eliminating the metal shell and the most important features is its improved safety make it more resistant to overcharge; less chance for electrolyte leakage.

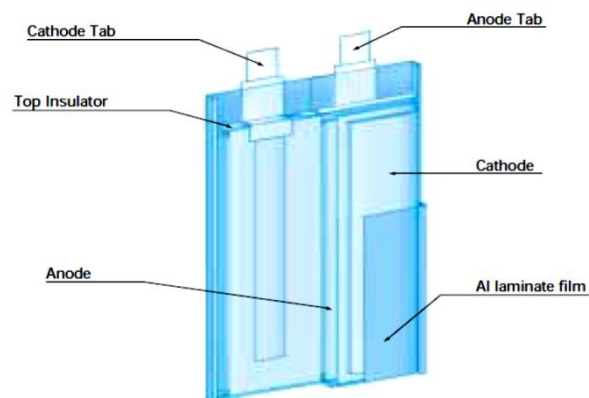


**Figure 2.4:** Lithium Polymer Battery (Sony, n.d.)

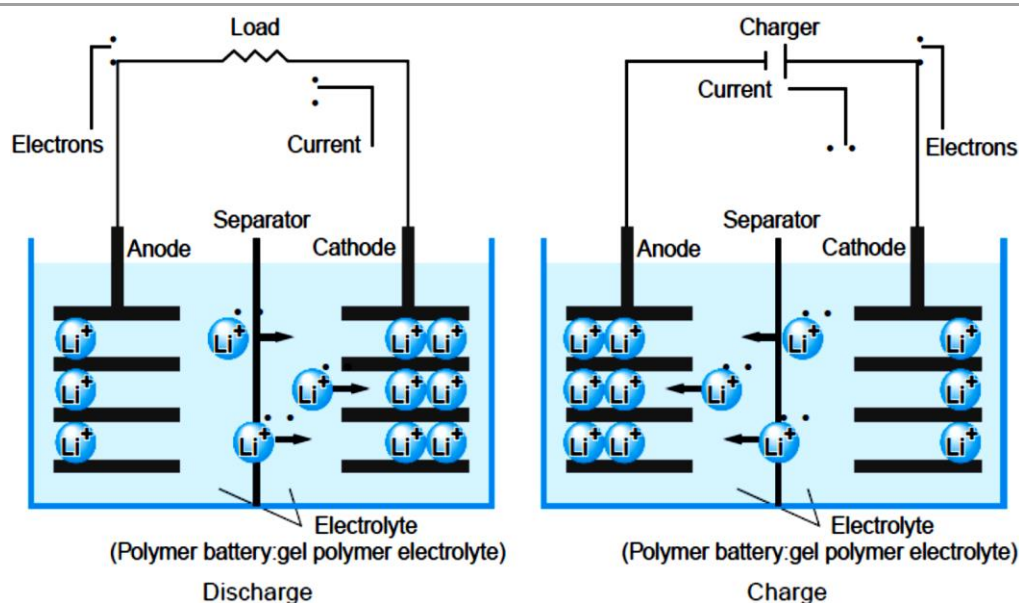


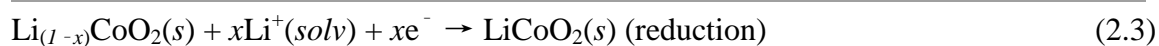
**Figure 2.5:** Schematic illustration of charge and discharge process for secondary battery (Sony, n.d.)

### 2.7.2 Charge/discharge mechanism

Battery charging and discharging occur through the migration of lithium ions between the cathodes and anodes and the exchange of electrons through intercalation and deintercalation. More specifically, during charging lithium is deintercalate from cathodes consisting of a lithium-containing compound, and the interlayers of carbon in anodes are intercalated with lithium. Conversely, during discharge lithium is deintercalate from between the carbon layers in anodes, and the compound layers in cathodes are intercalated with lithium. Reactions occurring in lithium ion rechargeable batteries employing lithium cobalt oxide in cathodes and carbon in anodes are shown in Figure 2.5. By means of the initial charging, which takes place during battery manufacture, lithium ions migrate from the lithium compound of the cathode to the carbon material of the anode (McQuarrie, Rock & Gallogly, 2011).

The half-cell reactions and overall cell equation for a typical lithium ion secondary cell are





and the overall cell equation is



### 2.7.3 Cathodes

The material for an ideal cathode of a rechargeable lithium battery should have following properties (Tao, Feng, Liu, Kan & Chen 2011).

- (i) Capable of reversibly intercalating/deintercalating Li ions at a large capacity and high potential.
- (ii) Minimal structural change during Li ion intercalating/deintercalating
- (iii) Minimal redox potential change during Li ion intercalating/deintercalating
- (iv) High electronic conductivity, high Li ion diffusion rate and conductivity
- (v) Chemically stable with electrode under operating potentials.

Currently, the most desirable compounds for cathode materials are  $\text{LiNi}_x\text{Mn}_y\text{Co}_{1-x-y}\text{O}_2$ ,  $\text{LiFePO}_4$  (lithium iron phosphate),  $\text{LiCoO}_2$  (lithium cobalt oxide),  $\text{LiNiO}_2$  (lithium nickelate), and  $\text{LiMn}_2\text{O}_4$  (spinel-structure lithium manganate) based system (Li, Daniel & Wood, 2011). On comparing the characteristics of these compounds,  $\text{LiCoO}_2$  was selected for use as the first generation's cathode active material due to its reversibility, discharge capacity, charge/discharge efficiency, discharge curve and other properties. Table 2.1 shows a comparison of typical cathode materials (Sony, n.d.).

**Table 2.1:** Comparison of Typical Cathode Materials ( Tao et al., 2011).

	<b>LiCoO<sub>2</sub></b>	<b>LiMnO<sub>4</sub></b>	<b>LiFePO<sub>4</sub></b>
<b>Theoretical Capacity (Ah Kg<sup>-1</sup>)</b>	145	148	170
<b>Commercial Capacity (Ah Kg<sup>-1</sup>)</b>	135~134	100~110	140~160
<b>Tap Density (Kg L<sup>-1</sup>)</b>	2.6~3.0	1.8~2.4	0.8~1.4
<b>Discharge Plateau (V)</b>	3.6	3.7	3.3
<b>Cycle Life (Cycles)</b>	500-800	1000-1500	>3000
<b>Working Temperature ( °C)</b>	-20~55	-20~50	-20~60
<b>Advantages</b>	1. Simple process 2. High volumetric capacity	1. Cheap 2. Simple process	1. Cheap 2. Eco-friendly 3. Safe
<b>Disadvantages</b>	1. Expensive 2. Toxic	1. Capacity fades at elevated temperature	1. Low conductivity 2. Complex process 3. Low volumetric capacity
<b>Applied Areas</b>	Portable Devices	Electric Vehicles	Electric Vehicles

### 2.7.4 Anodes

Anode materials should have the same properties as cathode for a good battery performance. Carbon-based materials are generally used in commercial Li ion batteries as the anode. However, based on the limitation of the theoretical gravimetric capacities of these materials (372 Ah Kg<sup>-1</sup>, LiC<sub>6</sub>), many efforts have been carried out to develop higher capacity anode materials such as Li-based materials, Tin-based materials, transition-metal oxides and silicon. Lithium was used as anode material owing to its high theoretical capacity of 3860 Ah Kg<sup>-1</sup>. It was reported that reaction of lithium with organic electrolytes lead to the formation of dendrite. This problem can be inhibited by



substitution of polymer electrolyte. Carbon materials with large doping capacities, and the possibility of lithium-carbon intercalation complexes exceeding the  $\text{LiC}_6$  stoichiometric composition, are being studied. There are three types of carbon material have been employed in anodes which are graphite, graphitizable carbon (soft carbon) and non-graphitizable carbon (hard carbon).

In hard carbon, the interlayer distances are large compared with those in graphite and soft carbon, and reversibility in charging and discharging is good, for excellent cycling characteristics. On the other hand, graphite materials have a little working voltage by the depth of discharge and exhibit excellent characteristics in constant-power discharge (Sony, n.d.). Transition-metal oxides (MO) were proposed as anode materials for their large capacity at low potentials. The reaction mechanism between MO (M is Co, Ni, Cu or Fe) and Li ion differs from the classical Li ion intercalation/deintercalation or Li-alloying processes. It involves the composition and decomposition of  $\text{Li}_2\text{O}$ , accompanied with the reduction and oxidation of the transition metal, respectively. The capacities of these transition-metals are all greater than  $700 \text{ Ah Kg}^{-1}$ , with high capacity retention and high recharging rate. These systems hold much promise for future development. Among MO materials, the capacities of Ti-based oxides are less than half that of graphite ( $175 \text{ Ah Kg}^{-1}$  for  $\text{Li}_4\text{Ti}_5\text{O}_{12}$ ). However, these materials have many advantages, such as outstanding stability, rapid charge rate, and wide operating temperature (range from  $-50^\circ\text{C}$  to  $75^\circ\text{C}$ ). The combination of these advantages results in ultra-long durability (around 20 years) and cycle life (9000 cycles). In addition, these batteries do not explode or result in thermal runaway under harsh conditions (Tao et al., 2011).

# **CHAPTER 3**

## **EXPERIMENTAL TECHNIQUES**

### 3.1 Sample Preparation

In this work, three types of polymer electrolyte systems were prepared. The first system is the plasticized PAN films where the amount of plasticizers EC and DMP was varied in different ratio and the amount of PAN is fixed. The second system is unplasticized PAN films doped with different amounts of  $\text{LiBF}_4$ . The final system is the plasticized PAN films doped with varied concentrations of  $\text{LiBF}_4$  and fixed ratio of plasticizers.

#### 3.1.1 Preparation of PAN-EC-DMP system

In this system, 2 grams of polyacrylonitrile (PAN) from Aldrich was dissolved in appropriate amount of dimethylformamide (DMF) solvent from R&M Chemicals. The mixtures consisting of PAN and DMF were stirred with heating at 60 °C until homogeneous polymer solution was obtained. The amounts of plasticizers, ethylene carbonate (EC) from Aldrich and dimethyl phthalate (DMP) from Merck with different ratios were added to the polymer solution as shown in Table 3.1. The mixtures were stirred for another 6 hours at 60 °C. The solutions were then cast on petri dishes and left to dry under vacuum for 2 days at 53 °C until free standing films were obtained. These films were prepared to determine the best combination of EC and DMP to be used for the polymer electrolyte preparation. Pure PAN films were prepared as reference.

**Table 3.1:** Compositions of PAN, EC and DMP in PAN-EC-DMP system

Sample	PAN (g)	EC (g)	DMP (g)
Pure PAN	2	0	0
PAN-EC	2	3	0
PAN-2EC-1DMP	2	2	1
PAN-EC-DMP	2	1.5	1.5
PAN-1EC-2DMP	2	1	2
PAN-DMP	2	0	3

### 3.1.2 Preparation of PAN-LiBF<sub>4</sub> system

LiBF<sub>4</sub> doped PAN films were prepared using the same method as mentioned in Section 3.1.1. Different amounts of LiBF<sub>4</sub> from Acro Organics varying from 5 wt% to 50 wt% were added into the polymer solution to form PAN-LiBF<sub>4</sub> films. The effect of the concentration of dopant salt, LiBF<sub>4</sub> was studied on PAN-LiBF<sub>4</sub> system.

### 3.1.3 Preparation of PAN-EC-DMP-LiBF<sub>4</sub> system

Another set of solutions containing same amount of 2 grams of PAN, fixed amount of EC and DMP in the ratio of 1 to 1 and LiBF<sub>4</sub> varying from 5 wt.% to 40 wt.% were prepared to form the PAN-EC-DMP-LiBF<sub>4</sub> system. A comparison between the unplasticized and plasticized system was studied in terms of their electrical, thermal, structural and electrochemical properties.

## 3.2 Measurement of Ionic Conductivity

### 3.2.1 Electrochemical Impedance Spectroscopy (EIS)

Electrochemical impedance spectroscopy (EIS) is a powerful tool for investigation of the rate of charge transfer and charge transport processes occurring in electrochemical systems (Bard & Faulkner, 2000; Lasia, 2002; Retter, 2002). Therefore,

it is widely used also for the characterization of conducting polymer films and membranes. Owing to the marginal perturbation from equilibrium (steady state) by low-amplitude (<5 mV) sinusoidal voltage, its advantage over other techniques involving large perturbations (e.g., chronoamperometry) is evident. For instance, even the potential dependence of the charge transport diffusion coefficient can be determined that may reveal the nature of charge carriers and interactions within the film.

Although there are several variations, usually an alternating voltage

$$U(t) = U_m \sin(\omega t) \quad (3.1)$$

is applied to an electrode and the resulting current response

$$I(t) = I_m \sin(\omega t + \varphi) \quad (3.2)$$

is measured, where  $\omega$  ( $\omega = 2\pi f$ , where  $f$  is the frequency) is the angular frequency of the sinusoidal potential perturbation,  $\varphi$  is the phase difference between the potential and the current, and  $U_m$  and  $I_m$  are the amplitudes of the sinusoidal voltage and current, respectively. The impedance ( $Z$ ) is defined as

$$Z = \frac{U(t)}{I(t)} = |Z| \exp(i\varphi) = Z_r + iZ_i \quad (3.3)$$

where  $Z'$  and  $Z''$  are the real and imaginary part of  $Z$ , respectively, and  $i = (-1)^{1/2}$ .

Where the impedance can be resolved into

$$Z_r = Z(\omega) \cos \varphi(\omega) \quad (3.4)$$

$$Z_i = Z(\omega) \sin \varphi(\omega) \quad (3.5)$$

In the impedance spectrum, also known as the Cole-Cole plot the real part of impedance is plotted against the imaginary part as Figure 3.1 for the data collected at various frequencies.

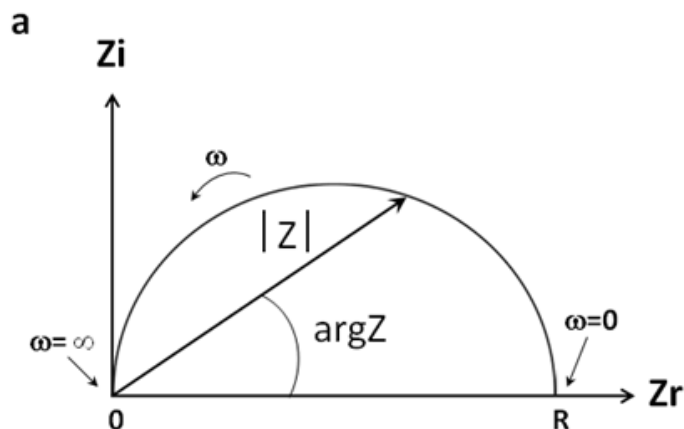


**Figure 3.1:** Cole-Cole plot (Andrade, Oliveira, Faulin, Hering & Abdalla, 2011)

From this plot the bulk resistance of the electrolyte ( $R_b$ ) is obtained. The bulk resistance for each film is measured for six times on different parts of the film. The conductivity,  $\sigma$  is then obtained from

$$\sigma = \frac{t}{R_b A} \quad (3.6)$$

where  $t$  is the thickness of sample,  $A$  is the contact area between electrode and sample and  $R_b$  is the bulk resistance.

### 3.2.2 Conductivity-Temperature Behaviour

The conductivity-temperature dependence data can be treated by the use of Arrhenius equation

$$\sigma = \sigma_o \exp(-E_a/kT) \quad (3.7)$$

The Arrhenius plot in which  $\log \sigma$  is plotted against  $1000/T$  shows straight line. The activation energy,  $E_a$  can be calculated from the slope of the Arrhenius plot (Hagenmuller & Van Gool, 1978; Plieth, 1995). The activation volume  $\Delta V^*$  from the plot of conductivities values on logarithmic scale as a function of pressure. The slopes

of straight lines plot allow a volume  $\Delta V^*$  to be determined by the relationship (Duclot, 2000)

$$\left(\frac{\partial \ln \sigma}{\partial P}\right)_T = \frac{\Delta V^*}{RT} \quad (3.8)$$

Usually the impedance is measured as a function of frequency, and its variation is characteristic to the electrical circuit consisting of passive and active circuit elements. Under appropriate conditions, that is, at well-selected cell geometry, working and auxiliary electrodes, and so forth, the impedance response will be related to the properties of the working electrode and the (ohmic) resistance between the working electrode and the reference.

The equations for the dielectric constant  $\varepsilon_r$  and the dielectric loss,  $\varepsilon_i$  can be obtained as shown in Equations 3.9- 3.11

$$\varepsilon_r = \frac{Z_i}{\omega C_c(Z_r^2 + Z_i^2)} \quad (3.9)$$

$$\varepsilon_i = \frac{Z_r}{\omega C_c(Z_r^2 + Z_i^2)} \quad (3.10)$$

$$C_c = \frac{\varepsilon_o A}{t} \quad (3.11)$$

where  $\varepsilon_o$  is permittivity of free space.

In this study, the electrical conductivity of polymer electrolytes was measured using HIOKI 3532-50 LCR Hi Tester which is interfaced to a computer for data acquisition over the frequency range between 50 Hz and 1 MHz. The film was placed between two stainless steel electrodes which acted as a blocking electrode for ions. The electrical conductivity is measured six times on different area of the samples. The

behaviour of conductivity was studied by conducting the measurement in the temperature range between 303K and 353K.

### 3.3 Ion transport number measurements

In polymer electrolytes both the ions (cations and anions) may be mobile. If free electrons are also present in the system, they will also take part in the conduction process. Measurement of transport number was done to know what fraction of current is carried by which mobile species. This measurement can be carried out using D.C. polarization and/or combined A.C./D.C. techniques. The transference number of a charge carrier is defined as the ratio of the conductivity due to itself and the total conductivity,  $\sigma_T$ . Hence, the total ionic transport number,  $t_{ion}$  is expressed as:

$$t_{ion} = \sigma_{ion} / \sigma_T = I_{ion} / I_T \quad (3.12)$$

and the electron /hole transport number,  $t_{e,h}$  is expressed as:

$$t_{e,h} = \sigma_{e,h} / \sigma_T = I_{e,h} / I_T \quad (3.13)$$

where symbol have their usual meanings i.e.  $\sigma_{ion}$  ( $I_{ion}$ ),  $\sigma_{e,h}$  ( $I_{e,h}$ ),  $\sigma_T$  ( $I_T$ ) are the ionic, electronic/ hole and total conductivity (current) respectively. Ideally, for pure ionic conductors  $t_{ion} = 1$  and  $t_{e,h} = 0$ . The transference number lies between 0 and 1 for mixed conductors with partially ionic and electronic conduction. In most of the liquid or aqueous electrolytes as well as ion conducting polymer electrolytes, cations and anions are the main contributors to the total ionic conductivity and the electron or hole conduction is negligibly small. Hence, cationic/anionic transport numbers are important parameters to be determined. The combination of A.C. and D.C. techniques as suggested by Evans, Vincent and Bruce ( 1987) and Watanabe, Nagano, Sanui and Ogata (1988) are widely used to evaluate cationic transference number ( $t_+$ ).



In the present study, both D.C. polarization and combined A.C./D.C. methods were used. These techniques are discussed in Section 3.3.1 and 3.3.2.

### 3.3.1 D.C. polarization technique for the evaluation of total ionic transport number

A D.C. electric potential is applied across the sample sandwiched between two blocking electrodes (stainless steel in present study) and the current is monitored as a function of time. The peak current obtained initially decreases rapidly with time due to polarization of mobile ions at the electrode-electrolyte interface, subsequently, the current either approaches zero (for pure ion conductor) or attains a residual constant value (for mixed ionic/electronic conductor). The initial total current ( $I_t$ ) is either due to ions solely or as a result of combined ionic and electronic conduction while the constant residual current is only due to electron conduction. From the current versus time plot, the ionic ( $t_{ion}$ ) and electron ( $t_e$ ) transport numbers can be determined using equation 3.14:

$$t_{ion} = 1 - \frac{i_e}{i_t} = 1 - t_e \quad (3.14)$$

### 3.3.2 Combined A.C./D.C. techniques for the evaluation of cationic transport number

Vincent & Bruce Technique (Evans et. al, 1987) was adopted to evaluate the cationic transport number. In this technique, the cell is in the configuration of: M | MX (Electrolyte) | M type is polarized potentiostatically upon applying a small D.C. voltage  $\Delta V$  and initial ( $I_0$ ) and final ( $I_s$ ) currents are recorded. The cell is also subjected to A.C. impedance measurements prior to and after the polarization to evaluate the resistance before ( $R_0$ ) and after ( $R_s$ ) the polarization. Eventually, the cationic transport number ( $t_+$ ) can be estimated following equation:

$$t_+ = \frac{I_s(\Delta V - I_0 R_0)}{I_0(\Delta V - I_s R_s)} \quad (3.15)$$

### **3.4 Morphology and Structural Studies**

#### **3.4.1 Field Emission Scanning Electron Microscopy (FESEM)**

FESEM is used to visualize very small topographic details on the surface or entire or fractioned objects. Researchers in biology, chemistry and physics apply this technique to observe structures that may be as small as 1 nanometer. Much like the traditional Scanning Electron Microscope, the Field Emission Scanning Electron Microscope uses electrons to illuminate a sample, instead of visible light as is used in optical microscopy. Since the wavelength of electrons is much smaller than that of visible light, scanning electron microscopes are capable of imaging at much higher magnification than light microscopes. FESEM is capable of reaching a magnification of 1000,000 times and a spatial resolution of up to 1.4 nm, making the FESEM a good choice for high magnification and high resolution imaging (ACMAL eTraining, 2013).

Figure 3.2 shows a schematic diagram of FESEM experiment. Electrons are liberated from a field emission source and accelerated in a high electrical field gradient. Within the high vacuum column these so-called primary electrons are focussed and deflected by electronic lenses to produce a narrow scan beam that bombards the object. As a result, secondary electrons are emitted from each spot on the object. In cold field emission electron microscopy, however, an electric field is applied to the tip of the electron source essentially "pulling" electrons from the emitter. The electrons are then accelerated off of the source by two anodes. Because of the microscopic size of the electron source, the beam produced by this emitter is one of the smallest available and contributes to the high resolution of the instrument. The angle and velocity of these secondary electrons relates to the surface structure of the object. A detector catches the secondary electrons and produces an electronic signal. This signal is amplified and transformed to a video scan-image that can be seen on a monitor or to a digital image that can be saved and processed further.

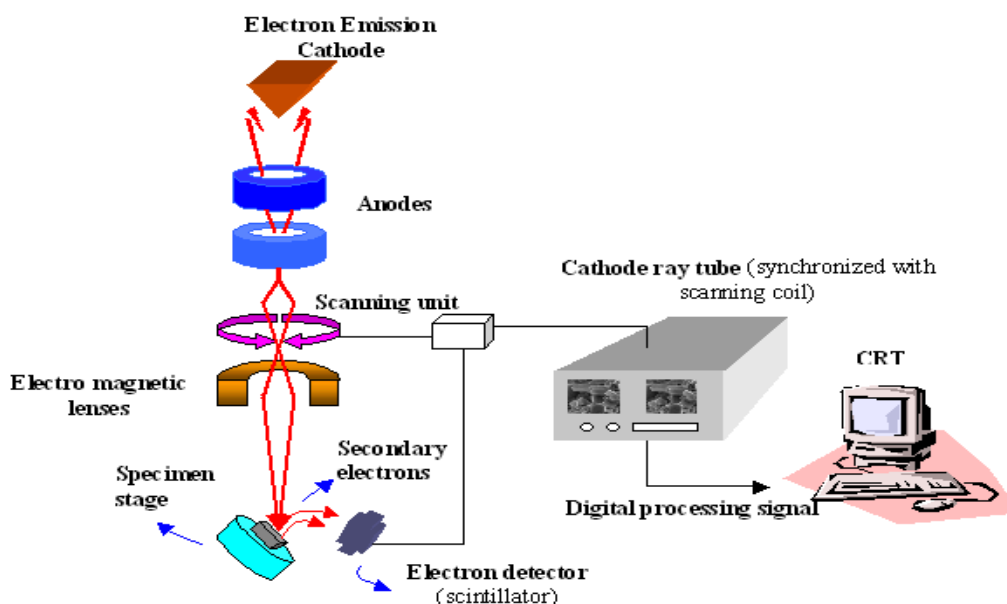


**Figure 3.2:** Schematic diagram of FESEM experiment (New Mexico Tech., n.d.)

In the present work, the morphological properties of the polymer electrolytes films were studied using micrographs obtained using FESEM. Quanta FEG 450 was used due to its variable vacuum strength which can retain the structure of the samples. The effect of addition of salt and plasticizers on the nature of the PAN films was revealed clearly using this technique.

### 3.4.2 X-ray Diffraction (XRD)

X-ray diffraction (XRD) is one of the most powerful techniques for qualitative and quantitative analysis of polymers, ceramics and semiconductor materials. The technique provides information that cannot be obtained any other way. The information obtained includes types and nature of crystalline phases present, structural make-up of phases, degree of crystallinity, amount of amorphous content, microstrain & size and orientation of crystallites.

X-ray diffractometers consist of three basic elements: an X-ray tube, a sample holder, and an X-ray detector as shown in Figure 3.3. X-ray diffraction is based on constructive interference of monochromatic X-rays and a crystalline sample. X-rays are

generated by a cathode ray tube, filtered to produce monochromatic radiation, collimated to concentrate, and directed toward the sample. The interaction of the incident rays with the sample produces constructive interference (and a diffracted ray) as shown in Figure 3.4 when conditions satisfy Bragg's Law ( $n\lambda = 2d \sin \theta$ ) (Geochemical, 2013). The position of diffracted peaks also provides information about how the atoms are arranged within the crystalline compound. The intensity information is used to assess the type and nature of atoms. Determination of lattice parameter helps understand extent of solid solution in a sample. The width of the diffracted peaks is used to determine crystallite size and micro-strain in the sample. This law relates the wavelength of electromagnetic radiation to the diffraction angle and the lattice spacing in a crystalline sample. These diffracted X-rays are then detected, processed and counted. By scanning the sample through a range of  $2\theta$  angles, all possible diffraction directions of the lattice should be attained due to the random orientation of the powdered material. Conversion of the diffraction peaks to d-spacings allows identification of the mineral because each mineral has a set of unique d-spacings. Typically, this is achieved by comparison of d-spacings with standard reference patterns.

The structural properties of the polymer electrolyte films were investigated by XRD studies using X'Pert PRO PANalytical diffractometer in order to examine the nature of crystallinity and the amorphousness of the SPE films. The influence of the amount of plasticizers and  $\text{LiBF}_4$  on the structural changes was observed.

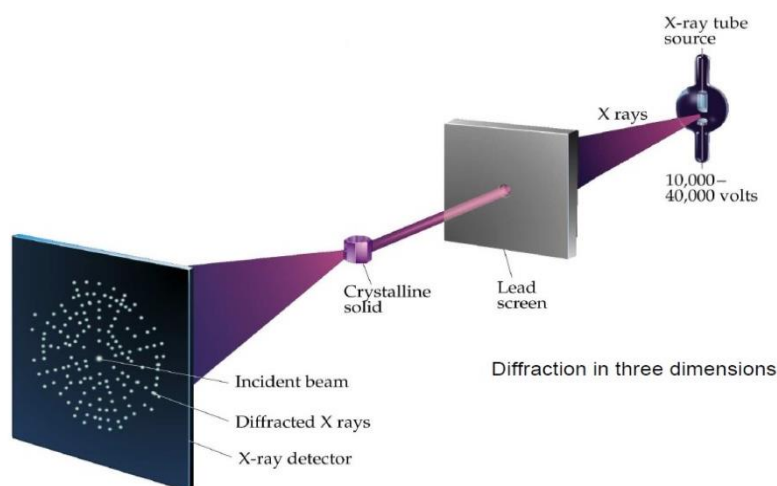


**Figure 3.3:** Principle of X-ray Diffraction (“X-rays”, n.d.)

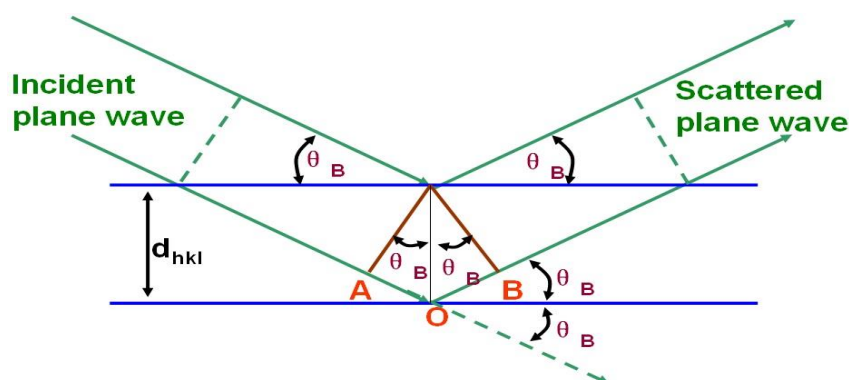


**Figure 3.4:** Schematic illustration of Bragg condition and Bragg's law (FEI, 2009)

### 3.5 Fourier Transform Infrared Spectroscopy (FTIR)

Infrared absorption spectroscopy is the study of interaction of infrared radiation with matter as a function of photon frequency. Fourier Transform Infrared Spectroscopy (FTIR) provides specific information about the vibration and rotation of the chemical bonding and molecular structures, making it useful for analyzing organic materials and certain inorganic materials. An infrared spectrum represents a fingerprint of a sample with absorption peaks which correspond to the frequencies of vibrations between the bonds of the atoms making up the material. Because each different material is a unique combination of atoms, no two compounds produce the exact same infrared spectrum. Therefore, infrared spectroscopy can result in a positive identification of every different

kind of material. In addition, the size of the peaks in the spectrum is a direct indication of the amount of material present. With modern software algorithms, infrared is an excellent tool for quantitative analysis.

The IR region is commonly divided into three smaller areas: near - IR ( $400 - 10\text{ cm}^{-1}$ ), mid - IR ( $4000 - 400\text{ cm}^{-1}$ ), and far - IR ( $14000 - 4000\text{ cm}^{-1}$ ). Infrared photons have enough energy to cause groups of atoms to vibrate with respect to the bonds that connect them. Like electronic transitions, these vibrational transitions correspond to distinct energies, and molecules absorb infrared radiation only at certain wavelengths and frequencies. Chemical bonds vibrate at characteristic frequencies, and when exposed to infrared radiation, they absorb the radiation at frequencies that match their vibration modes. Measuring the radiation absorption frequency produces a spectrum that can be used to identify functional groups and compounds. Some impurities produce their own characteristic bands in infrared region. Spectral measurements of these bands are used to determine concentration of the impurities and their bonding with the host materials (Silverstein, Bassler & Morrill, 1981).

The schematic diagram of an FTIR spectrometer is shown in Figure 3.5. The normal instrumental process is as follows:

- (i) Source: Infrared energy is emitted from a glowing black-body source. This beam passes through an aperture which controls the amount of energy presented to the sample (and, ultimately, to the detector).
- (ii) Interferometer: The beam enters the interferometer where the 'spectral encoding' takes place. The resulting interferogram signal then exits the interferometer.
- (iii) Sample: The beam enters the sample compartment where it is transmitted through or reflected off of the surface of the sample, depending on the type of analysis being accomplished. This is where specific frequencies of energy, which are uniquely characteristic of the sample, are absorbed.

- (iv) Detector: The beam finally passes to the detector for final measurement. The detectors used are specially designed to measure the special interferogram signal.
- (v) Computer: The measured signal is digitized and sent to the computer where the Fourier transformation takes place. The final infrared spectrum is then presented to the user for interpretation and any further manipulation.

In this present work, the infrared spectra for all samples were taken with Thermo Scientific Nicolet iS 10 FT-IR spectrometer in the number region between  $650\text{ cm}^{-1}$  and  $4000\text{ cm}^{-1}$  with resolution of  $1\text{ cm}^{-1}$ .

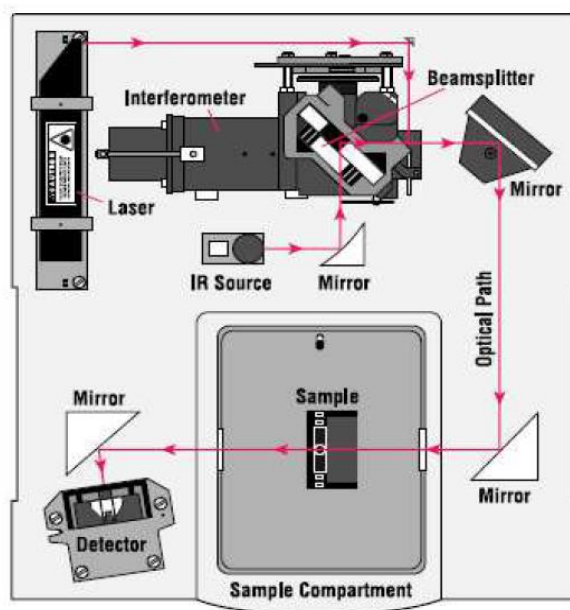


**Figure 3.5:** Schematic Diagram of FTIR (Thermo Nicole, n.d.)

### 3.6 Thermal Analysis

#### 3.6.1 Thermogravimetric Analysis (TGA)

Thermogravimetric analyzer is employed in research and testing to characterize materials such as inorganic compounds, monomers, polymers or organic compounds, to determine

- (i) Degradation temperatures.
- (ii) Absorbed moisture content of materials.
- (iii) The level of inorganic and organic components in materials.
- (iv) Decomposition points of explosives.
- (v) Decomposition points.
- (vi) Temperatures that solvent residues are driven off (“Thermal Gravimetric Analysis”, n.d.).

Figure 3.6 shows a schematic diagram of a thermobalance. A TGA consists of a sample pan that is supported by a precision balance. That pan resides in a furnace and is heated or cooled during the experiment. The mass of the sample is monitored during the experiment. A sample purge gas controls the sample environment. This gas may be inert or a reactive gas that flows over the sample and exits through an exhaust.

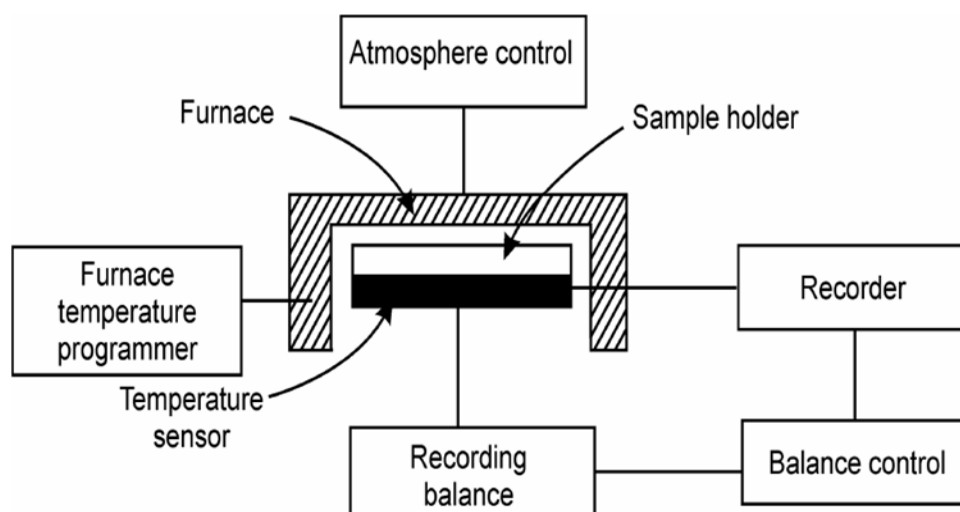


**Figure 3.6:** Block Diagram of a Thermobalance



A thermogravimetric analyzer is used to complement a DSC, and measures mass changes of a sample as a function of temperature or time. For example, if one sees an endothermic or exothermic reaction using a DSC, the TGA measurements will help determine whether the change is physical or chemical in nature. The reaction is chemical in nature if a mass change is associated with it and physical if no mass change occurs. It is based on the measurement of mass loss of material as a function of temperature. In thermogravimetry a continuous graph of mass change against temperature is obtained when a substance is heated at a uniform rate or kept at constant temperature. A plot of mass change versus temperature ( $T$ ) is referred to as the thermogravimetric curve (TG curve). For the TG curve, we generally plot mass ( $m$ ) decreasing downwards on the y axis, and temperature ( $T$ ) increasing to the right on the  $x$  axis as illustrated in Figure 3.7 where plateau A and C represents constant mass region and plateau B represent mass loss portion.

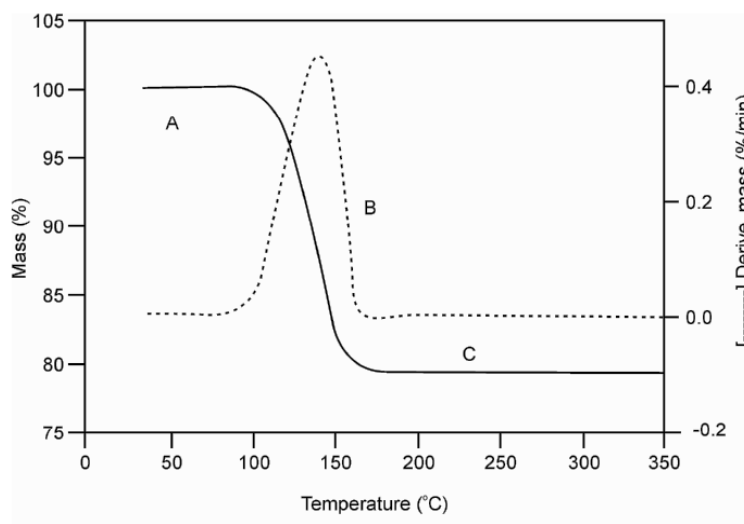


**Figure 3.7:** TG Curve.

In this work, TG graphs for all the samples were obtained using Perkin Elmer Instrument. The experiment is conducted from room temperature to 800 °C with heating

rate 10 °C/min. The thermograms provide information such as the thermal stability and percentage weight loss of the component(s) of the polymer electrolyte films.

### 3.6.2 Differential Scanning Calorimetry (DSC)

DSC is a method of thermal analysis that is widely used to study thermal transitions, i.e., solid-solid transitions as well as solid-liquid and various other transitions and reactions. A solid-solid phase transition would be if the material had its structure altered, but not gain enough energy to become a liquid. Using thermal analysis, it is possible to understand what is happening in a material, even if there is no visual evidence that a change has occurred (Brown, 2001). By understanding the technique and instrumentation of DSC, it is possible to understand what the materials go through during energy gain or loss.

Differential scanning calorimetry (DSC) monitors heat effects associated with phase transitions and chemical reactions as a function of temperature. In a DSC, the difference in heat flow to the sample and a reference at the same temperature is recorded as a function of temperature. The reference is an inert material such as alumina, or just an empty aluminium pan. The temperature of both the sample and reference are increased at a constant rate.

The calorimeter consists of a sample holder and a reference holder as shown in Figure 3.8. Both are constructed of platinum to allow high temperature operation. Under each holder are a resistance heater and a temperature sensor. Currents are applied to the two heaters to increase the temperature at the selected rate. The difference in the power to the two holders, necessary to maintain the holders at the same temperature, is used to calculate  $\Delta dH/dt$ . A flow of nitrogen gas is maintained over the samples to create a reproducible and dry atmosphere. The nitrogen atmosphere also eliminates air oxidation of the samples at high temperatures.

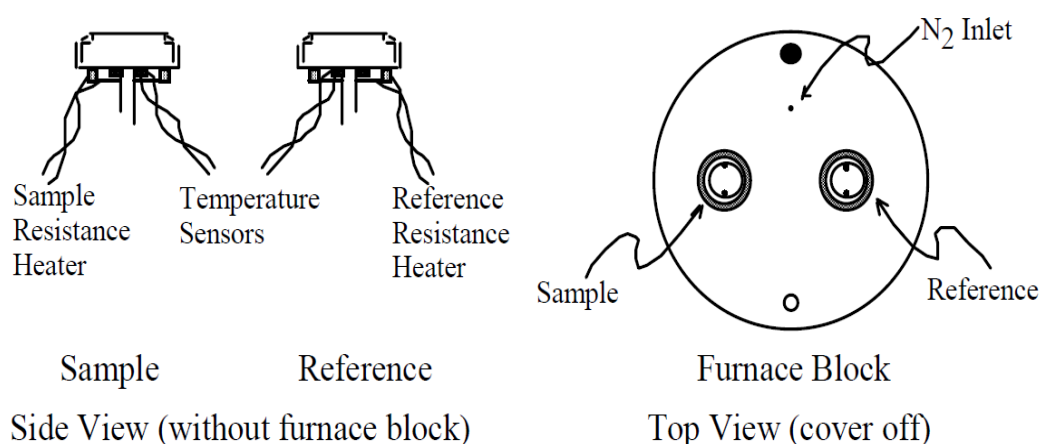


**Figure 3.8:** Differential scanning calorimeter sample and reference holder.

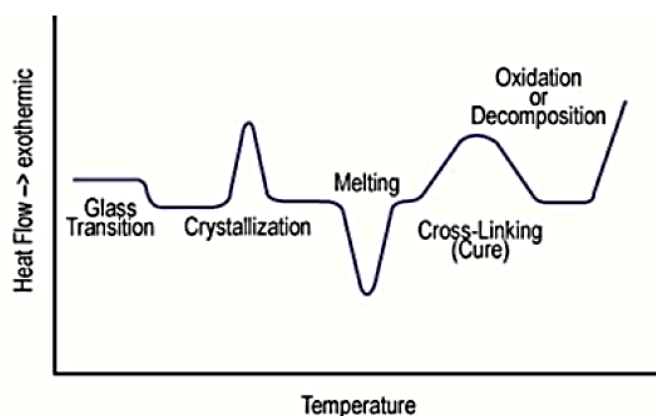


**Figure 3.9:** DSC Thermogram (TA Instruments, Inc)

During the heating of a sample, for example, from room temperature to its decomposition temperature, peaks with positive and negative  $\Delta dH/dt$  may be recorded; each peak corresponds to a heat effect associated with a specific process, such as crystallization or melting as shown in Figure 3.9.

In this work, DSC results of the SPE samples are obtained using Perkin Elmer DSC Instrument. The temperature range used ranging from room temperature until 350 °C with heating/cooling rate at 10 °/min. The DSC plots were analyzed using TA Instrument Explorer software in order to find the glass transition temperature  $T_g$  (midpoint) and decomposition temperature ( $T_d$ ) of the SPE films.

### 3.7 Potential Sweep Voltammetry

Potential also known as voltammetric sweep methods provide an efficient and straightforward assessment of the redox behaviour of molecular systems. In all potential sweep methods, the potential (V) of the working electrode is varied continuously with time according to a predetermined potential waveform, while the current ( $I$ ) is concurrently measured as a function of the potential. The applied potential at the working electrode is measured against a reference electrode of choice, while a counter electrode is required to balance the I-V applied. Thus, three electrodes are required which are working electrode, reference electrode and counter electrode (Bard & Faulkner, 2000).

#### 3.7.1 Linear Sweep Voltammetry (LSV)

The simplest type of voltammetry is called Linear Sweep Voltammetry (LSV). Linear sweep voltammetry involves applying a linear potential sweep to the working electrode (the electrode under study) whilst monitoring simultaneously the current flowing in the circuit. A signal generator produces a voltage sweep from  $E_i$  to  $E_f$  and a potentiostat applies this potential wave to the electrode under study. The scan direction can be positive or negative and in principle, the sweep rate can possess any constant value:

$$\text{Sweep rate} = dE/dt \quad (3.16)$$

This method of analysis is commonly employed in polarography whereby under well-defined conditions, the limiting current derived from a redox process in solution during LSV may be used to quantitatively determine the concentration of electroactive species in solution. As the electrode potential is constantly rising (or decreasing) throughout the experiment, a level of capacitive or ohmic current flows continuously.

These currents are due to the capacitive charging of the working electrode's double layer. Faradaic current will also flow when the potential reaches values at which the species in solution can undergo electrochemical conversions (Velasco, 1997).

In this research work, linear sweep voltammetry were performed on stainless steel working electrode, with counter and reference electrode of lithium metal at scanning rate of 1.0 mV/s using WonATech system to estimate the electrochemical stability window of the polymer electrolytes.

### **3.7.2 Cyclic Voltammetry (CV)**

Cyclic voltammetry is a method for investigating the electrochemical behaviour of a system. It was first reported in 1938 and described theoretically by Randles (1948). In this technique current flowing between the electrode of interest (whose potential is monitored with respect to a reference electrode) and a counter electrode is measured under the control of a potentiostat. The voltammogram determines the potentials at which different electrochemical processes occur. The working electrode is subjected to a triangular potential sweep, whereby the potential rises from a start value  $E_i$  to a final value  $E_f$  then returns back to the start potential at a constant potential sweep rate. The sweep rate applied can vary from a few millivolts per second to a hundred volts per second. The current measured during this process is often normalised to the electrode surface area and referred to as the current density. The current density is then plotted against the applied potential, and the result is referred to as a cyclic voltammogram. A peak in the measured current is seen at a potential that is characteristic of any electrode reaction taking place. The peak width and height for a particular process may depend on the sweep rate, electrolyte concentration and the electrode material (Gileadi, Kirowa-Einsner & Penciner, 1975; Bard & Faulkner, 2000)

Cyclic voltammetry makes possible the elucidation of the kinetics of electrochemical reactions taking place at electrode surfaces (Bockris & Khan, 1993; Brett & Brett, 1993). In a typical voltammogram, there can be several peaks. From the sweep-rate dependence of the peak amplitudes, widths and potentials of the peaks observed in the voltammogram, it is possible to investigate the role of adsorption, diffusion, and coupled homogeneous chemical reaction mechanisms (Bard & Faulkner, 2000).

In this work, cyclic voltammetry and complex impedance studies have been carried out in order to confirm the  $\text{Li}^+$  ion conduction in the polymer electrolyte systems. The cycle stability was estimated from the voltammograms obtained. Cyclic Voltammetry was performed on symmetrical cells  $\text{SS} | \text{SPE} | \text{SS}$  and  $\text{Li} | \text{SPE} | \text{Li}$  for the most electrochemically stable films for both unplasticized and plasticized systems (predetermined from LSV) at room temperature using three electrode systems.

### 3.8 Lithium Polymer Cell Fabrication

In order to examine the practicability of the PAN-based polymer electrolyte as electrolyte in battery applications, some important parameters such as battery capacity and cyclic performance will be examined. The most electrochemically stable polymer electrolyte film which carries high conductivity at room temperature was used as the electrolyte for the lithium polymer cell fabrication.  $\text{LiCoO}_2$  was chosen as the cathode material. A  $\text{Li} | \text{SPE} | \text{LiCoO}_2$  cell was assembled by sandwiching the respective electrodes and the SPE film in a sealed container. Charge/discharge cycling was carried out by using an electrochemical analyzer, WPG100e potentiostat/galvanostat system with a constant current of 0.05 mA. The cycle test of the cell was performed in the 2.5-4.3 V range by a galvanostatic method.

# **CHAPTER 4**

## **RESULTS AND DISCUSSIONS**

## 4.1 Electrical Studies

### 4.1.1 Impedance Spectroscopy Analysis

The electrical characteristics of polymer electrolytes were investigated using impedance spectroscopy by measuring the response of the material to an applied A.C. signal. The response to the applied A.C. signal is represented graphically by a plot of the measured impedance and dielectric constant in the complex plane. While the electrical response of materials with significant dielectric losses is usually graphically represented by an impedance plot which reveals the relation between the real and the imaginary part of the complex impedance. Impedance measurements of PAN based polymer electrolytes systems were made in the frequency range of 50 Hz to 1 MHz to obtain the conductivity values at room temperature. The dependence of the conductivity on temperature was further investigated in the temperature range from 303 K to 353 K.

### 4.1.2 Room temperature electrical conductivity studies

#### 4.1.2.1 PAN plasticized with varying amounts of EC and DMP

Figure 4.1 shows the impedance plot of pure PAN film. The bulk resistance  $R_b$  was determined from the intercept of the lower frequency end of the extrapolated semicircle with the  $Z_r$  axis. The average bulk resistance of pure PAN film is  $3.65 \times 10^8 \Omega$ . The impedance plot for a plasticized PAN film containing EC and DMP with mass ratio of 1:1 is shown in Figure 4.2. The bulk resistance of plasticized film exhibited an average value of four orders lower in magnitude than pure PAN film. Comparing both impedance plots, the pure PAN film consisted of a small portion of a depressed semicircle while PAN-EC-DMP films shows two well defined regions: semicircle at the high frequency region represents the bulk electrolyte impedance while the linear plot in the low frequency region attribute to the formation of double layer at



the blocking electrodes that causes the inclination (Bruce, 1995). The amount of inclination of the straight line is related to the width of relaxation time distributed in the sample film (Selvasekarapandian, Baskaran & Hema, 2005). The amount of the plasticizers in different mass ratio, average bulk resistance,  $R_b$  and the average conductivities films of the PAN-EC-DMP system at room temperature are listed in Table 4.1. It was observed that the addition of plasticizer has drastically reduced the bulk resistance hence increased the conductivity values of the films. This result indicates that the presence of plasticizers improve the segmental flexibility of the polymer back bone, and consequently enhance the segmental mobility. The variation of conductivity of PAN-EC-DMP films containing difference amount of EC and DMP in ratio is presented in Figure 4.3. A notable difference in conductivity enhancement is observed when EC: DMP in ratio 1:1 was added to PAN-EC-DMP system, the conductivity of  $1.11 \times 10^{-6} \text{ S cm}^{-1}$  which is increased by more than five orders of magnitude at room temperature.

**Table 4.1:** Average bulk resistances and conductivity values of plasticized PAN films with different ratio of EC and DMP

Mass Ratio of EC:DMP	Average bulk resistance, $R_b$ ( $\Omega$ )	Average conductivity, $(\sigma \pm \Delta\sigma)$ ( $\text{S cm}^{-1}$ )
0:0	$3.65 \times 10^8$	$(1.83 \pm 0.19) \times 10^{-11}$
0:1	$1.50 \times 10^5$	$(1.45 \pm 0.22) \times 10^{-7}$
1:0	$3.73 \times 10^4$	$(5.11 \pm 0.40) \times 10^{-7}$
1:1	$1.32 \times 10^4$	$(1.11 \pm 0.03) \times 10^{-6}$
1:2	$1.58 \times 10^5$	$(1.51 \pm 0.18) \times 10^{-7}$
2:1	$9.79 \times 10^4$	$(1.49 \pm 0.48) \times 10^{-7}$

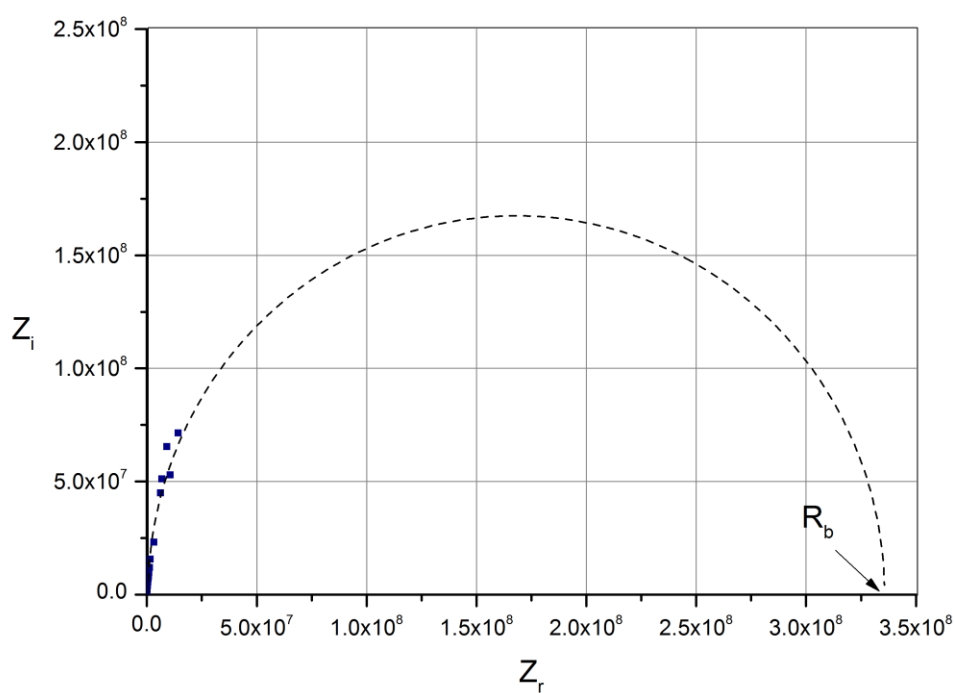


**Figure 4.1:** The complex impedance plot for pure PAN film.

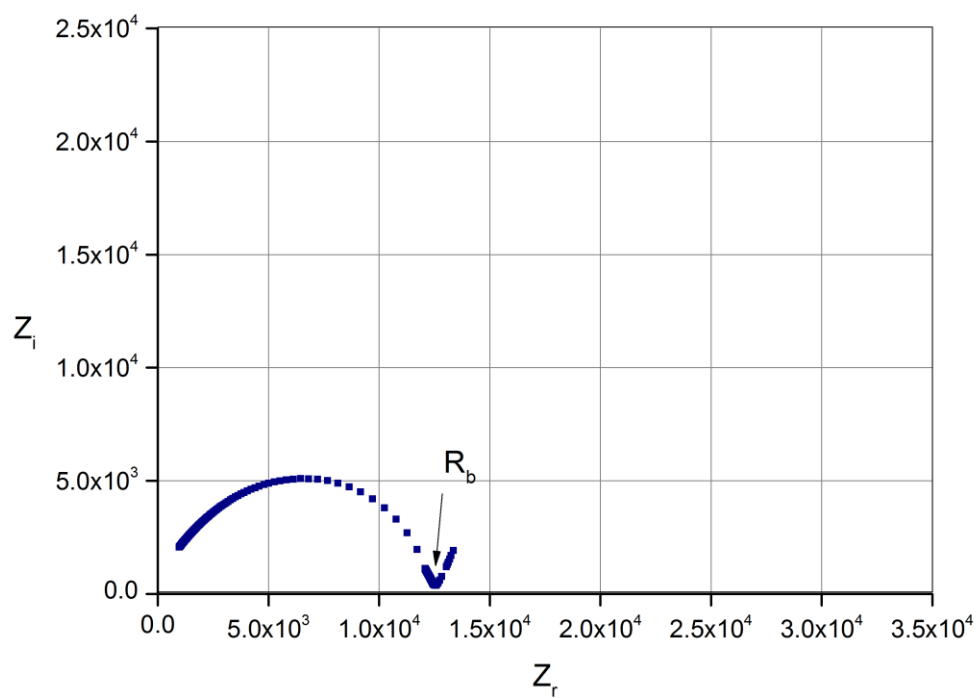


**Figure 4.2** The complex impedance plot for PAN-EC-DMP film.

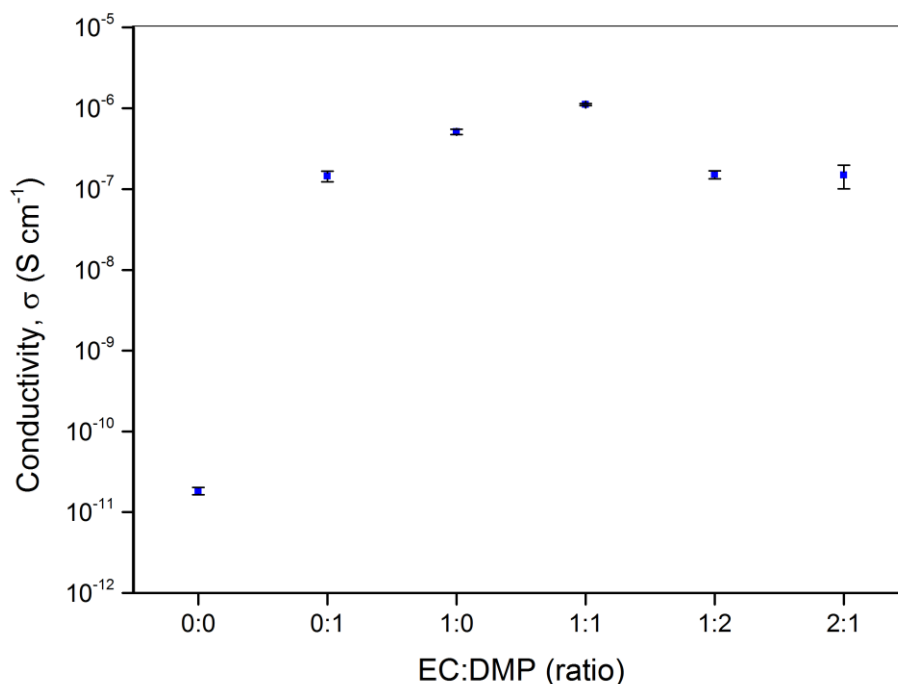


**Figure 4.3:** Variation of conductivity with different ratio of EC and DMP in the PAN-EC-DMP system.

#### 4.1.2.2 PAN-LiBF<sub>4</sub> system

The A.C. responses for the lowest and the highest conducting PAN-LiBF<sub>4</sub> electrolytes are depicted in Figure 4.4 and Figure 4.5, respectively. The complex impedance spectra pattern of PAN film containing 5 wt. % of LiBF<sub>4</sub> at room temperature comprises of a depressed semi-circular arc attributed to bulk sample contribution as shown in Figure 4.4. Its electrical equivalent circuit consists of a parallel combination of resistance ( $R$ ), capacitance ( $C$ ) and constant phase element (CPE). The impedance of CPE can be expressed as

$$Z_{CPE}^* = [A(j\omega)^n]^{-1} \quad (4.1)$$

where  $A$  is a constant that is independent of frequency and  $n$  is an exponential index which is a measure of arc-depression (Bard & Reichman, 1980). As comparison, impedance spectra of the highest conducting film containing 50 wt.% of LiBF<sub>4</sub> as

shown in Figure 4.5 displayed a linear spike at high frequency region and the semicircle is completely disappeared. This result suggests that the charge carriers within the materials are predominantly ions and this leads one to further conclude that the total conductivity is mainly the result of ion conduction (Jacob, Prabakaran & Radhakrishna, 1997).

The average bulk resistances and average conductivity values of electrolyte films with different compositions of  $\text{LiBF}_4$  is summarized in Table 4.2. The highest conductivity achieved at  $1.83 \times 10^{-3} \text{ S cm}^{-1}$  for film containing 50 wt. % of  $\text{LiBF}_4$ . The bulk resistances were observed to be declining with concentration of salt and lead to increase in conductivity of the films. Figure 4.6 shows the variation of conductivity of the system containing different amounts of  $\text{LiBF}_4$  in weight percentage. An abrupt increase in conductivity value from  $1.83 \times 10^{-11} \text{ S cm}^{-1}$  of pure PAN film to  $2.71 \times 10^{-9} \text{ S cm}^{-1}$  was observed from when 5 wt.%  $\text{LiBF}_4$  was added. It can be observed that the conductivity of the films rose gradually until a maximum was achieved at  $1.83 \times 10^{-3} \text{ S cm}^{-1}$  for film containing 50 wt. % of  $\text{LiBF}_4$ . The magnitude of the ionic conductivity of the electrolyte is generally depends on the charge carrier concentration,  $n$ , charge of the mobile carrier,  $q$  and carrier mobility,  $\mu$ , as described by the relation  $\sigma = nq\mu$  (Ramya, Selvasekarapandian, Savitha, Hirankumar & Angelo, 2007). In this work, the conductivity values vary linearly with the charge carrier concentration which was achieved by increasing salt concentration in polymer matrix. In addition,  $\text{BF}_4^-$  was reported as the anion having the highest mobility among the most common anions encountered (Ue, 1994; Ue & Mori, 1995). The increase of conductivity values upon addition of salt may attribute to the combined effect as mentioned.

Dielectric relaxation gives a measure of the dynamic and relaxation behaviour of the electric dipoles in the matrix. The effect of salt concentration on the dielectric response has been studied for PAN films containing varying amounts of  $\text{LiBF}_4$ .

Figure 4.7 and Figure 4.8 show the frequency response of permittivity  $\epsilon_r$  and loss  $\epsilon_i$  for PAN-LiBF<sub>4</sub> system. All samples exhibited a dielectric dispersion in the low frequency region is contributed by the charge accumulation at the electrode-electrolyte interface. (Howell, Bose, Macedo & Moynihan, 1974). On contrary, sharp decrease of  $\epsilon_r$  and  $\epsilon_i$  towards high frequency region was observed. The periodic reversal of external electric field occurs very fast at high frequency. Consequently, there is no net ion diffusion in the direction of field causes inhibition to the orientation of dipoles and decrease in polarization (Ramesh & Arof, 2001). It can be observed that the dielectric constant and dielectric loss increase with the salt content is in accordance to the conductivity and vice versa. It should be noted that the highest conducting sample carries the highest  $\epsilon_r$  and  $\epsilon_i$ . This result infers that there is an increase in charge carrier density at high salt concentrations hence leads to enhancement in conductivity.

**Table 4.2:** Compositions, bulk resistance,  $R_b$  and conductivity of films in the PAN-LiBF<sub>4</sub> system.

LiBF <sub>4</sub> content in PAN-LiBF <sub>4</sub> system ( wt. %)	Average Bulk Resistance, $R_b$ ( $\Omega$ )	Average Conductivity, ( $\sigma \pm \Delta\sigma$ ) (S cm <sup>-1</sup> )
5	$6.60 \times 10^6$	$(2.71 \pm 0.58) \times 10^{-9}$
10	$8.30 \times 10^3$	$(1.43 \pm 0.38) \times 10^{-6}$
15	$1.60 \times 10^3$	$(3.91 \pm 0.53) \times 10^{-6}$
20	$8.19 \times 10^2$	$(1.80 \pm 0.52) \times 10^{-5}$
25	$1.39 \times 10^2$	$(6.87 \pm 0.84) \times 10^{-5}$
30	$7.80 \times 10^1$	$(2.25 \pm 0.32) \times 10^{-4}$
35	$3.27 \times 10^1$	$(3.02 \pm 0.71) \times 10^{-4}$
40	$2.20 \times 10^1$	$(8.97 \pm 0.89) \times 10^{-4}$
45	$1.80 \times 10^1$	$(1.36 \pm 0.33) \times 10^{-3}$
50	$1.41 \times 10^1$	$(1.83 \pm 0.47) \times 10^{-3}$

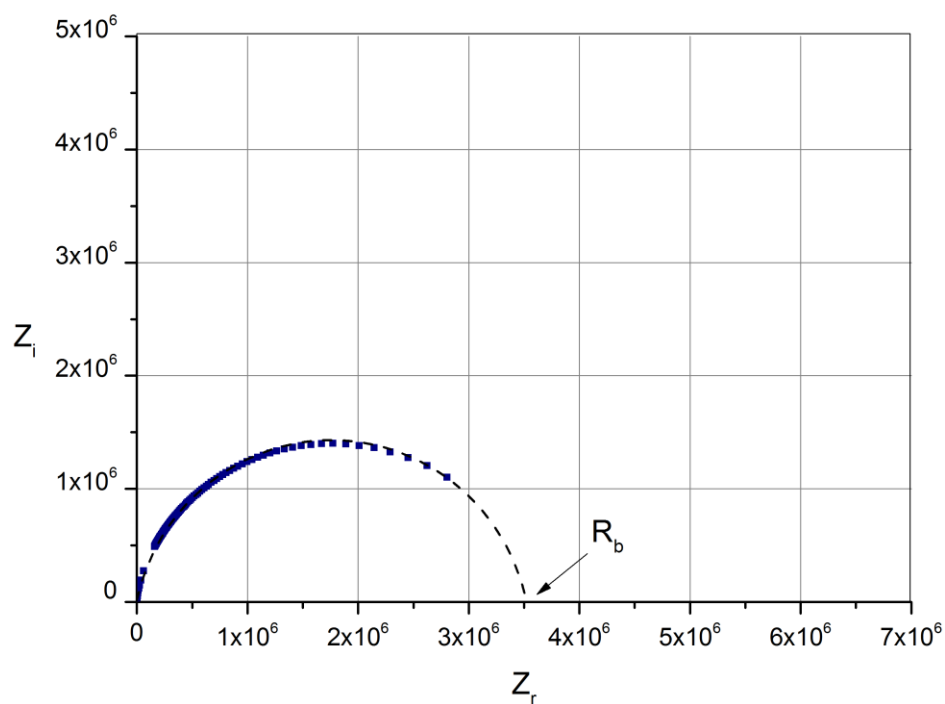


**Figure 4.4:** Impedance plot for PAN film containing 5 wt% of  $\text{LiBF}_4$ .

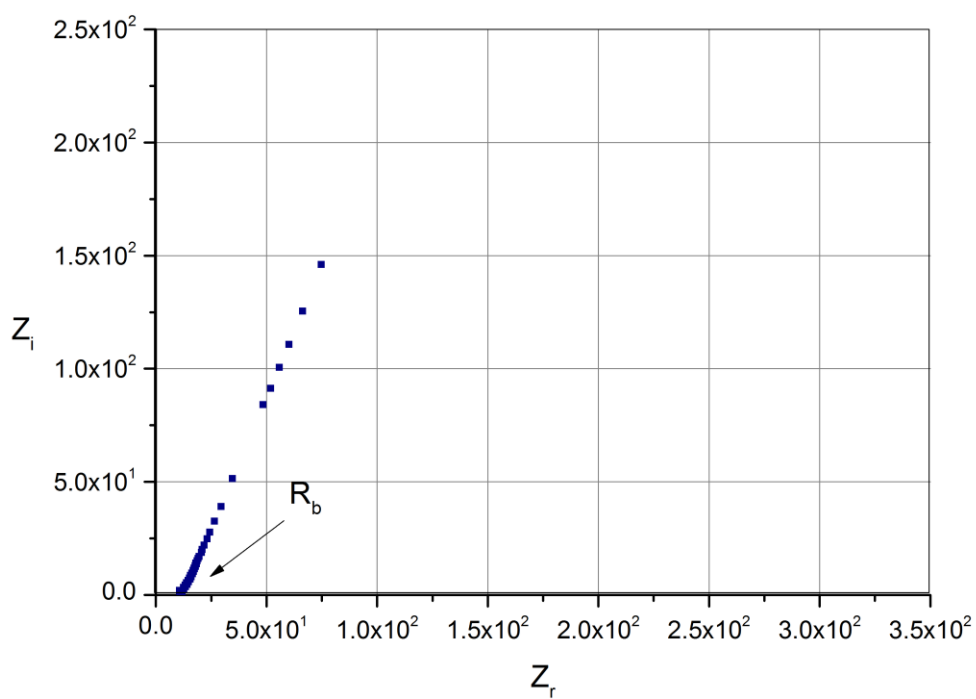


**Figure 4.5:** Impedance plot for PAN film containing 50 wt.% of  $\text{LiBF}_4$ .

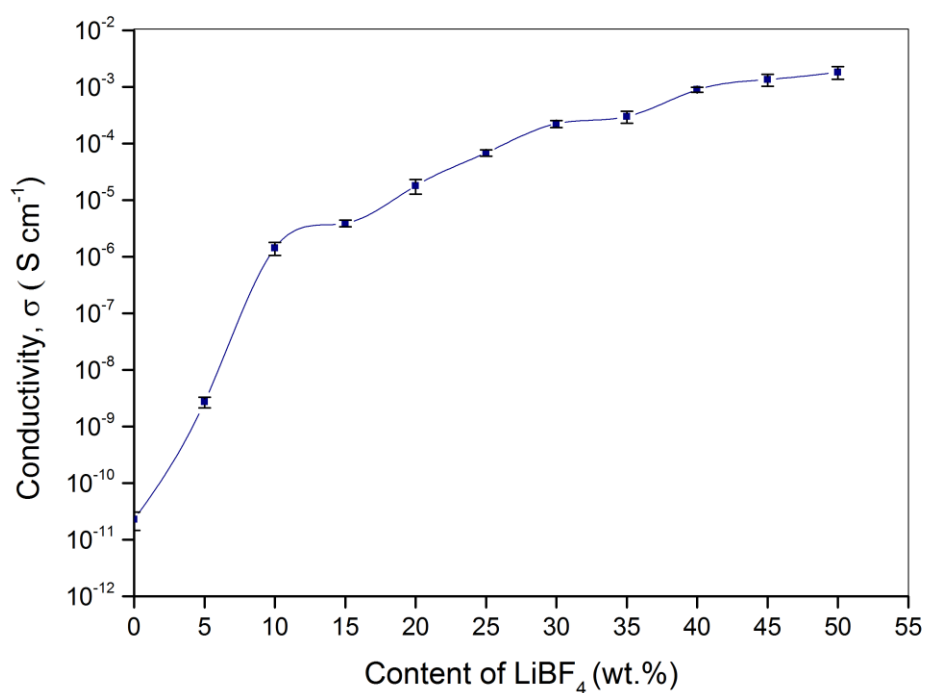


**Figure 4.6 :** Variation of conductivity with different amounts of salt in PAN-LiBF<sub>4</sub> system

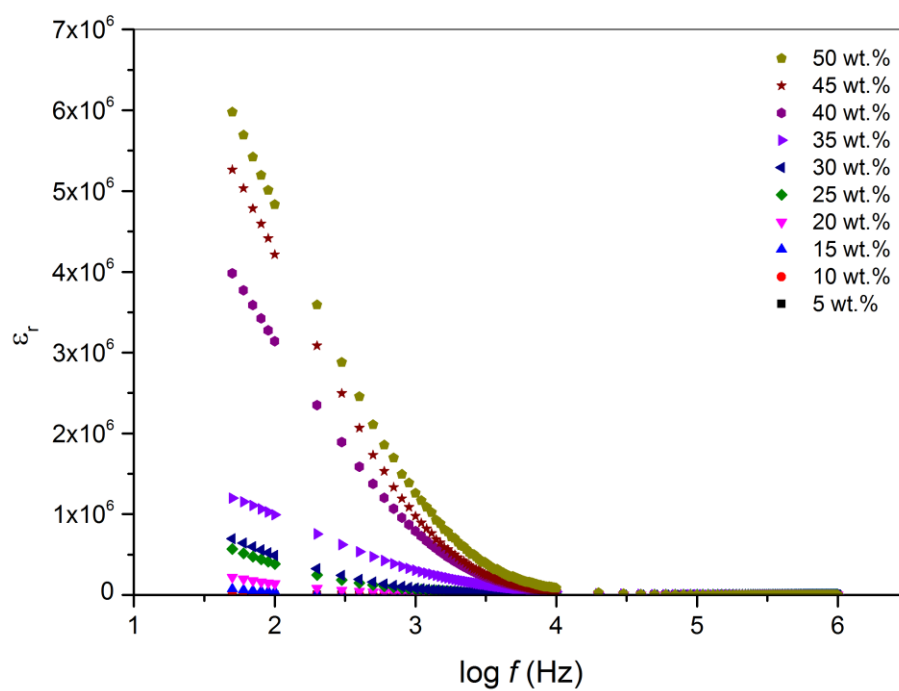


**Figure 4.7:** Dielectric constant versus frequency for films in PAN-LiBF<sub>4</sub> system

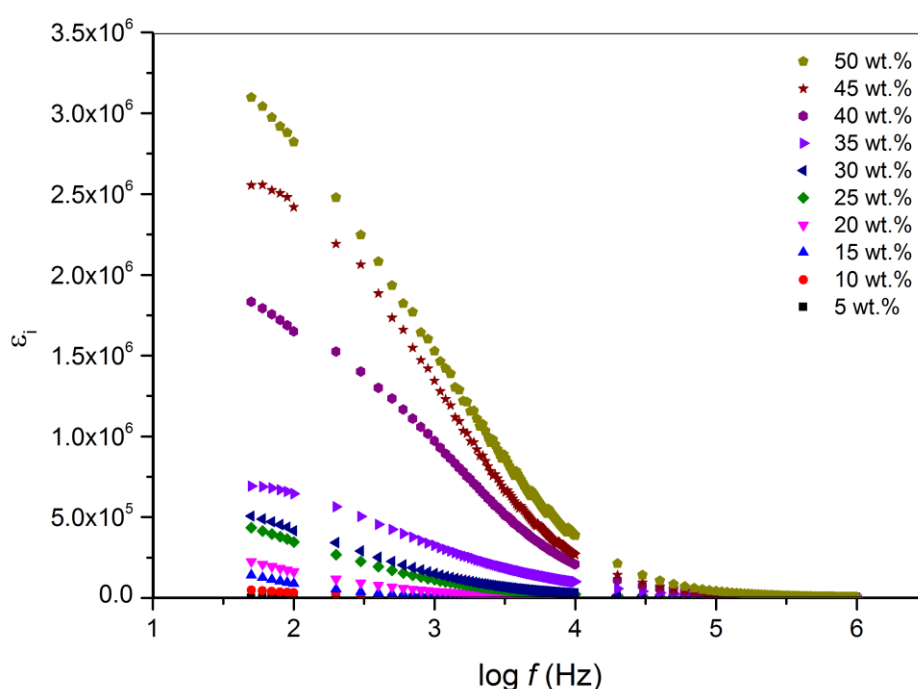


**Figure 4.8:** Dielectric loss versus frequency for films in PAN-LiBF<sub>4</sub> system

#### 4.1.2.3 PAN-EC-DMP-LiBF<sub>4</sub> system

The A.C. responses for the lowest and the highest conducting electrolytes of PAN-EC-DMP-LiBF<sub>4</sub> system at room temperature are depicted in Figure 4.9 and Figure 4.10, respectively. The spectra clearly indicate that for the plasticized polymer electrolyte system, at high frequency region the shape of semicircle is disappeared in all plots, thus suggesting capacitive behavior of the electrolyte over the studied frequency range. Moreover, the spectrum shows a linear spike even at low salt concentration as shown in Figure 4.9. The disappearance of semicircle with the addition of plasticizers leads to the conclusion that the charge carriers are ions which lead to the increase in conductivity (Klassen, Aroca, Nazri & Nazri, 1998). The average bulk resistances and average conductivity values of electrolyte films with different compositions of LiBF<sub>4</sub> is summarized in Table 4.3. The conductivity of the polymer electrolyte shows a linear relationship with the salt concentration. Figure 4.11 shows the variation of conductivity



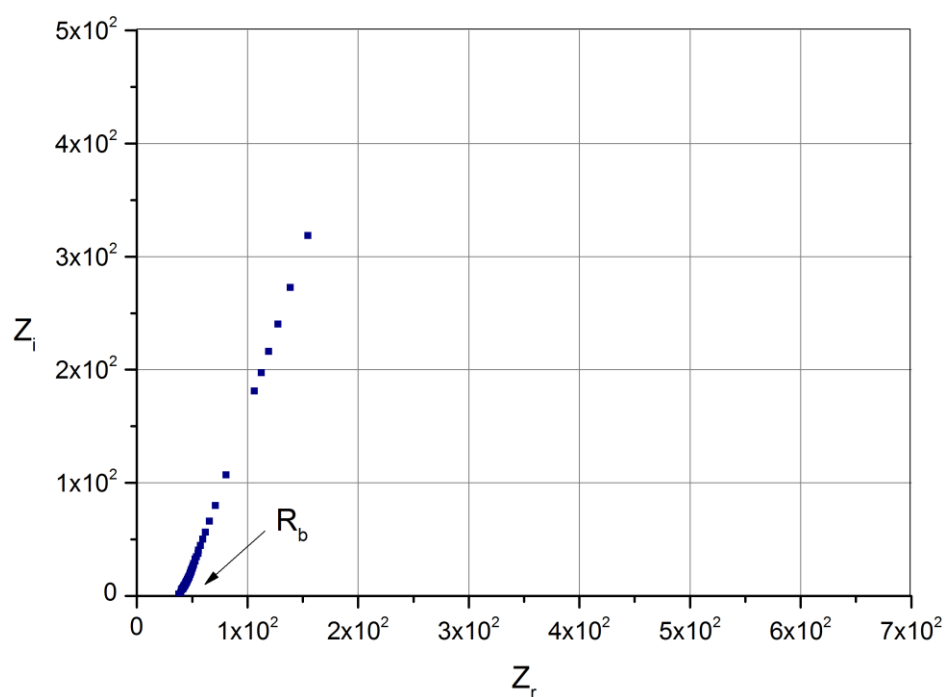
of the system containing different amount of  $\text{LiBF}_4$  in weight percentage. Similar behaviour was observed in the plasticized system, the conductivity value jump abruptly from  $1.11 \times 10^{-6} \text{ S cm}^{-1}$  of PAN-EC-DMP film to  $3.89 \times 10^{-4} \text{ S cm}^{-1}$  when 5 wt.%  $\text{LiBF}_4$  was added. With addition of salt, the conductivity value shows a continuous increase until a maximum was achieved at  $1.08 \times 10^{-2} \text{ S cm}^{-1}$  for film containing 40 wt. % of  $\text{LiBF}_4$ . The conductivity values of this system fall within the range of  $10^{-3} \sim 10^{-2} \text{ Scm}^{-1}$  as required for practical applications (Park, 2012). Once again, plasticization is proven as an effective method to increase the conductivity of polymer electrolytes based on two factors ( Rhoo, Kim, Park & Hwang, 1997):

- a) Increased ionic mobility by opening up the narrow rivulet of plasticizer rich phase
- b) Effective dissociation of salt takes place and creates the facile pathway for ionic conduction

Dielectric relaxation properties for selected samples for PAN-EC-DMP- $\text{LiBF}_4$  were examined in the same frequency range at equally similar conditions. The frequency dependence of the dielectric constant and dielectric loss curves are shown in Figure 4.12 and Figure 4.13, respectively. The same manner as discussed in PAN- $\text{LiBF}_4$  system can be observed in these figures. In addition, the value of  $\epsilon_r$  and  $\epsilon_i$  for this system is greater than PAN- $\text{LiBF}_4$  system may be credited to the salt dissociation ability of plasticizers. With the presence of plasticizers, the number of free ions is greatly enhanced which in turns contribute to the high value of  $\epsilon_r$  and  $\epsilon_i$  due to charge accumulation at the electrode and electrolyte interface at low frequency (Osman, Ibrahim & Arof, 2001).

**Table 4.3:** Compositions, bulk resistance,  $R_b$  and conductivity of films in the PAN-EC-DMP-LiBF<sub>4</sub> system.

LiBF <sub>4</sub> content in PAN-EC-DMP-LiBF <sub>4</sub> system ( wt. %)	Average Bulk Resistance, $R_b$ ( $\Omega$ )	Average Conductivity, ( $\sigma \pm \Delta\sigma$ ) (S cm <sup>-1</sup> )
5	$4.93 \times 10^1$	$(3.89 \pm 0.41) \times 10^{-4}$
10	$2.39 \times 10^1$	$(1.11 \pm 0.28) \times 10^{-3}$
15	$1.37 \times 10^1$	$(2.07 \pm 0.40) \times 10^{-3}$
20	$0.84 \times 10^1$	$(3.23 \pm 0.27) \times 10^{-3}$
25	$0.71 \times 10^1$	$(5.40 \pm 0.78) \times 10^{-3}$
30	$0.58 \times 10^1$	$(8.64 \pm 0.40) \times 10^{-3}$
35	$0.57 \times 10^1$	$(9.02 \pm 0.31) \times 10^{-3}$
40	$0.46 \times 10^1$	$(1.08 \pm 0.12) \times 10^{-2}$

**Figure 4.9:** Impedance plot for PAN-EC-DMP film containing 5 wt.% of LiBF<sub>4</sub>.

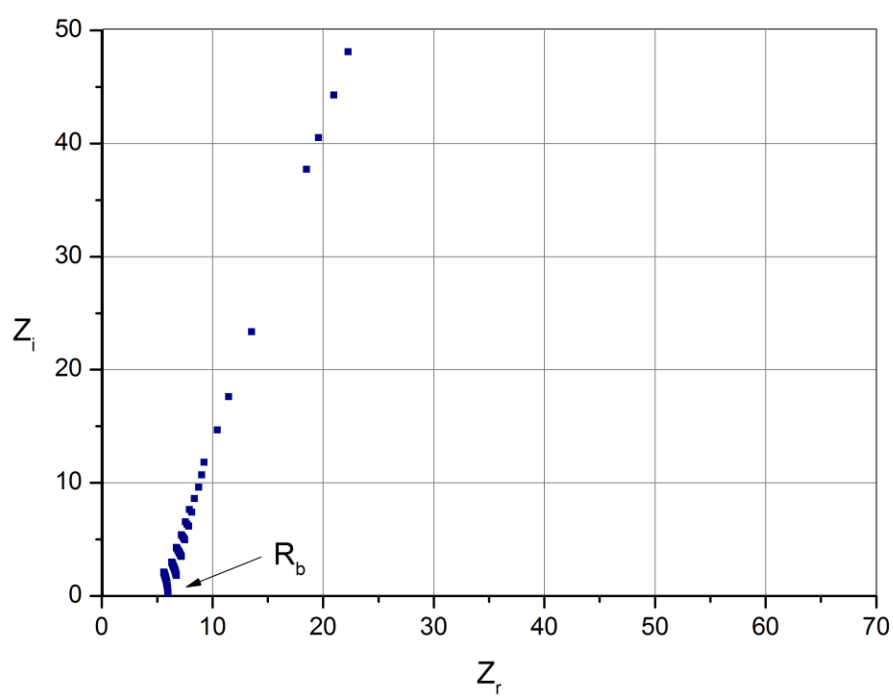


**Figure 4.10:** Impedance plot for PAN-EC-DMP film containing 40 wt.% of  $\text{LiBF}_4$ .

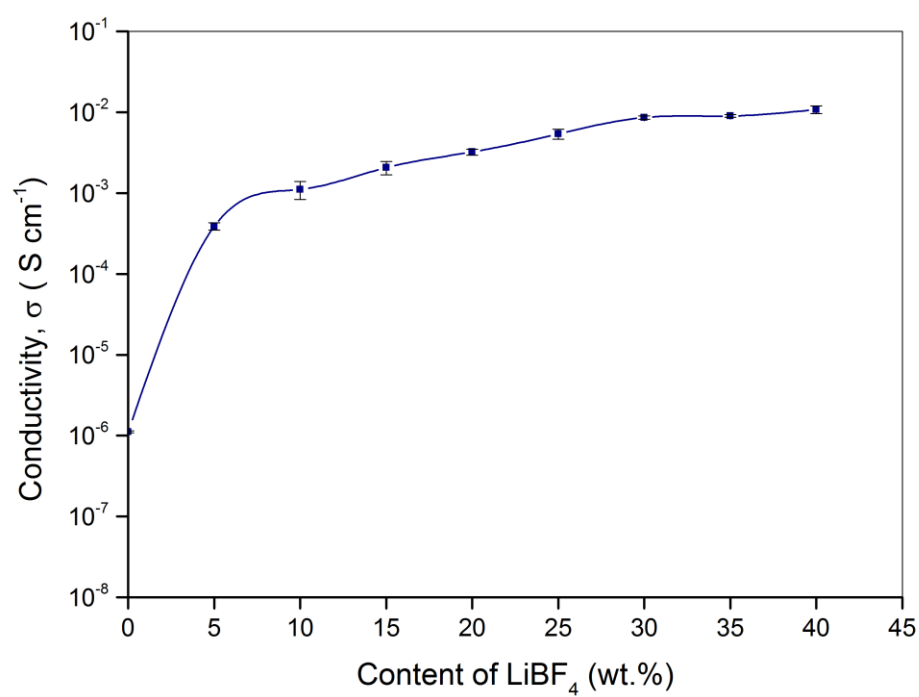


**Figure 4.11 :** Variation of conductivity with different amounts of salt in PAN-EC-DMP- $\text{LiBF}_4$  system

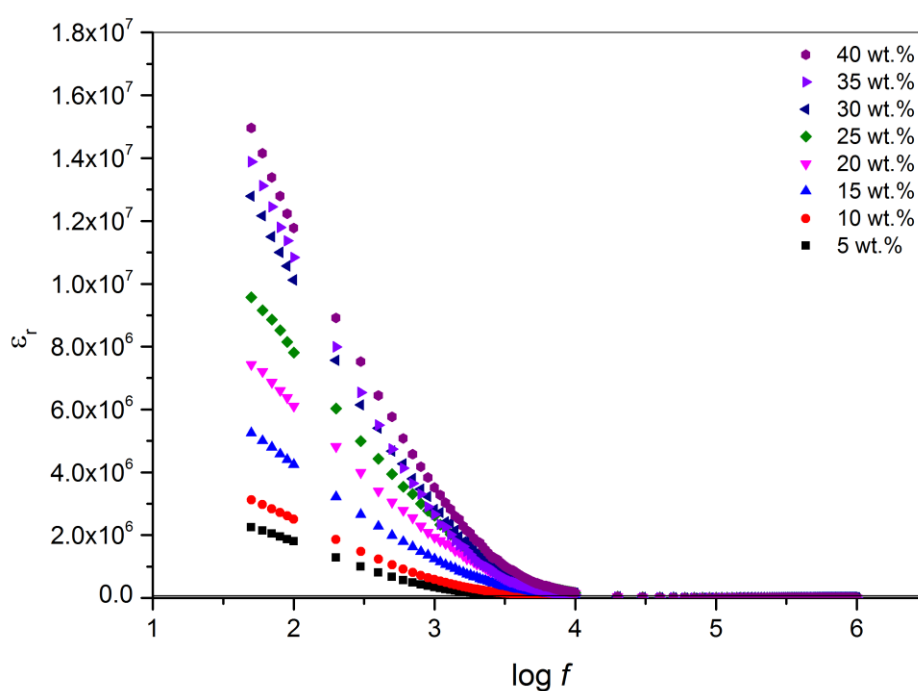


**Figure 4.12:** Dielectric constant versus frequency for films in PAN-EC-DMP-LiBF<sub>4</sub> system

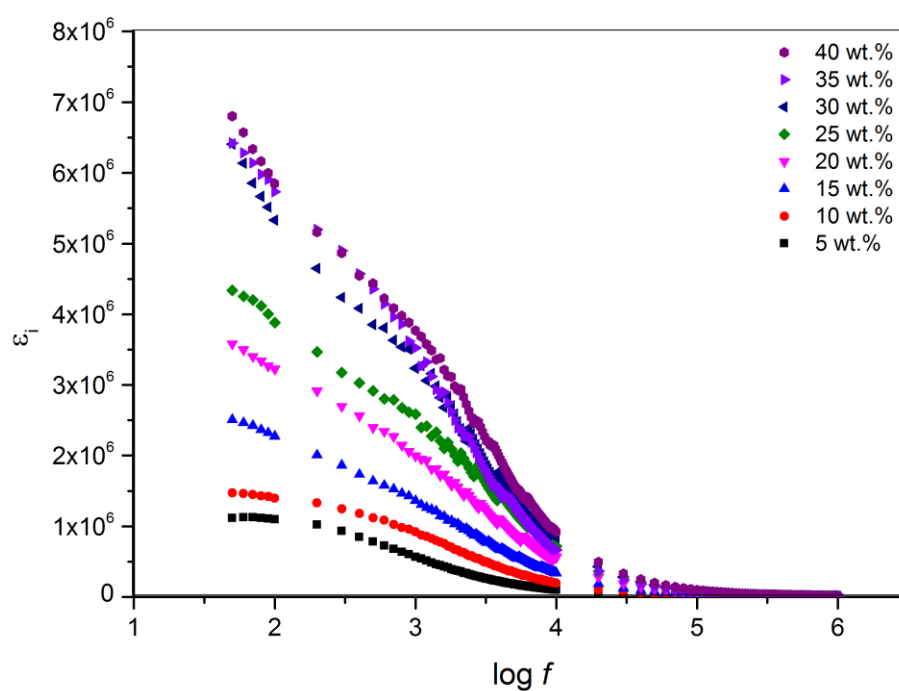


**Figure 4.13:** Dielectric loss versus frequency for films in PAN-EC-DMP-LiBF<sub>4</sub> system

### 4.1.3 Elevated temperature electrical conductivity studies

#### 4.1.3.1 PAN-LiBF<sub>4</sub> System

In order to understand the mechanism of ionic conduction, the electrical conductivity was studied as a function of temperature from 303 K to 353 K. Figure 4.14 depicts the temperature dependence of conductivity for selected samples in PAN-LiBF<sub>4</sub> system. A linear relationship is perceived from the plots with regression values close to unity suggesting that the temperature dependent ionic conductivity for PAN-LiBF<sub>4</sub> complexes obey the Arrhenius rule. The Arrhenius relationship indicates the presence of the hopping mechanism. In the context of polymer electrolytes, the ion is usually “loosely bound” to a site with donor electrons. When the coordinated ion has acquired sufficient energy upon heating, decoupling process is initiated (Buraidah, Teo, Majid & Arof, 2009). The continuous decoupling process leads to formation of vacant sites in the polymer chain. Hence, the neighbouring ions from adjacent sites tend to occupy these vacant sites and coordinate with the polymer chain again. The movement from one site to another result in the conduction of charge and the energy for this conduction is the activation energy. In order to probe the ion dynamic of polymer electrolytes, activation energy,  $E_a$  can be obtained from the slope of the Arrhenius plot. It can be observed that  $E_a$  decreases as conductivity of sample increases implying that the ions in highly conducting samples require lower energy for migration. Table 4.4 lists the activation energy value for all samples studied. The activation energy decreases with salt concentration until a minimum of 0.29 eV for the highest conducting sample in the PAN-LiBF<sub>4</sub> system.

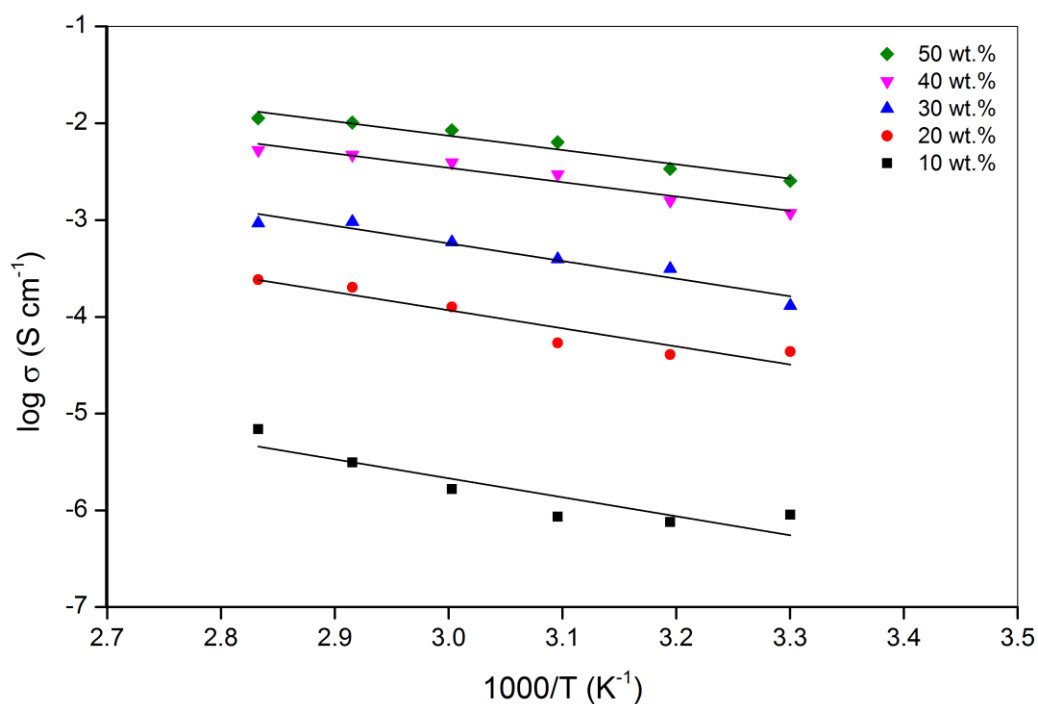


**Figure 4.14:** Temperature dependence of ionic conductivity of PAN-LiBF<sub>4</sub> system.

**Table 4.4:** Activation energies for films in PAN-LiBF<sub>4</sub> system.

LiBF <sub>4</sub> content (wt%)	Activation energy, $E_a$ (eV)
10	0.38
20	0.37
30	0.36
40	0.31
50	0.29

---

#### 4.1.3.2 PAN-EC-DMP-LiBF<sub>4</sub> system

The evolution of the ionic conductivity of the films in PAN-EC-DMP-LiBF<sub>4</sub> system with reciprocal temperature is displayed in Figure 4.15. It can be observed from Figure 4.15 that the conductivity values do not show abrupt increase with temperature indicating that these electrolytes exhibit a completely amorphous structure (Michael, Jacob, Prabakaran & Radhakrishna, 1997). This result has confirmed by XRD analysis in Section 4.2. Similar to the PAN-LiBF<sub>4</sub> system, the temperature dependence conductivity follows Arrhenius relationship. This theory states the ion jumps from its normal position on the lattice to an adjacent equivalent but empty site. Enhancement in conductivity is normally accompanied by the decrease in activation energy. The activation energies for electrolyte films in this system marks a decrease upon addition of salt as listed in Table 4.5. It should be noted that the overall activation energy in this system shows lower value than unplasticized system. The low activation energy for the lithium ion transport is due to the completely amorphous nature of the polymer electrolytes that facilitate the fast ionic motion in the polymer network. It is known that plasticizer can make the sample more amorphous and the increase in amorphousity can enhance conductivity (Michael et al., 1997).

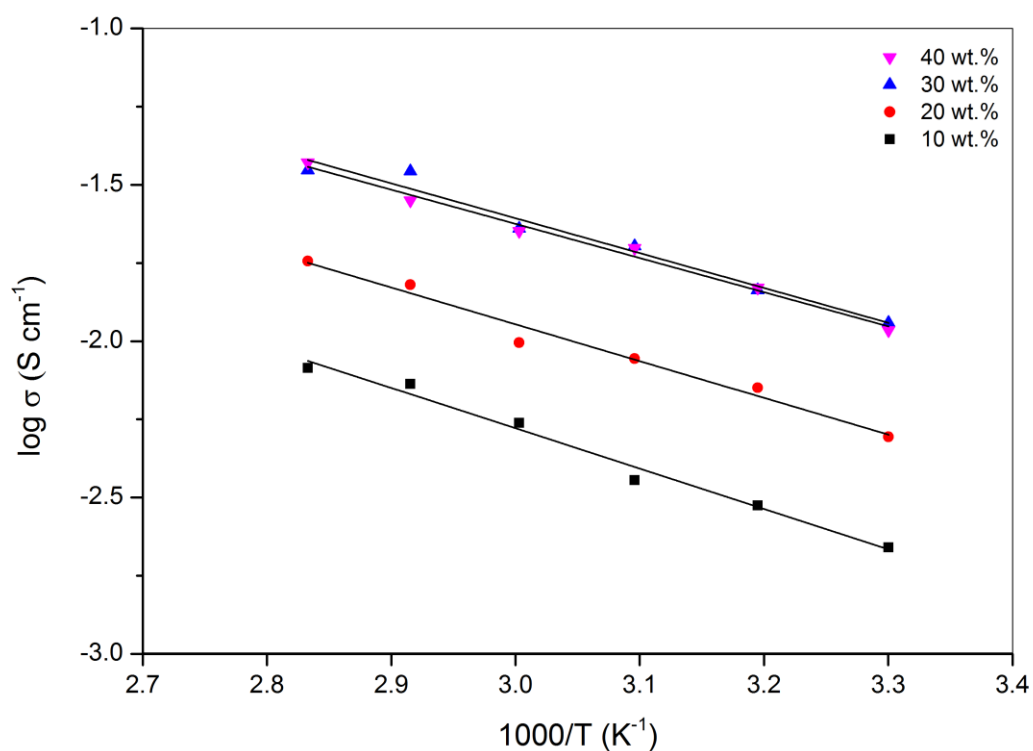


**Figure 4.15:** Temperature dependence of ionic conductivity of PAN-EC-DMP-LiBF<sub>4</sub> system.

**Table 4.5:** Activation energies for films in PAN-EC-DMP-LiBF<sub>4</sub> system

LiBF <sub>4</sub> content (wt%)	Activation energy, $E_a$ (eV)
10	0.26
20	0.23
30	0.22
40	0.22



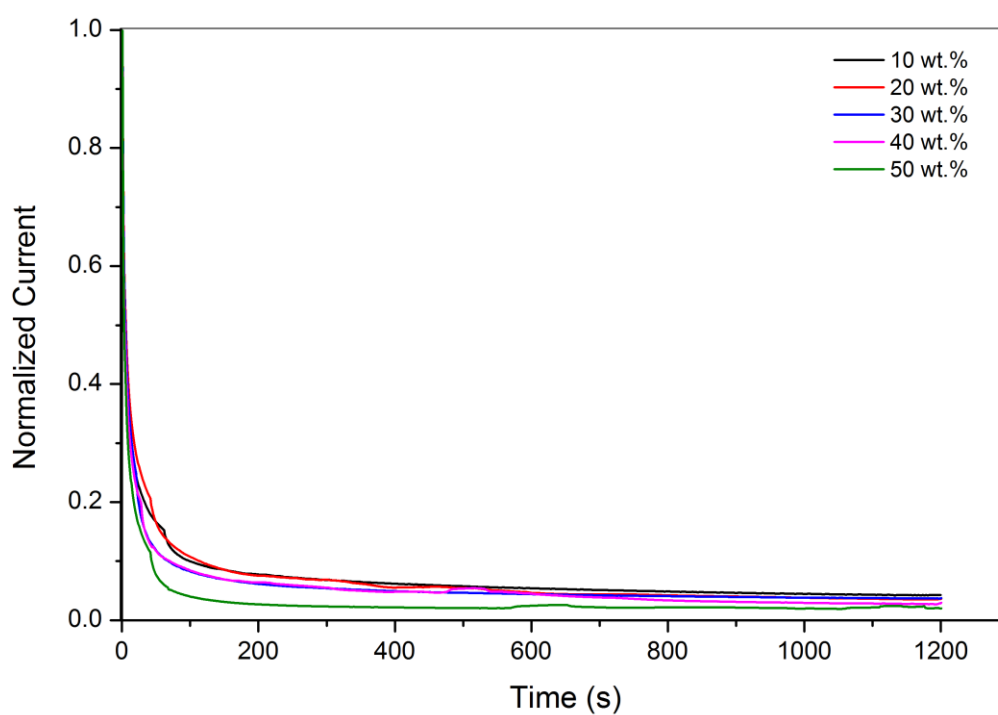
#### 4.1.4 Transport Number

##### 4.1.4.1 Ionic Transport Number

Ionic transport number is dimensionless parameter which informs about the contribution of the particular charged species present in the electrolyte to the overall charge transport across the cell. The conductivity behaviour of the PAN films was reported in earlier section, yet conductivity alone does not reflect the full characteristics of a solid electrolyte, as the ionic transference number less than unity results in the formation of concentration overvoltage. Therefore, the contributions of possible charge carriers into the charge transfer process are of practical importance as well (Lewandowski, Stępniaak & Grzybowski, 2001). Transport number measurement was done by supplied D.C. electric potential of 0.5 V across the sample sandwiched between two blocking electrodes where current is monitored as a function of time. Figure 4.16 and 4.17 show the variation of normalized current with time for both PAN-LiBF<sub>4</sub> and PAN-EC-DMP-LiBF<sub>4</sub> systems. The steady state was developed at a short interval implies that the charge transport is mainly due to ions. The ionic transport number calculated using eq. 3.14 for both systems is listed in Table 4.6. It is observed that the values of ionic transference number of all the samples in both systems are found to be more than 0.9 suggesting that the charge carrier within the polymer electrolyte is predominantly ions (Kumar & Hashmi, 2010). It should be noted that the  $t_i$  value increases in accordance with conductivity values agree with the idea that the number of charge carrier increases upon addition of salt. Besides, the  $t_i$  values for the samples in the plasticized system is found to be slightly higher may attribute to the salt dissociating ability of the plasticizers which has amplified the charge carrier density.

**Table 4.6:** Ionic transport number for PAN-LiBF<sub>4</sub> and PAN-EC-DMP-LiBF<sub>4</sub> systems.

Salt Content (wt.%)	Ionic Transport Number	
	PAN-LiBF <sub>4</sub>	PAN-EC-DMP-LiBF <sub>4</sub>
10	0.958	0.957
20	0.964	0.967
30	0.962	0.983
40	0.970	0.986
50	0.980	-

**Figure 4.16:** Normalized current versus time plots for films in PAN-LiBF<sub>4</sub> system.

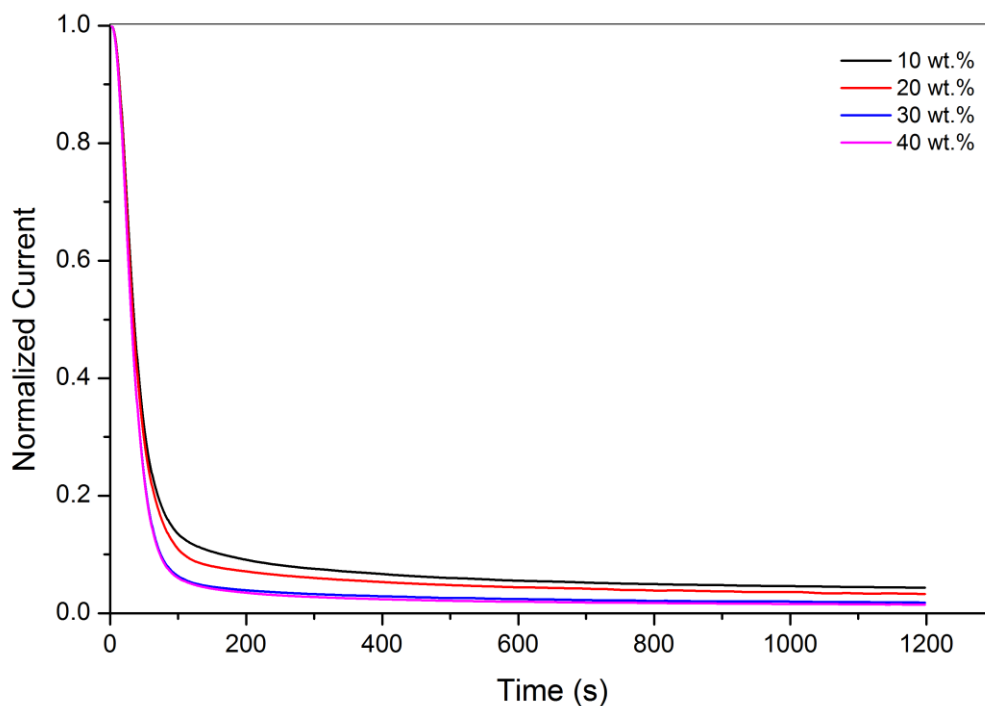


**Figure 4.17:** Normalized current versus time plots for films in PAN-EC-DMP-LiBF<sub>4</sub> system.

#### 4.1.4.2 Cationic Transport Number

The cationic transport number was determined by using a combination of D.C. polarization and A.C. impedance measurement. The symmetrical Li| SPE |Li cell was subjected to A.C. impedance measurements prior to and after the polarization. The values of electrode-electrolyte contact resistances were obtained from the impedance plots as shown in Figure 4.18. In the D.C. potentiostatic polarization of the electrode-electrolyte interface, a constant potential of 0.5 V was applied to the symmetrical Li| SPE |Li cell and the current flowing through the cell was recorded as a function of the time. As shown in Figure 4.10, there is a current  $I_0$  at the very beginning of the polarization. After a longer time of polarization, a steady state is established and the current stabilises at  $I_s$ . When an electric field is applied to the polymer electrolyte, the cation constituent Li is carried toward the cathode by  $\text{Li}^+$ ,  $\text{Li}_2\text{BF}_4^+$ , etc., while  $\text{BF}_4^-$ ,

$\text{Li}(\text{BF}_4)^{2-}$  etc. migrate toward the anode. Hence, the movement of both the cationic and anionic species contribute to the total ionic conductivity (Choe, Carroll, Pasquariello & Abraham, 1997).

The difference between the fluxes of Li-containing species directed toward the cathode and anode was measured as the cationic transport number. After a certain time, a steady state is developed, where the current drop is due to the growth of passivation layers on the electrodes and the establishment of concentration gradient. The  $t_+$  was calculated using equation 3.15. The cationic transport number measurement was conducted on sample for both unplasticized and plasticized systems. However, only the  $t_+$  of two highest conducting samples in the PAN-EC-DMP-LiBF<sub>4</sub> system is measurable. The  $t_+$  for sample containing 30 wt.% and 40 wt.% of LiBF<sub>4</sub> was calculated as 0.16 and 0.17. This indicates the cationic species in the plasticized system relatively contribute more to the overall conductivity than unplasticized system which explains the high conductivity of these two samples with the order of  $\sim 10^{-2} \text{ S cm}^{-1}$ . However, the anionic species are apparently the main contributor to the total ionic conductivity. The  $t_+$  values obtained in this present work are within the range of 0.1 to 0.3 for PAN-based polymer electrolytes as reported by Choe et al. (1997) and Chen et al. (2002). This behaviour illustrates the similarity in the conductivity mechanisms in plasticized polymer electrolytes and conventional liquid electrolytes (Abraham, Jiang & Carroll, 1997).

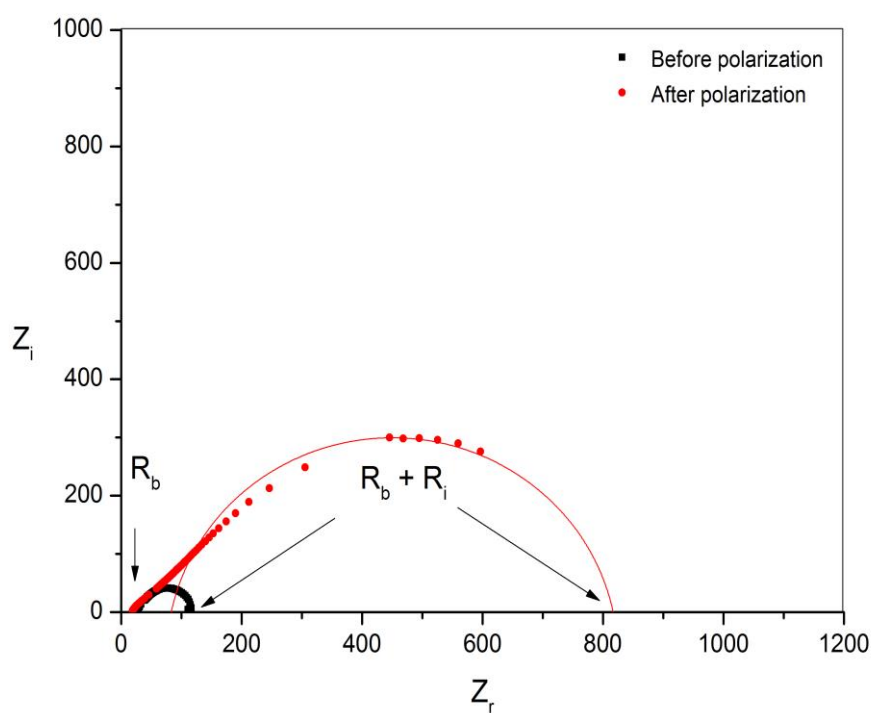


**Figure 4.18:** A.C. complex impedance plot before and after D.C. polarization of a typical symmetric Li |SPE |Li cell.

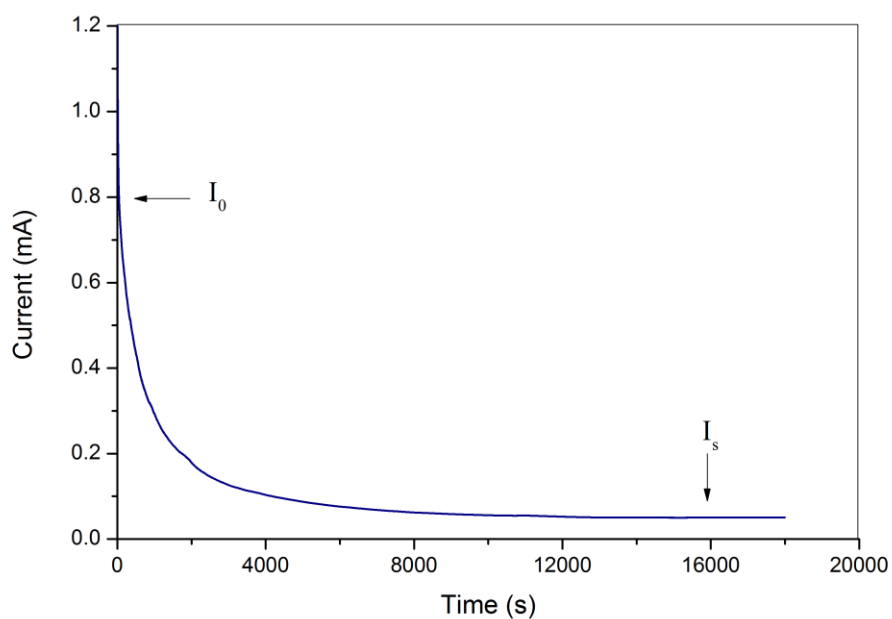
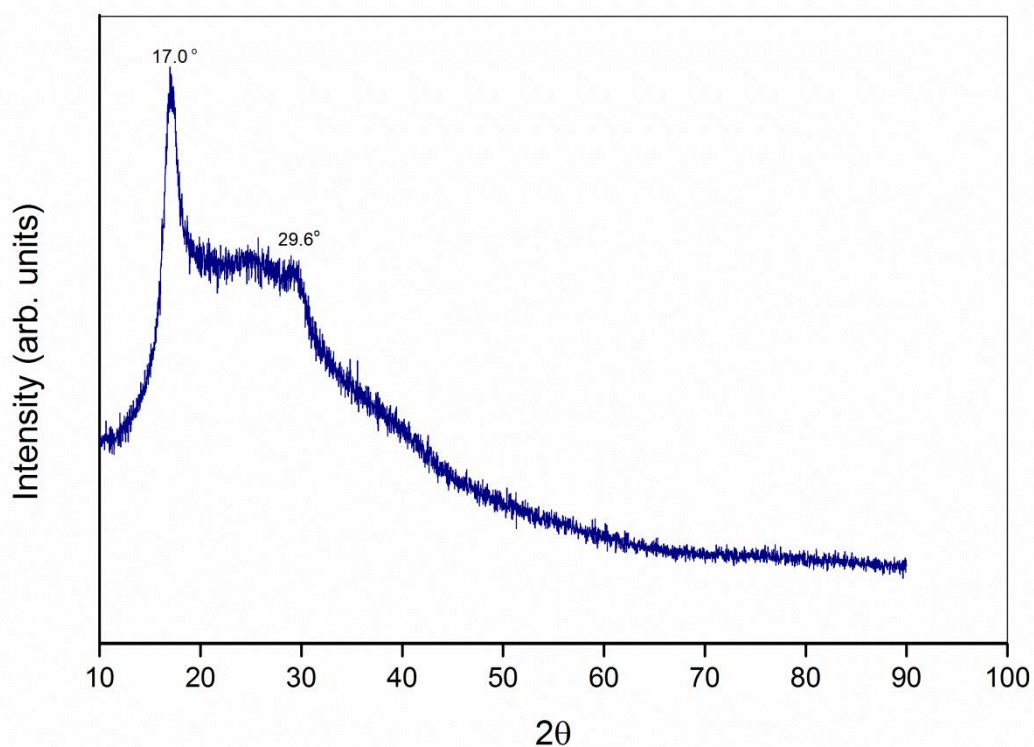


**Figure 4.19:** Polarization current plot as a function of time for the highest conducting film in PAN-EC-DMP-LiBF<sub>4</sub> system with Li |SPE |Li cell.

## 4.2 X-ray Diffraction (XRD) Studies

### 4.2.1 X-ray Diffraction Analysis

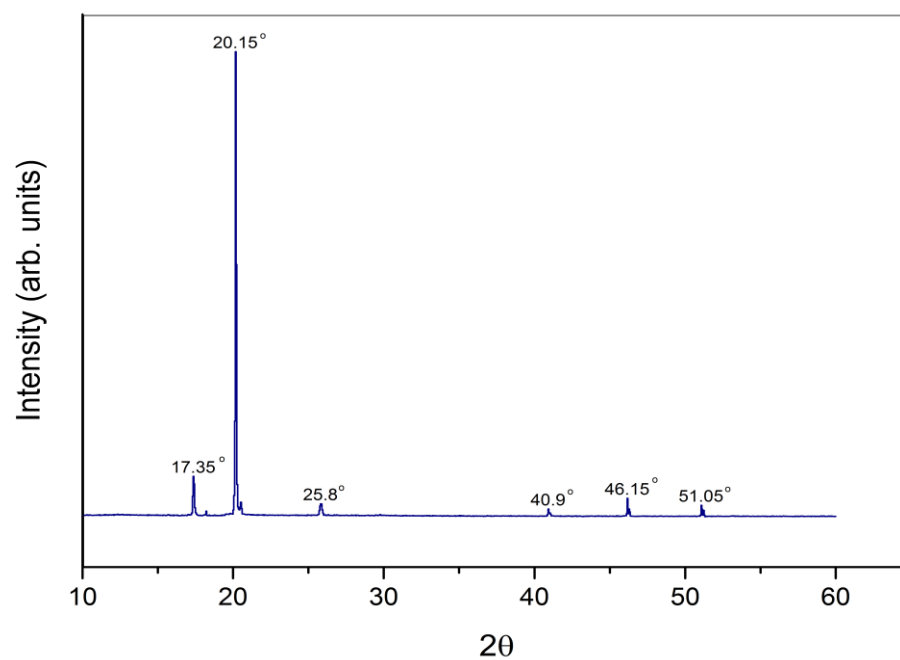
X-ray diffraction analysis is a versatile technique used for phase identification of a material available in both crystalline and amorphous region that aids in explaining the ionic conductivity. It was performed on polymer electrolytes at room temperature. The X-ray diffraction patterns of pure PAN film,  $\text{LiBF}_4$ , EC will be presented. The effect of the incorporation of different amounts of salt and plasticizers to the changes in the structural properties and crystallization of polymer-salts complex will be discussed as well.



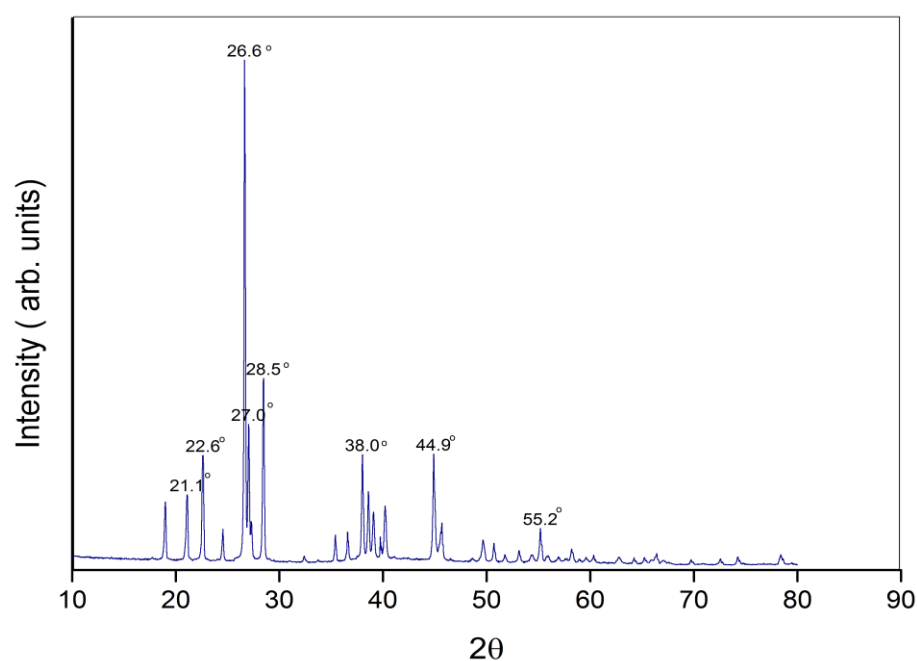
**Figure 4.20:** X-ray diffractogram of pure PAN

Figure 4.20 depicts the diffraction pattern of pure PAN film which reveals the semi crystalline nature of PAN. The observed sharp intense diffraction peak centered at  $2\theta = 17^\circ$  and a weak diffraction peak at  $29.6^\circ$  are the characteristic peaks of plane of

PAN crystallites (Prasanth, Aravindan & Srinivasan, 2012). The XRD patterns of EC and  $\text{LiBF}_4$  are illustrated in Figure 4.21 and 4.22, respectively. The presence of sharp intense peaks in both diffractograms indicates the crystalline nature EC and  $\text{LiBF}_4$ .



**Figure 4.21:** X-ray diffractogram of EC



**Figure 4.22:** X-ray diffractogram of  $\text{LiBF}_4$

### 4.2.2 PAN-LiBF<sub>4</sub> system

In order to further understand the structural alteration and complex formation that takes place in PAN-LiBF<sub>4</sub> system, a few selected samples with different LiBF<sub>4</sub> contents were subjected to this analysis. Figure 4.23 depicts the diffraction patterns of pure PAN film, pure LiBF<sub>4</sub>, and PAN electrolyte film containing 10 wt. % to 50 wt. % of LiBF<sub>4</sub> at room temperature. The characteristics peaks corresponds to LiBF<sub>4</sub> were found to be absent in the polymer electrolytes which correlates to the complete dissolution of LiBF<sub>4</sub> in the PAN matrix (Rajendran, Sivakumar & Subadevi, 2003). It was noted that as the amount of LiBF<sub>4</sub> in the polymer electrolyte increases the diffraction peak substantially decreased in intensity accompanied by an increase in broadness. The relative intensity of the characteristics peak of PAN at 17 ° is observed to decrease followed by a gradually diminishing of peak at 29.6 ° indicates the reduction of crystalline phase in polymer complexes. With the addition of salt, besides a slight shifting of peak at 17 ° was observed, this peak was split into two small peaks for sample containing the highest salt concentration as shown in Figure 4.23(a). This observation suggests that further structural conversion had taken place at that particular angle and more free volume were available for the movement of ions. The amorphous nature produces greater ionic diffusivity providing high ionic conduction (Frech & Chintapalli, 1996). Thus, polymer electrolyte containing 50 wt. % of LiBF<sub>4</sub> exhibited the highest amorphousity is the highest conducting sample concurrent with earlier findings.

### 4.2.3 PAN-EC-DMP-LiBF<sub>4</sub> system

X-ray diffraction measurements were performed on selected plasticized PAN electrolyte films. The diffractograms in Figure 4.24 clearly indicate the fact that the semi-crystalline nature in PAN-EC-DMP-LiBF<sub>4</sub> matrix was further being disrupted by the addition of LiBF<sub>4</sub>. Similar to the highest conducting sample in PAN-LiBF<sub>4</sub> system,



the diffraction peak of PAN at the angle of  $17^\circ$  was observed to be splitting into two weak peaks and subsequent decrease in the peak intensity as the concentration of  $\text{LiBF}_4$  increases. In addition, the weak peak corresponding to PAN at  $29.6^\circ$  was found disappearing with salt concentration. These observations mark the decline in the degree of crystallinity in PAN matrix as more  $\text{LiBF}_4$  is incorporated in the PAN-EC-DMP- $\text{LiBF}_4$  system. As a comparison, it was observed that the humps of each peak in the plasticized system are relatively broader than the unplasticized films in PAN- $\text{LiBF}_4$  system as shown in Figure 4.24 indicates further suppression of the crystalline region of the host matrix. The associated reduction in crystallinity was caused by the significant structural reorganisation by the presence of EC and DMP that induces greater structural disorderness. The complexation between these four pure constituents was further supported by the absence of characteristic peaks of EC and  $\text{LiBF}_4$ . Plasticizers play the role in expanding the amorphous phase of the polymer matrix which works as the ionically conducting pathways lead to higher conductivity. With reference to the results, it can be clarified that greater structural changes occur predominantly in the highest  $\text{LiBF}_4$  containing sample, allowing it to present in highly amorphous morphology which provides greater free volume for the movement of ions. Thus, this polymer electrolyte composition appears as the highest conducting sample.

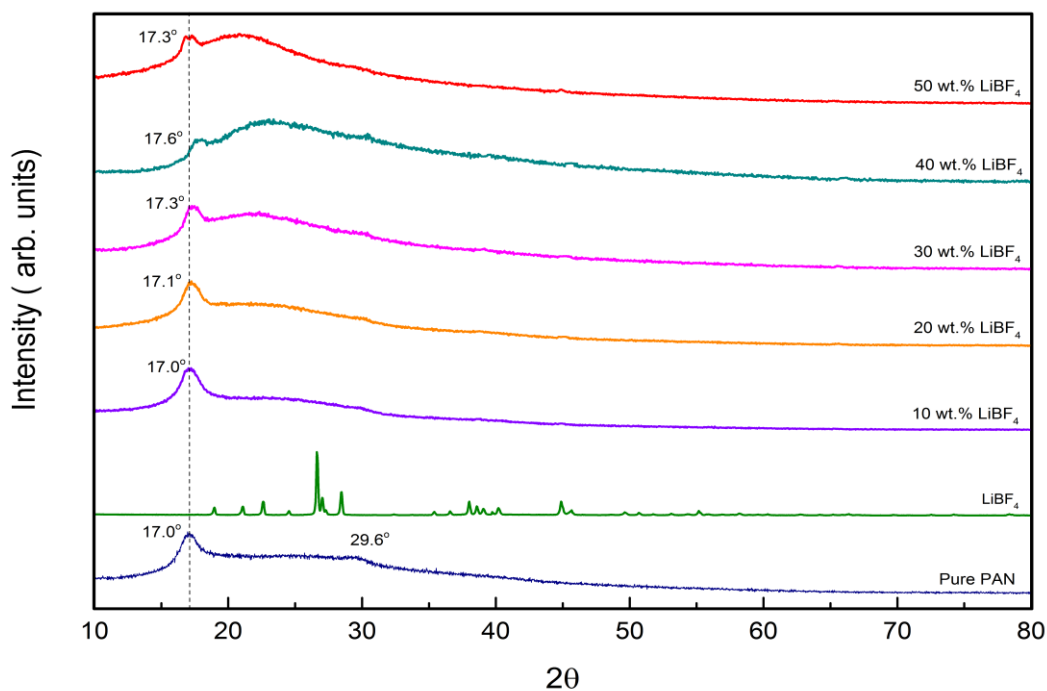


**Figure 4.23:** X-ray diffractogram of the films in the PAN-LiBF<sub>4</sub> system

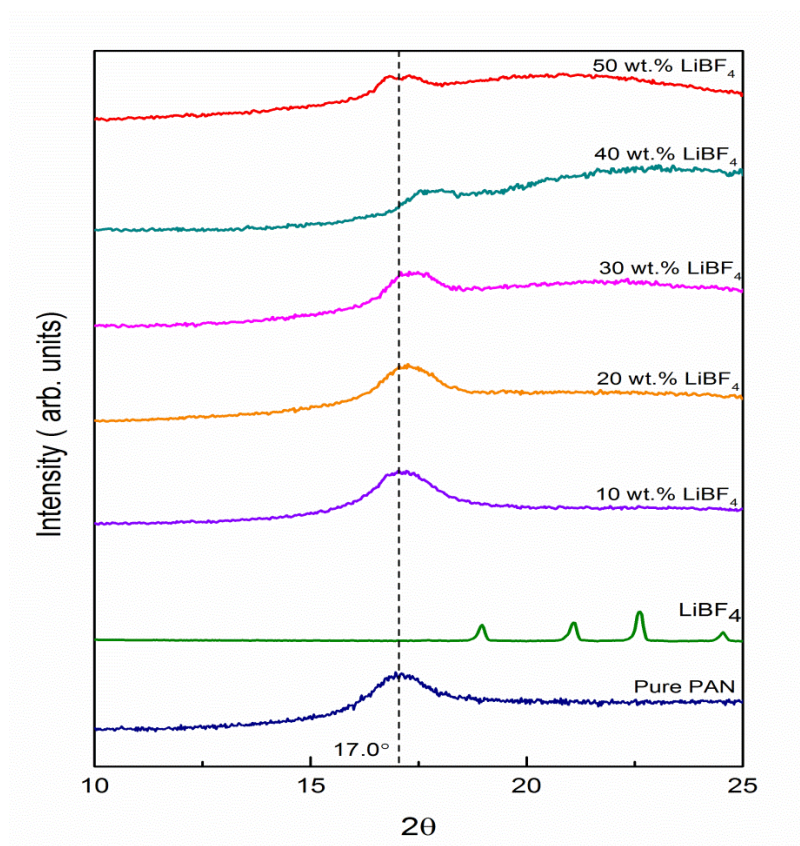


**Figure 4.23(a):** Variation of peak intensity at  $17^\circ$  with concentration of LiBF<sub>4</sub> salt.

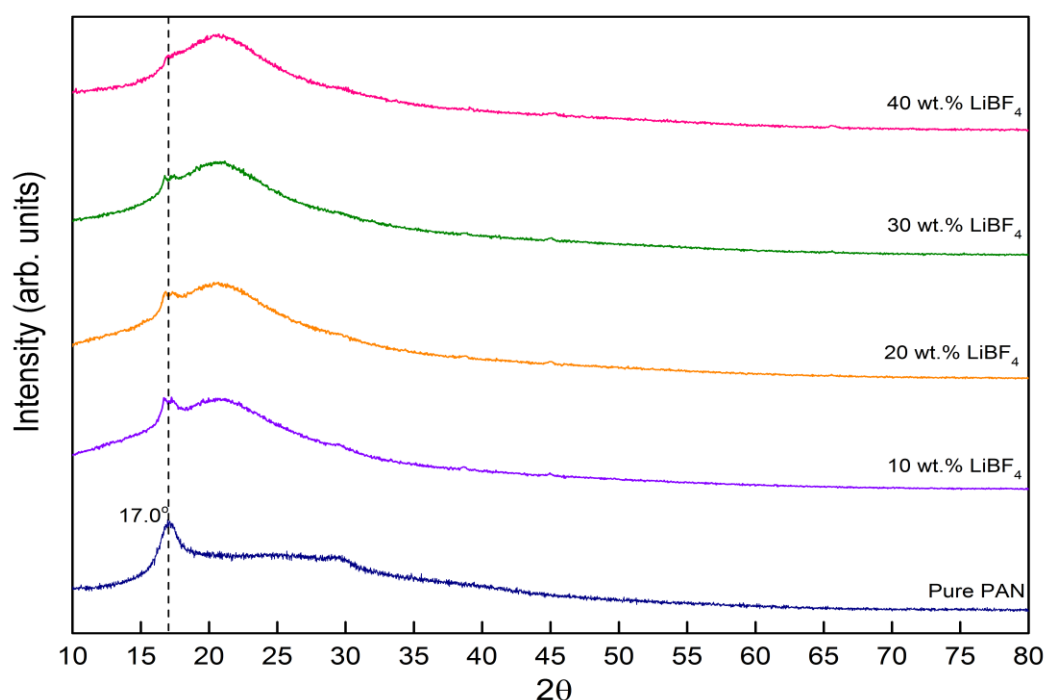


**Figure 4.24:** X-ray diffractogram of the films in PAN-EC-DMP-LiBF<sub>4</sub> system.

### 4.3 Fourier Transform Infrared (FTIR) studies

#### 4.3.1 Introduction

FT-IR spectroscopy was used to obtain the information of the interactions among PAN, EC, DMP and LiBF<sub>4</sub> in the polymer electrolytes. This analysis is a promising method to deduce the complexation between the chemical constituents present in both crystalline and amorphous phase. The occurrence of complexation can be deduced by relying on the alternations in the cage peaks in terms of the frequency shifting, shape, relative intensity, disappearance of existing peak and even through the formation of new peaks. Wang et al. (1996,1999) has reported investigation of interactions among components and ion transport mechanism in PAN-based electrolytes using spectroscopic techniques. The coordination of cations with polar group of PAN can be observed by curve fitting of Gaussian-Lorentzian peak to the nitrile absorbance

region for the polymer electrolytes (Chen et al., 2011). In this study, the Fourier Transform Infrared (FTIR) analysis is performed by using Thermo Scientific Nicolet is10 Smart ATR spectrophotometer in the wave number range from 650 to 4000  $\text{cm}^{-1}$  with resolution of 1  $\text{cm}^{-1}$ .

### 4.3.2 Infrared spectra of pure substances

#### 4.3.2.1 Pure Polyacrylonitrile (PAN)

The band assignments for respective pure PAN were summarised in Table 4.7. The existence of functional groups of pure PAN was determined using infrared spectra. Figure 4.25 shows FTIR spectrum of pure PAN in the region of 1000 and 3500  $\text{cm}^{-1}$ . It can be observed that PAN shows peaks at 2936, 2243, 1664 and 1456  $\text{cm}^{-1}$ . The sharp and strong peak at 2243  $\text{cm}^{-1}$  is assigned to nitrile band and this is due to dominant functional groups in polyacrylonitrile structure. Another strong peak at 1664  $\text{cm}^{-1}$  is due to C – H bending. C – H<sub>2</sub> scissoring and CH<sub>2</sub> symmetrical stretching were observed at 1456 and 2936  $\text{cm}^{-1}$  respectively.

**Table 4.7:** The vibrational modes and wavenumbers of pure PAN film.

<b>Vibrational modes</b>	<b>Wavenumbers (<math>\text{cm}^{-1}</math>)</b>	<b>References</b>	<b>Results observed</b>
C – H <sub>2</sub> scissoring	1453, 1455	(Büttiker, Ebert, Hinderling, Adlhart, 2011; Smith, 1988)	1456
C-H in plane bending	1640	(Moreno, Ana, Gonzalez & Benavente, 2010)	1664
C $\equiv$ N symmetrical stretching	2243,2244	(Rajendran, Kannan, Mahendran, 2001b; Tsutsumi & Kitagawa, 2006)	2243
CH <sub>2</sub> Symmetrical stretching	2940,2939	(Rajendran et al., 2001b; Ouyang, Cheng, Wang & Li, 2008)	2936

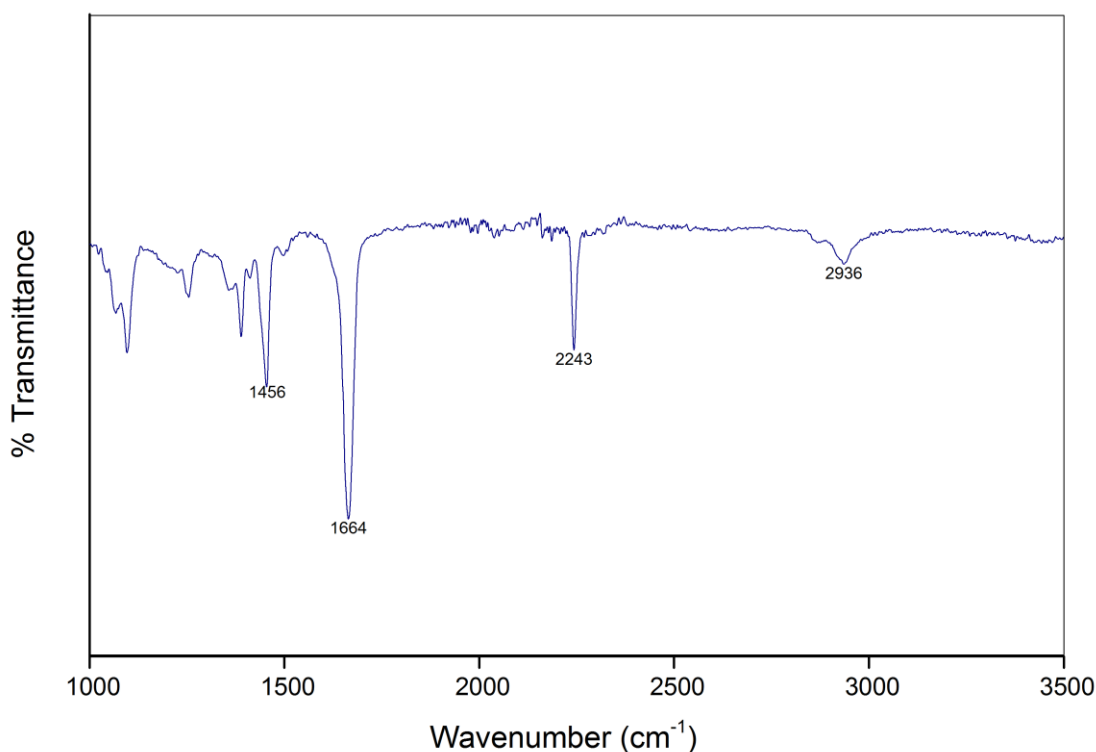


**Figure 4.25:** FTIR spectra of pure PAN film in the region from 1000 to 3500  $\text{cm}^{-1}$

#### 4.3.2.2 Ethylene carbonate (EC)

The vibrational modes and wavenumbers of ethylene carbonate are listed in Table 4.8. Figure 4.26 represents the infrared spectrum of ethylene carbonate in the region from 650 to 3500  $\text{cm}^{-1}$ . The carbonate group has the chemical formula  $\text{CO}_3$ . A carbonate contains a  $\text{C}=\text{O}$  double bond and two  $\text{C}-\text{O}$  single bonds. An intrinsic vibrational band of  $\text{C}=\text{O}$  group in carbonate species is usually located at about 1800  $\text{cm}^{-1}$  as reported by Wang et al. (1996). It can be observed that the  $\text{C}=\text{O}$  symmetric stretching bands of pure EC are split into two intense doublets at 1771  $\text{cm}^{-1}$  and 1791  $\text{cm}^{-1}$ . This phenomenon is similar with the result obtained by previous work and a further explanation has been reported (Angell, 1956; Fini, Mirone & Fortunato, 1973). The  $\text{C}=\text{O}$  bending mode and ring breathing mode of EC were observed at 715 and 892  $\text{cm}^{-1}$  respectively. The second important group wavenumber is the asymmetric

stretching of the two C – O bonds. The O – C – O stretch of EC falls at  $1217\text{ cm}^{-1}$ . The skeletal stretching bands which fall at  $972$ ,  $1060$  and  $1136\text{ cm}^{-1}$  accompanied by  $\text{CH}_2$  wagging mode at  $1391$ ,  $1420\text{ cm}^{-1}$  and  $\text{CH}_2$  bending at  $1472\text{ cm}^{-1}$  are associated with the alkyl group of the carbonate.

#### 4.3.2.3 Dimethyl Phthalate (DMP)

The vibrational modes and wavenumbers of dimethyl phthalate are listed in Table 4.9. Figure 4.27 represents the infrared spectrum of dimethyl phthalate in the region from  $700$  to  $3500\text{ cm}^{-1}$ . The strong out-of-plane C-H bend at  $743\text{ cm}^{-1}$  and ring mode at  $1489\text{ cm}^{-1}$  confirms the presence of an aromatic ring. The three most intense bands in the spectrum are at  $1723$ ,  $1276$  and  $1120\text{ cm}^{-1}$  follows the rule of three bands for esters which correspond to C = O stretching, C – C – O stretching and O – C – C stretching of an aromatic ester. The peak appearing at  $2953\text{ cm}^{-1}$  is assigned to methyl C – H stretches.

**Table 4.8:** The vibrational modes and wavenumbers exhibited by ethylene carbonate.

Vibrational modes	Wavenumbers ( $\text{cm}^{-1}$ )	References	Results observed
C = O bending	717	(Chintapalli & Frech, 1996)	715
Ring Breathing	1067, 890	(Wang et al., 1996)	892
Skeletal stretching	970, 1076, 1180	(Angell, 1956)	972, 1060, 1136
$\text{CH}_2$ wagging	1394, 1420	(Wang et al., 1996)	1391, 1420
$\text{CH}_2$ bending	1480	(Angell, 1956)	1472
O – C – O Stretch	1210-1250	(Smith, 1998)	1217
C = O stretching	1810-1870, 1760-1790, 1773 and 1798	(Angell, 1956; Smith, 1998; Wang et al., 1996))	1771, 1791

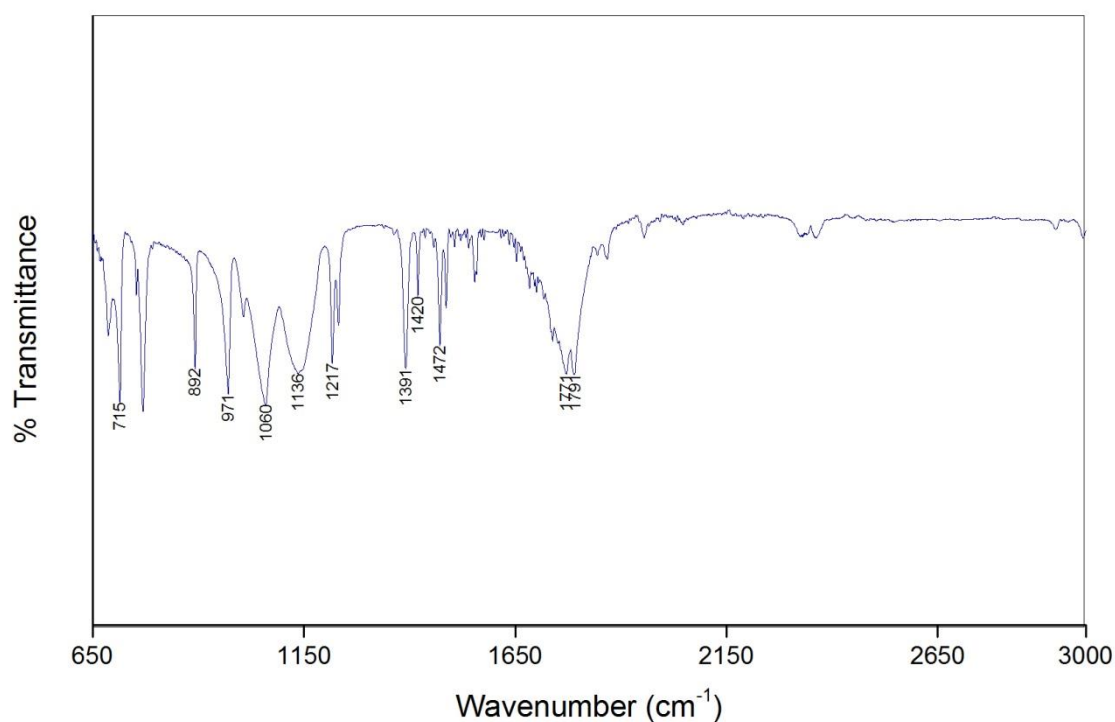


**Figure 4.26:** FTIR spectra of ethylene carbonate in the region from 650 to 3000  $\text{cm}^{-1}$

**Table 4.9:** The vibrational modes and wavenumbers of dimethyl phthalate.

Vibrational modes	Wavenumbers ( $\text{cm}^{-1}$ )	References	Results observed
Aromatic out of plane C – H bend	744	(Smith, 1998)	743
Aromatic ester O – C – C stretch	1122	(Smith, 1998; Uma & Rajendran, 2000)	1120
Aromatic ester C – C – O stretch	1286	(Smith, 1998)	1276
Aromatic ring mode	1488	( Rajendran et al., 2003)	1489
C = O stretching	1728	(Smith, 1998; Uma & Rajendran, 2000 )	1723
Methyl C – H stretches	2962 2954	(Smith, 1998; Rajendran et al., 2003)	2953

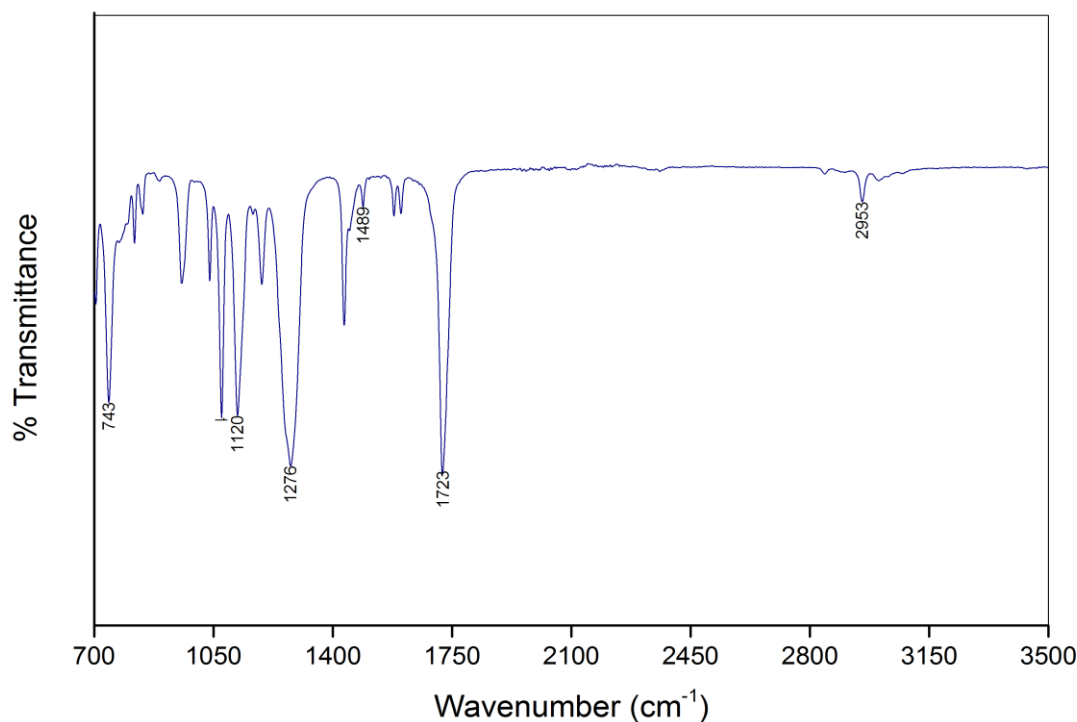


**Figure 4.27:** FTIR spectra of dimethyl phthalate in the region from 700 to 3500  $\text{cm}^{-1}$

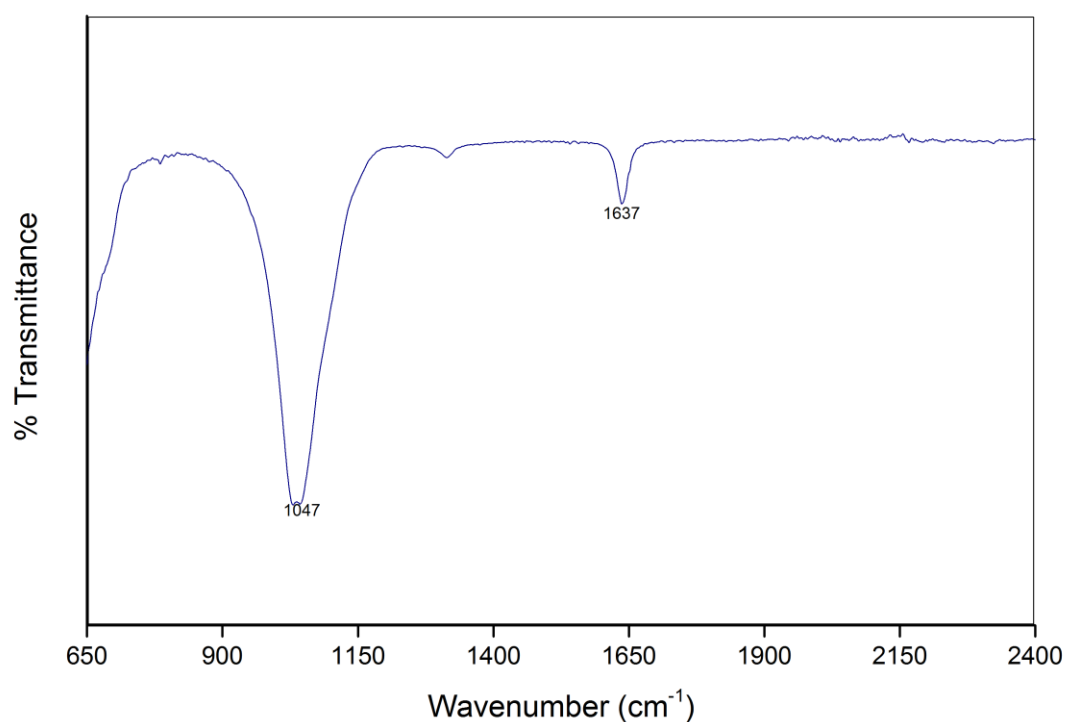
#### 4.3.2.4 Lithium Tetrafluoroborate ( $\text{LiBF}_4$ )

The vibrational modes and wavenumbers of  $\text{LiBF}_4$  are listed in Table 4.10. Figure represents the infrared spectrum of lithium tetrafluoroborate.  $\text{LiBF}_4$  has a tetrahedral structure, similar to  $\text{ClO}_4^-$ , it has four vibrational modes, which are symmetric stretching ( $\nu_s$ ) at  $777 \text{ cm}^{-1}$ , two degenerate in-plane bending ( $\delta_d$ ) at 360 and  $533 \text{ cm}^{-1}$  and degenerate stretching ( $\nu_d$ ) at  $1070 \text{ cm}^{-1}$ . However, only  $\delta_d$  and  $\nu_d$  are infrared active (Nakamoto, 1922). From Figure 4.28, a noticeable intense peak at  $1047 \text{ cm}^{-1}$  assigned to degenerate stretching ( $\nu_d$ ) of  $\text{BF}_4^-$ . Due to highly hygroscopic nature of  $\text{LiBF}_4$ , the peak observed at  $1637 \text{ cm}^{-1}$  peak is believed to be H–O–H bending of water molecules associated to water adsorption on the lithium salt (Dawy, 2000; Chang, Huang, Yeh & Lin, 2000).



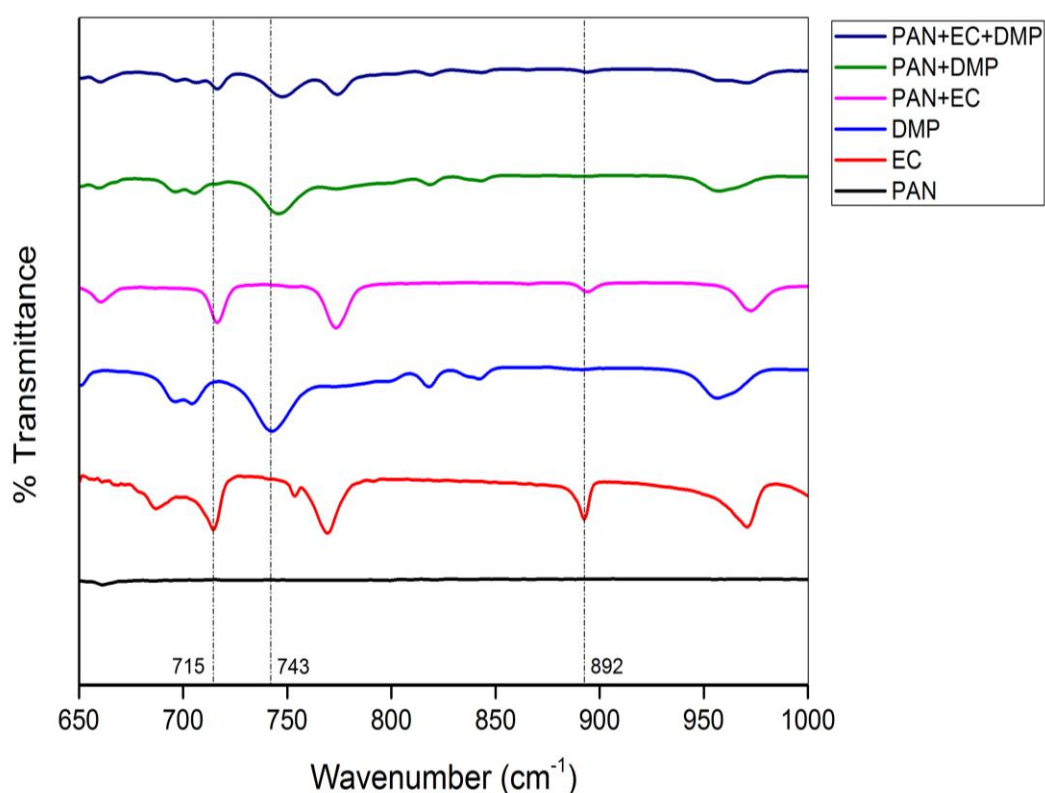
**Table 4.10:** The vibrational modes and wavenumbers of lithium tetrafluoroborate.

Vibrational modes	Wavenumbers ( $\text{cm}^{-1}$ )	References	Results observed
symmetric $\text{BF}_4$ stretching ( $\nu_s$ )	777, 766, 778	( Nakamoto, 1922; Jacob & Arof , 2000; Papke, Ratner & Shriver, 1982)	785
Degenerate $\text{BF}_4$ stretching ( $\nu_d$ )	1089, 1070	(Rajendran, Kannan & Mahendran, 2001a; Nakamoto, 1922)	1047

**Figure 4.28:** FTIR spectra of lithium tetrafluoroborate in the region from 650 to 2400  $\text{cm}^{-1}$

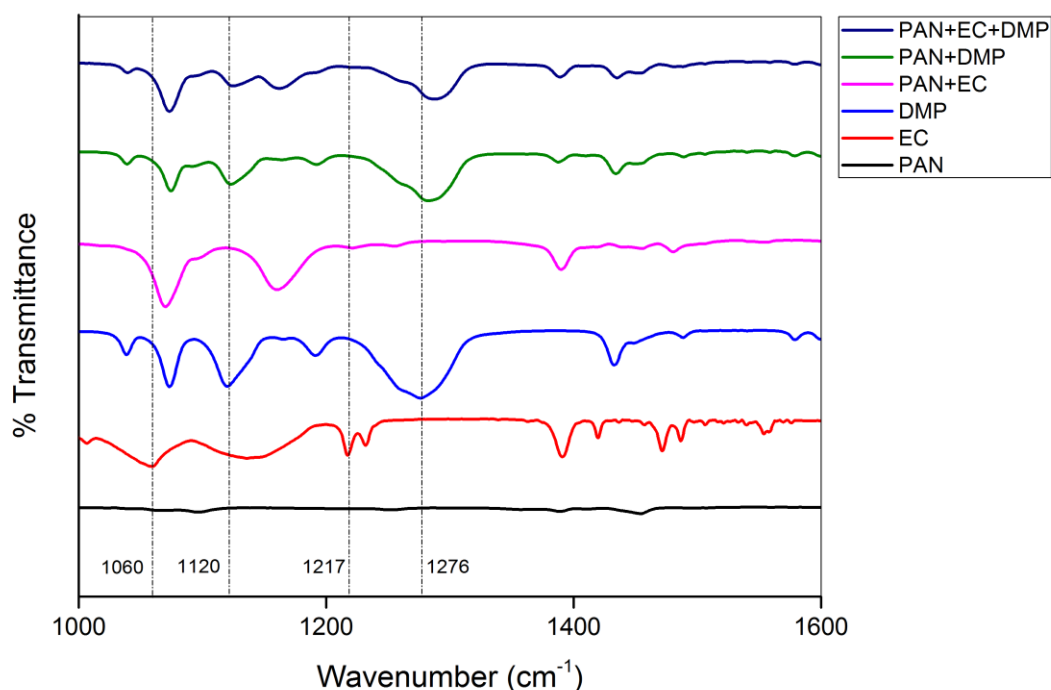
### 4.3.3 Interaction between PAN and Plasticizers

The infrared spectra of plasticized PAN films in different frequency regions were shown in Figure 4.29-4.32. Spectra for pure constituents are also included for comparison. In the frequency range from 650 to 1000  $\text{cm}^{-1}$ , there is no observable peak for PAN. However, there are significant changes observed on the plasticized film. The C=O bending of EC at 715 was slight shifted to 717  $\text{cm}^{-1}$  in the PAN-EC film while the intensity of this band is greatly reduced in PAN-EC-DMP film. The intensity of peak at 892  $\text{cm}^{-1}$  corresponding to the ring breathing of EC shows a large suppression in PAN-EC film and almost diminished in PAN-EC-DMP film. The only noticeable peak of DMP in this frequency range is the aromatic C-H band peaking at 743  $\text{cm}^{-1}$ . It was observed that this peak is slight shifted followed by decreased in intensities in both PAN-DMP and PAN-EC-DMP films.



**Figure 4.29:** Infrared spectra of plasticized-PAN film with different ratios of EC and DMP in the region 650 to 1000  $\text{cm}^{-1}$ .

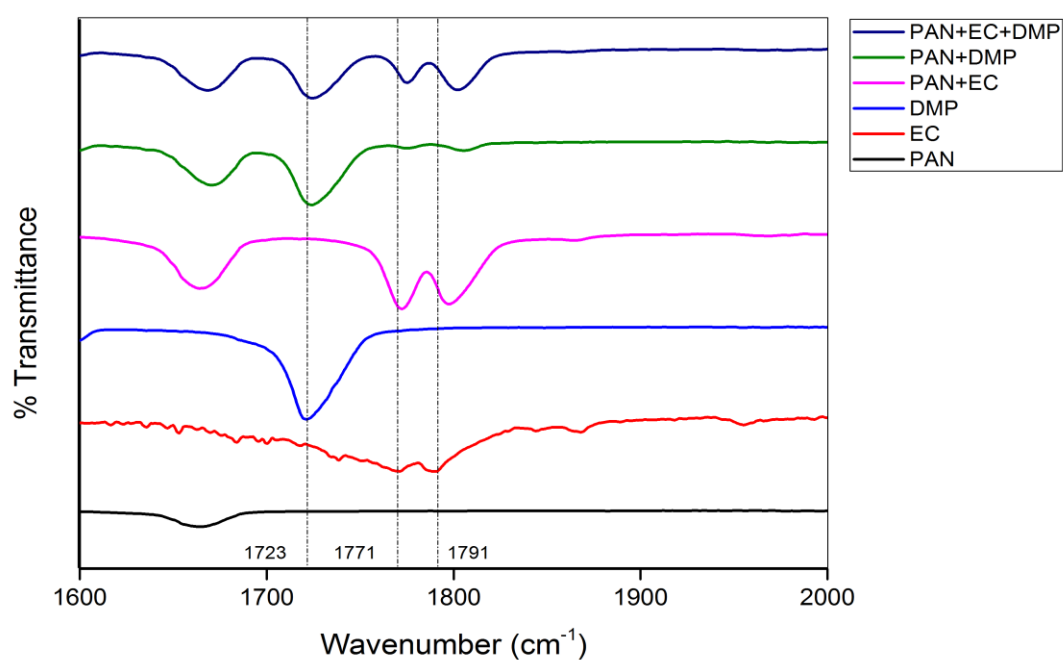
Figure 4.30 depicts the infrared spectra of the PAN, EC, DMP and plasticized PAN films in frequency region between 1000 and 1600  $\text{cm}^{-1}$ . The ring breathing mode at 1060  $\text{cm}^{-1}$  of EC moved upwards to 1070  $\text{cm}^{-1}$ , accompanied with increasing intensity and decreasing width in PAN-EC film. A similar manner was observed in PAN-EC-DMP film with a shift moves 16  $\text{cm}^{-1}$  towards the high frequency side of the spectra and reduced peak intensity as compared to PAN-EC film. The O–C–O stretch of EC at 1217  $\text{cm}^{-1}$  was found to be totally disappeared in the spectra of both systems. The intensity of the peak 1120  $\text{cm}^{-1}$  which assigned to O – C – C stretch of the ester group of DMP has greatly reduced in PAN-DMP film and a further reduction was discovered in PAN-EC-DMP film. Being one of the most intense peaks in DMP structure, the peak 1276  $\text{cm}^{-1}$  due to C–C–O stretch of ester was shifted to 1280  $\text{cm}^{-1}$  and 1291  $\text{cm}^{-1}$  in PAN-DMP and PAN-EC-DMP films respectively. The intensity of this peak was found to be smallest in the PAN-EC-DMP film.



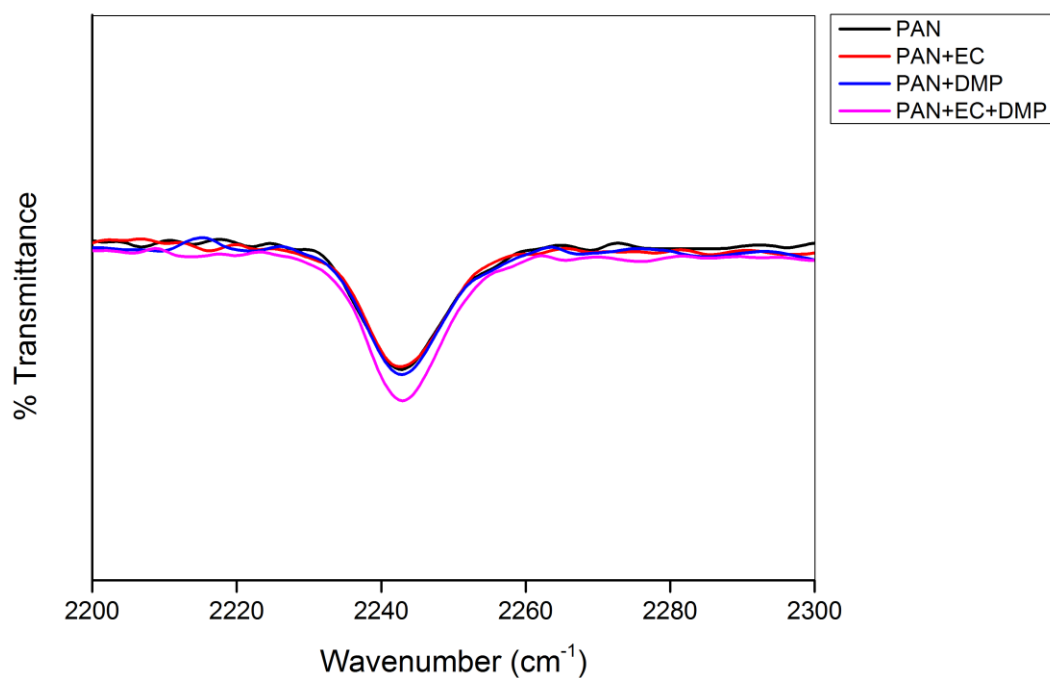
**Figure 4.30:** Infrared spectra of plasticized-PAN film with different ratios of EC and DMP in the region 1000 to 1600  $\text{cm}^{-1}$ .

Figure 4.31 represents the same spectra in the frequency range from 1600 to 2000  $\text{cm}^{-1}$ . The peaks at 1723, 1771 and 1791  $\text{cm}^{-1}$  are assigned to C=O bending of DMP and EC. The intensity of peak at 1723  $\text{cm}^{-1}$  displayed an obvious reduction in PAN-DMP and PAN-EC-DMP films. The doublet of the carbonyl bending mode of EC was found to be increased in intensity for PAN-EC film and a slight band shifting. However, a greater shifting was observed in PAN-EC-DMP films which are peaking at 1775 and 1803  $\text{cm}^{-1}$ .

The structure of PAN involves only a simple C-C backbone and a high density of  $\text{C}\equiv\text{N}$  groups, the change if the vibrational due to the presence of other components can provide an important concerning the interaction between the nitrile group and plasticizers. Figure 4.32 shows the FTIR spectra of pure PAN, PAN films plasticized with EC, DMP and mixture of EC-DMP in ratio of 1:1 in the frequency region between 2200 and 2300  $\text{cm}^{-1}$ . It can be observed that the intensity and position at this band remains unchanged with the presence of EC and DMP alone. This result revealed a weak interaction of EC and DMP with the nitrile group of PAN. However, PAN film plasticized with mixture of EC and DMP gives an exceptional behaviour at which exhibiting a relatively greater intensity indicating this combination makes a better interaction with the polymer host. The structural changes observed on the spectra of PAN-EC, PAN-DMP and PAN-EC-DMP indicates there is a rather strong interaction between PAN, EC and DMP. However, the influence of plasticizers on the spectral features of PAN is not obvious as the finding reported by Wang et al. According to Wang et al, this behaviour is plausibly due to the difference in strength of the  $\text{C}\equiv\text{N}$  bond and C=O bond which can bring different effects on different bonds.



**Figure 4.31:** Infrared spectra of plasticized-PAN film with different ratios of EC and DMP in the region 1600 to 2000  $\text{cm}^{-1}$ .



**Figure 4.32:** Infrared spectra of plasticized-PAN film with different ratios of EC and DMP in the region 2200 to 2300  $\text{cm}^{-1}$ .

### 4.3.4 Interaction between PAN and LiBF<sub>4</sub> salt

Figure 4.33 shows gives the spectra of PAN doped with different concentrations of LiBF<sub>4</sub> in the region from 900 to 1800 cm<sup>-1</sup>. As reported earlier, the vibrational band at ~1070 cm<sup>-1</sup> of BF<sub>4</sub><sup>-</sup> anion observed has been used as an indicator for dissociation of LiBF<sub>4</sub> (Uma & Rajendran, 2000; Shanti, Mathew, Ulaganathan & Rajendran, 2013). However, as reported in previous section, this peak was observed at 1047 cm<sup>-1</sup> which is similar to Song et al. (2004) findings. The peak intensity of this vibrational band is greatly reduced in the PAN matrix with a maximum shift of 10 cm<sup>-1</sup> towards higher frequency side signifies the dissociation of LiBF<sub>4</sub>. The band of C – H in plane bending at 1664 cm<sup>-1</sup> of PAN is slightly shifted and the peaks have apparently become more intense and sharp upon addition of salt. With the increase of LiBF<sub>4</sub> content in the polymer matrix, there are new bands formed at 1254 and 1389 cm<sup>-1</sup>. The strong stretching vibrations of nitrile groups such as C≡N are observed at 2243 cm<sup>-1</sup> for sample containing 10 wt.% to 50 wt.% of LiBF<sub>4</sub> salt as shown in Figure 4.34. In acrylonitrile based electrolytes, the Li<sup>+</sup> ions associate with the nitrogen atom of the electron rich nitrile group. Based on Figure 4.34, it is observed that the characteristic peak intensity corresponding to C≡N is decreased with the increase of salt concentration. This behaviour reflects the interaction between Li<sup>+</sup> ions and nitrile group is similar to the work presented by Shanti et al (2013). There is a pair of unbounded electrons on the nitrogen atom in the C ≡ N group and the Li<sup>+</sup> ion has an empty orbital. Therefore, it is possible for Li<sup>+</sup> ions to bond with the nitrogen atom and an associate is formed (Wang et al., 1999).

The symmetric B-F stretch ( $\nu_1$ ) mode is mostly used to study the ion association involving BF<sub>4</sub><sup>-</sup>. As discussed in section 4.3.2.4, the vibrational modes of BF<sub>4</sub><sup>-</sup> are formally forbidden in infrared. However, this band could be activated in infrared region by other species. Many attempts have been done to study the ion

association of  $\text{LiBF}_4$  with different solvents have brought out distinguishable vibrational bands which ascribed to the free ions and ions pair of  $\text{LiBF}_4$ . The band at  $766\text{ cm}^{-1}$  is the free ions, while the band at  $770\text{ cm}^{-1}$  originates from the contact ion pairs and at  $782\text{ cm}^{-1}$  assigned to the dimers (Xuan, Zhang, Wang & Wang, 2004; Qiao et al., 2008). In this system, these bands were detectable when  $\text{LiBF}_4$  is added into the polymer host that are free ions band at  $\sim 766\text{ cm}^{-1}$  and ion pairs band at  $\sim 777\text{ cm}^{-1}$ . Accordingly, the curve fitting of a Gaussian- Lorentzian peak to the  $\text{BF}_4^-$  absorbance region for selected samples was applied and is shown in Figure 4.35. Similar to Qiao et al. (2008) findings, in the studied concentration ranges, only two distinct bands had been observed. It can be observed the intensity and the integrated area corresponds to free ions curves increases with salt concentration and this explains the gradual increase in conductivity of the films from 10 wt. % to 50. wt% The position and integrated area of the free ions and ion pairs are summarized in Table 4.11.

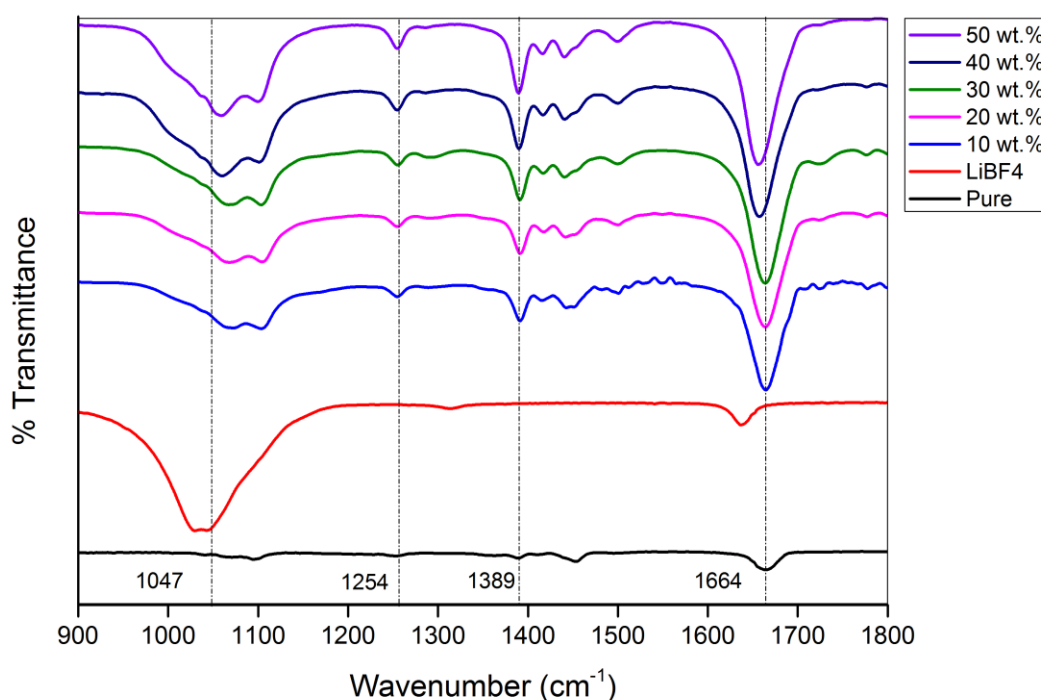


**Figure 4.33:** Infrared spectra of PAN film doped with varying amounts of  $\text{LiBF}_4$  in the region  $900$  to  $1800\text{ cm}^{-1}$ .

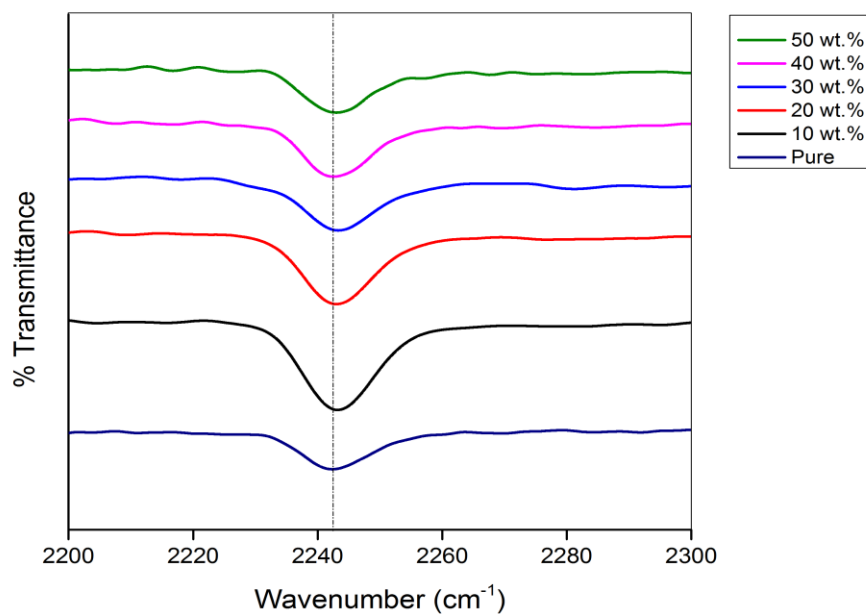


**Figure 4.34:** Infrared spectra of PAN film doped with varying amounts of LiBF<sub>4</sub> in the region 2200 to 2300 cm<sup>-1</sup>.

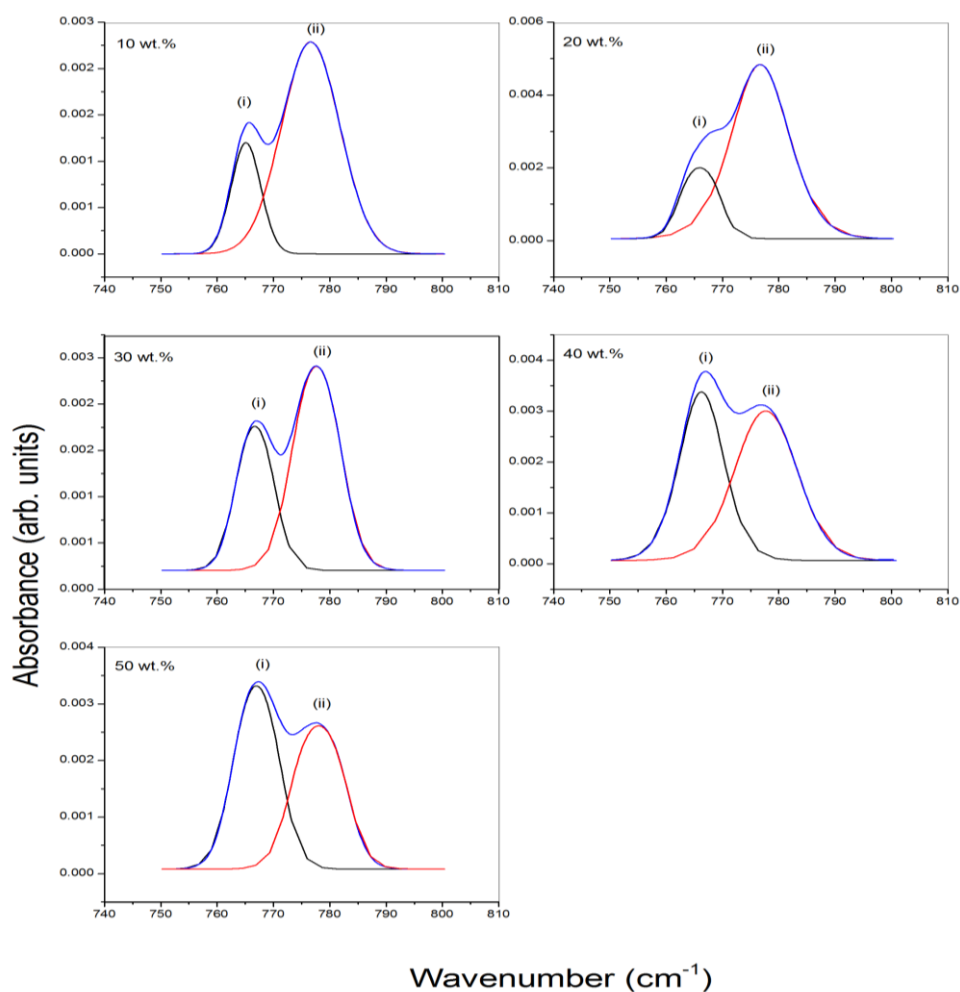


**Figure 4.35:** Infrared spectra of the ν<sub>1</sub> mode of BF<sub>4</sub><sup>-</sup> correspond to (i) free ions (ii) ion pairs for films at different concentrations of LiBF<sub>4</sub> in PAN-LiBF<sub>4</sub> system.



**Table 4.11:** Band-Fitting Results in the Tetrafluoroborate Anion  $\nu_1(A1)$  Manifold FTIR Spectra of  $\text{LiBF}_4$  in PAN- $\text{LiBF}_4$  system.

Salt Content (wt.%)	Position ( $\text{cm}^{-1}$ )		Integrated Area (%)	
	Free ions	Ion Pairs	Free Ions	Ion Pairs
10	765	777	20.1	79.9
20	766	777	20.3	79.7
30	767	778	36.1	63.9
40	766	778	40.1	59.9
50	767	778	52.9	47.1

#### 4.3.5 Interaction between PAN-EC-DMP and $\text{LiBF}_4$ salt

Figure 4.36 shows the infrared spectra for EC-DMP plasticized PAN films doped with varying amounts of  $\text{LiBF}_4$  in the region  $900\text{-}1900\text{ cm}^{-1}$ . Infrared spectrum of undoped plasticized PAN film is included for comparison. The spectral changes of the unperturbed B-F stretching modes at  $1047\text{ cm}^{-1}$  is obvious in this system as compared to PAN- $\text{LiBF}_4$  system. This band is totally disappeared upon addition of salt indicates the dissociation of  $\text{LiBF}_4$  and a greater interaction between plasticizer and  $\text{LiBF}_4$  than PAN alone. The ring breathing and carbonyl stretching doublets of EC at  $1076$ ,  $1775$  and  $1803\text{ cm}^{-1}$  were found to be depressing in intensity when salt content increases even though no obvious shifting was observed. Addition of salt also causes a reduction in intensity of the O – C – C stretch of ester and the carbonyl stretching of DMP at  $1291$  and  $1727\text{ cm}^{-1}$ . Figure 4.37 shows the spectral changes of nitrile band of plasticized PAN doped with varying amount of  $\text{LiBF}_4$ . Similar to PAN- $\text{LiBF}_4$  system, the interaction between  $\text{Li}^+$  ion and PAN can be seen clearly in Figure 4.37. There is almost no difference in the shape of this band or the vibrational frequency of the nitrile stretching band. However, upon addition of 10 wt. % salt, the intensity of this peak was

greatly reduced and a growth was observed when the salt concentration increases. This means that weak strong interaction exists between  $\text{Li}^+$  ions and the nitrile group.

Summarizing the above results and discussion, the interactions of  $\text{Li}^+$  with nitrile band observed in PAN- $\text{LiBF}_4$  system is more likely than PAN-EC-DMP- $\text{LiBF}_4$ . It can be concluded that the polymer host and the plasticizer interfere with each other in their association with the  $\text{Li}^+$  ions. Competitions exist between the ion associations of plasticizer and PAN with the  $\text{Li}^+$  ions as reported by Wang et al. (1996).

The band fitting of the  $\text{BF}_4^-$  absorbance region was done for system in order to study the ion dissociation of the salt. The curve fitting of a Gaussian- Lorentzian peak to the  $\text{BF}_4^-$  absorbance region for selected samples was applied and is shown in Figure 4.38. Based on Figure 4.38, again, only two distinct bands were observed. However, the positions of the bands are different from those observed in PAN- $\text{LiBF}_4$  system. The first distinct peak was observed at  $752\text{ cm}^{-1}$  while the second peak falls at  $776\text{ cm}^{-1}$ . The free ions band at  $766\text{ cm}^{-1}$  was found to be overlapped with the aromatic C – H band of DMP as observed in PAN-EC-DMP system and a single band formed at  $\sim 752\text{ cm}^{-1}$ . Thus, the integrated area of the free ions band is less reliable to be referred as indication of dissociation of the salt. Hence, the band corresponds to the paired  $\text{BF}_4^-$  ions were studied instead. The position and integrated area of ion pairs are summarized in Table 4.12. It was noticed that the area of the band of the ion pairs decreases with salt concentrations indicates more free ions are dissociated which is responsible for the high conductivity values of the polymer electrolyte. On the other hand, the change in the  $\text{C}\equiv\text{N}$  vibration absorbance was studied to analyse the interaction related to the polymer chains. According to Chen-Yang et al. (2002), the absorbance can be deconvoluted into two contributions, the unbounded  $\text{C}\equiv\text{N}$  between  $2235$  and  $2250\text{ cm}^{-1}$ , and the bonded  $\text{C}\equiv\text{N}$  between  $2255$  and  $2270\text{ cm}^{-1}$ . Figure 4.39 shows the band fitting of the  $\text{C}\equiv\text{N}$  absorbance for films in PAN-EC-DMP- $\text{LiBF}_4$  system. The position and

integrated area of the unbonded and bonded  $\text{C}\equiv\text{N}$  band are summarized in Table 4.13. The percentage of the bonded  $\text{C}\equiv\text{N}$  groups was found to be less than 20% implying that the interaction between the ions and plasticizers are stronger. In addition, the percentage of the bonded  $\text{C}\equiv\text{N}$  group decreases as more salt is added which explains that effective dissociation of salt even at high salt concentration with the presence of plasticizers. This observation is also consistent with the conductivity values.

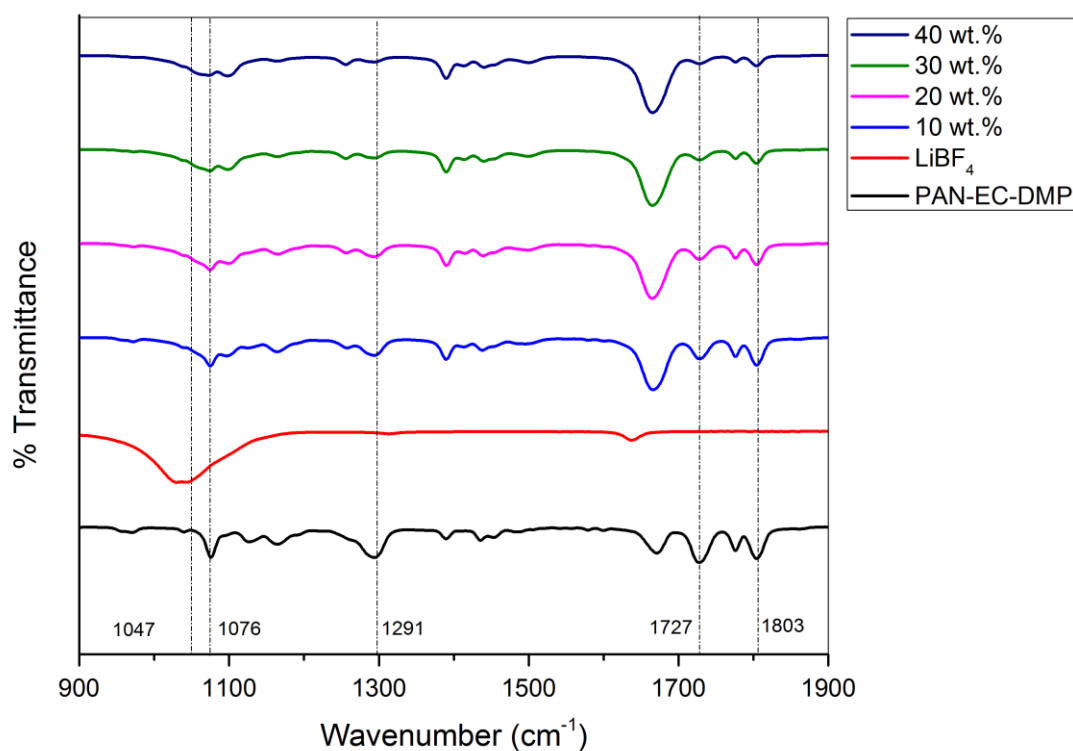


**Figure 4.36:** Infrared spectra of PAN-EC-DMP film doped with varying amount of  $\text{LiBF}_4$  in the region 900 to 1900  $\text{cm}^{-1}$ .

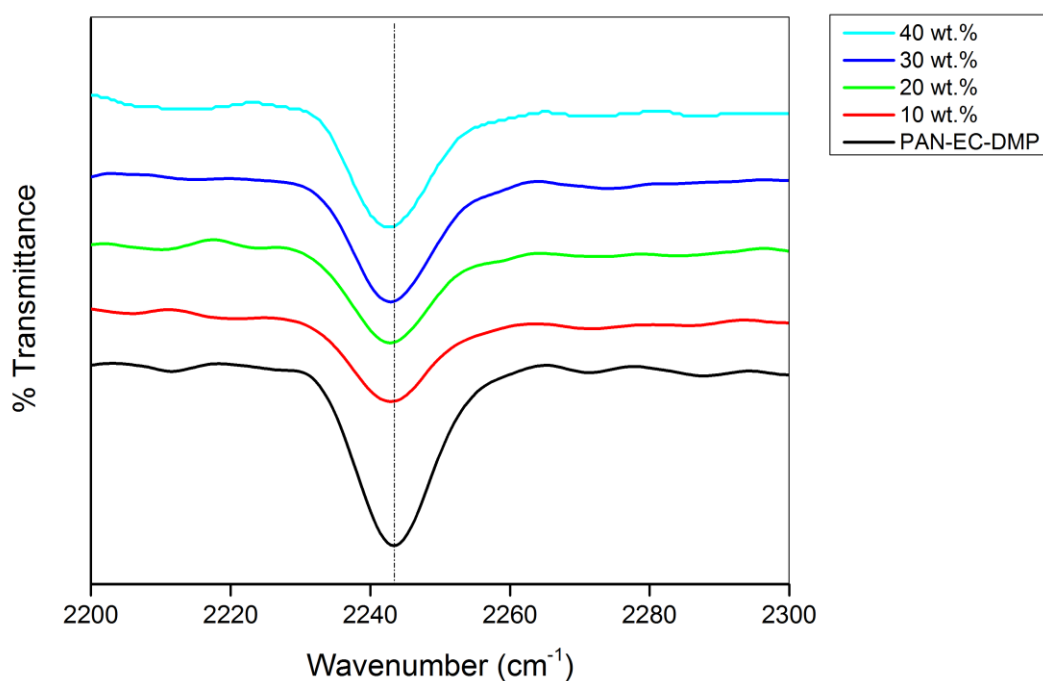


**Figure 4.37:** Infrared spectra of PAN-EC-DMP film doped with varying amount of  $\text{LiBF}_4$  in the region 2200 to 2300  $\text{cm}^{-1}$ .

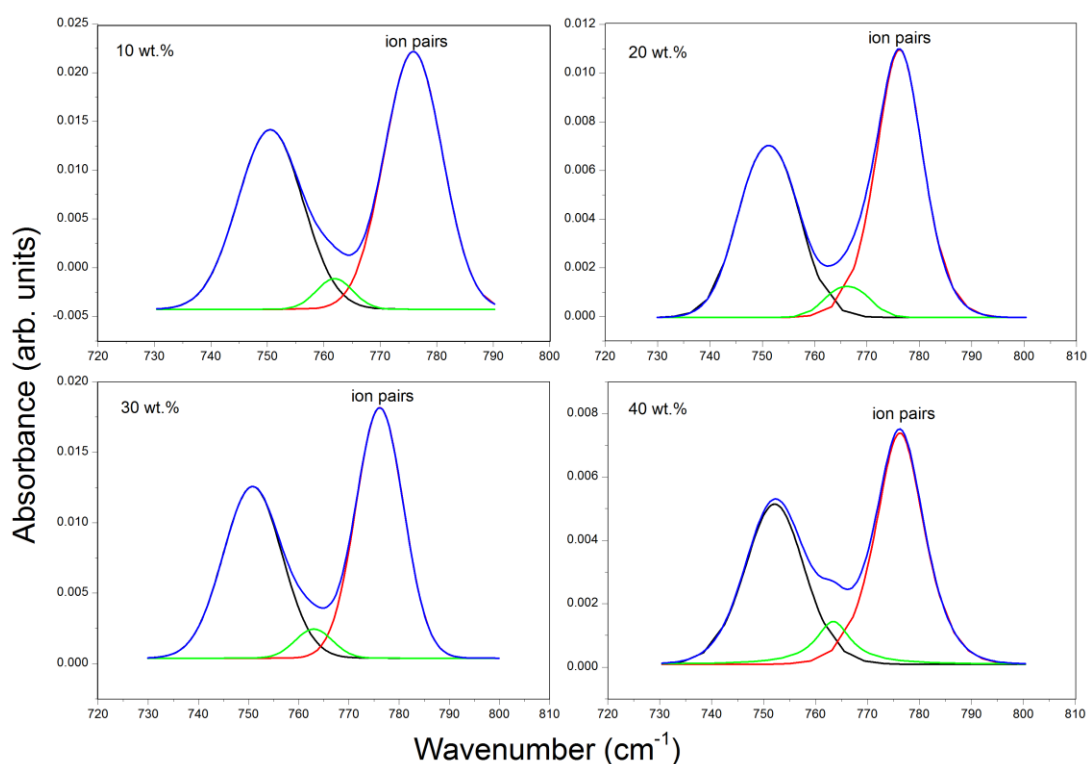


**Figure 4.38:** Infrared spectra of the  $\nu_1$  mode of  $\text{BF}_4^-$  for films containing different concentrations of  $\text{LiBF}_4$  in PAN-EC-DMP- $\text{LiBF}_4$  system.

**Table 4.12:** The position and integrated area of paired tetrafluoroborate ions formed in films of different  $\text{LiBF}_4$  content in PAN-EC-DMP- $\text{LiBF}_4$  system.

Salt Content (wt.%)	Position ( $\text{cm}^{-1}$ )	Integrated Area (%)
10	776	53.8
20	776	53.1
30	776	51.7
40	776	50.4

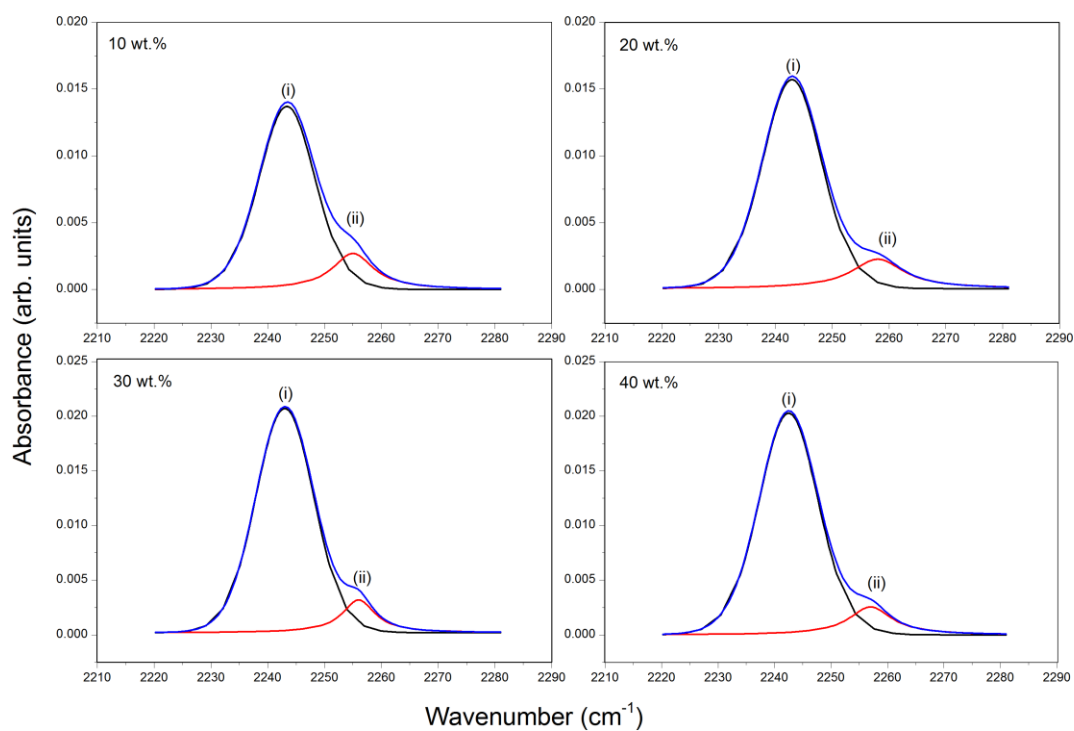


**Figure 4.39:** Infrared spectra of the (i) unbonded (ii) bonded nitrile band of films at different concentrations of  $\text{LiBF}_4$  in PAN-EC-DMP- $\text{LiBF}_4$  system.

**Table 4.13:** Band-Fitting Results of the  $\text{C} \equiv \text{N}$  absorbance for PAN in PAN-EC-DMP- $\text{LiBF}_4$  system.

Salt Content (wt.%)	Position ( $\text{cm}^{-1}$ )		Integrated Area (%)	
	Unbonded	Bonded	Unbonded	Bonded
10	2243	2255	83.7	16.3
20	2243	2258	86.2	13.8
30	2243	2257	89.1	10.9
40	2243	2256	89.6	10.4

## 4.4 Field emission Scanning Electron Microscopy (FESEM) Analysis

### 4.4.1 Introduction

Morphology features of the polymer electrolytes are very much related to the ionic conductivity performance as it is the interface between the two active solid electrodes, permitting the migration of ions. This study was relied in order to examine the morphology changes on the surface of the polymer electrolytes with the addition of EC, DMP and  $\text{LiBF}_4$ . The morphology images of selected polymer electrolytes were captured using Quanta FESEM with the model 450 FEG at 5kV. The micrographs for PAN films were obtained with the magnification factor of 20000 X.

### 4.4.2 Pure PAN film

Figure 4.40 shows the micrograph for pure PAN film. It is shown clearly a smooth and uniform surface morphology of PAN. The appearance of visible and evenly distributed small pores may due to preoccupation of moisture in the film. The hydrophilic groups in DMF traps water molecules. The rapid evaporation of the entrapped water molecules and DMF from the film at 50 °C under vacuum leaving pores on the surface of the film (Kuo, Chen, Wen & Gopalan, 2002).

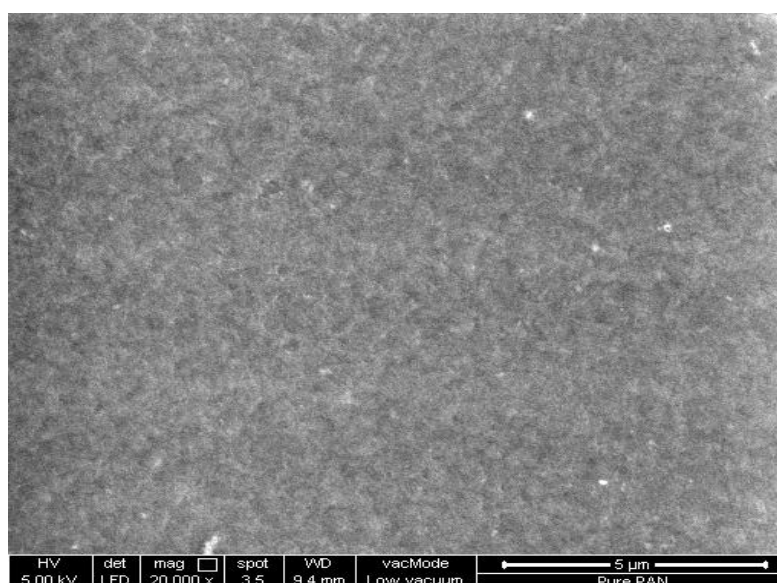


**Figure 4.40:** Micrograph of pure PAN film

#### 4.4.3 PAN-EC-DMP film

Figure 4.41 depicts the FESEM micrograph for the PAN-EC-DMP film at magnification of 20000 X. There are no separate phases were observed suggesting complete miscibility between plasticizers and PAN. Plasticizers are able to permeate into the free volume around the polymer chains which in turn increases intermolecular distance which results in some swelling and increased free volume (Wypych, 2004). The surface morphology of the film appears homogenous with greater pore size indicates that the amorphous phase has taken place on addition of plasticizers. It can therefore be inferred that the complexation between polymer, PAN and the plasticizers, EC and DMP has occurred. The porous structure is believed to be involved in ionic conduction and lead to the enhancement in ionic conductivity.

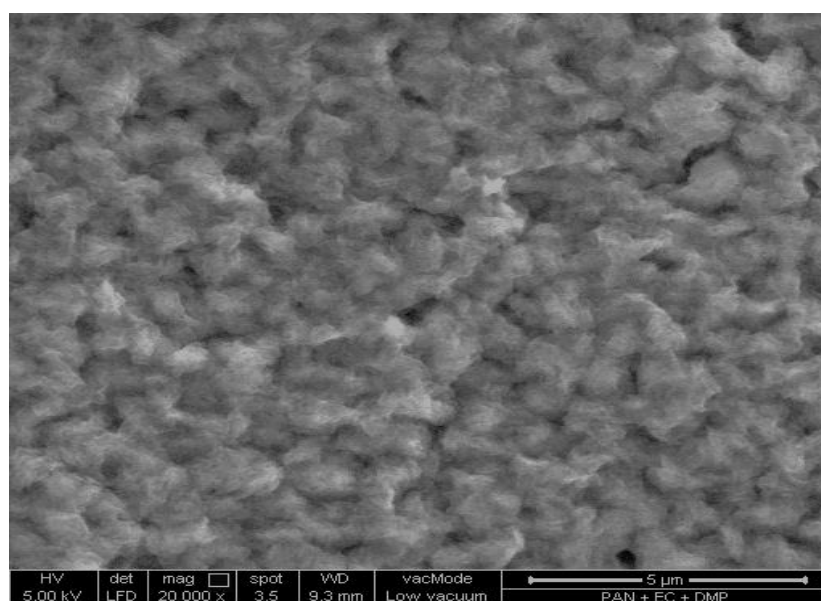


**Figure 4.41:** Micrograph of PAN-EC-DMP film



#### 4.4.4 PAN-LiBF<sub>4</sub> system

Figure 4.42 (a-c) shows the micrographs for PAN containing 10 wt.%, 40 wt.% and 50 wt.% of LiBF<sub>4</sub>, respectively. There are no salt crystal observed in the micrographs even at high salt concentration indicates complete dissolution of salt in the polymer matrix coincides with the XRD result. The morphology of PAN changes as soon as 10 wt. % of LiBF<sub>4</sub> is incorporated into the polymer; the porous structure of PAN has become more distinguishable. When higher amounts of lithium salt are added into the polymer, i.e. 40 wt.% and 50 wt.%, the surface morphology changes drastically and starts to show layered features. Figure 4.42(c) shows the FESEM micrograph for the highest conducting sample, the morphology becomes significantly more layered and the appearance of number of uniform tracks (dark region) of few micrometer sizes is responsible for the appreciable ionic conductivity of the electrolyte (Ulaganathan, Nithya & Rajendran, 2012). The overlapping layers shorten the pathway for the intra and inter-molecular coordination between ions and the polymer chains at the same time providing enough channels for the migration of ions, accounting for better ionic conductivity.

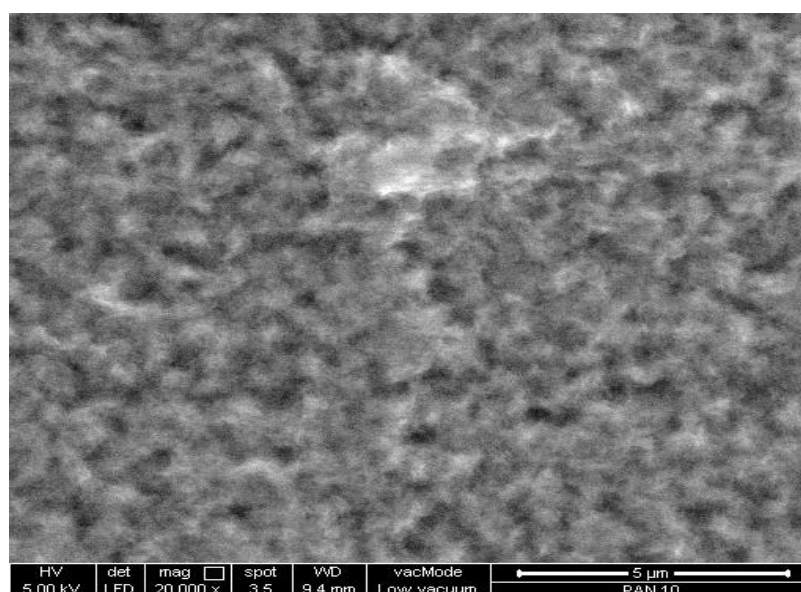


**Figure 4.42(a):** Micrograph of PAN film containing 10 wt.% of LiBF<sub>4</sub>

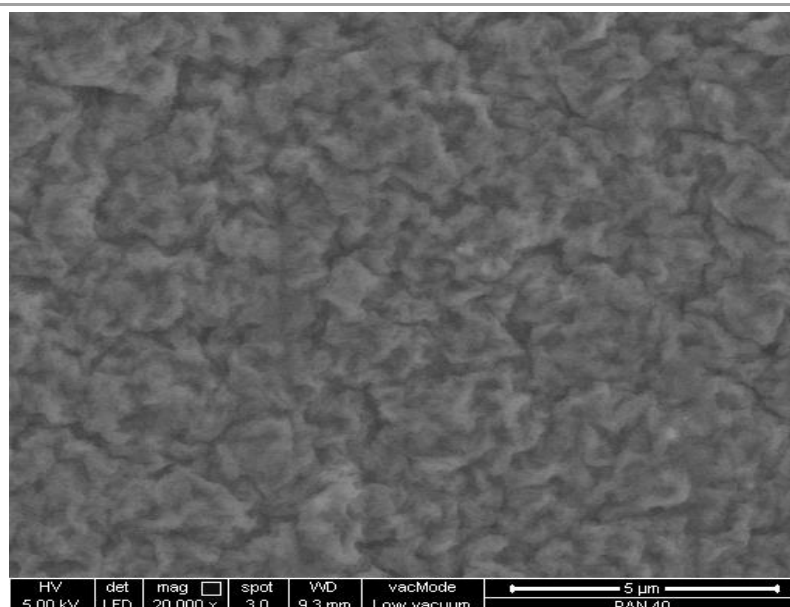


**Figure 4.42(b):** Micrograph of PAN film containing 40 wt.% of  $\text{LiBF}_4$

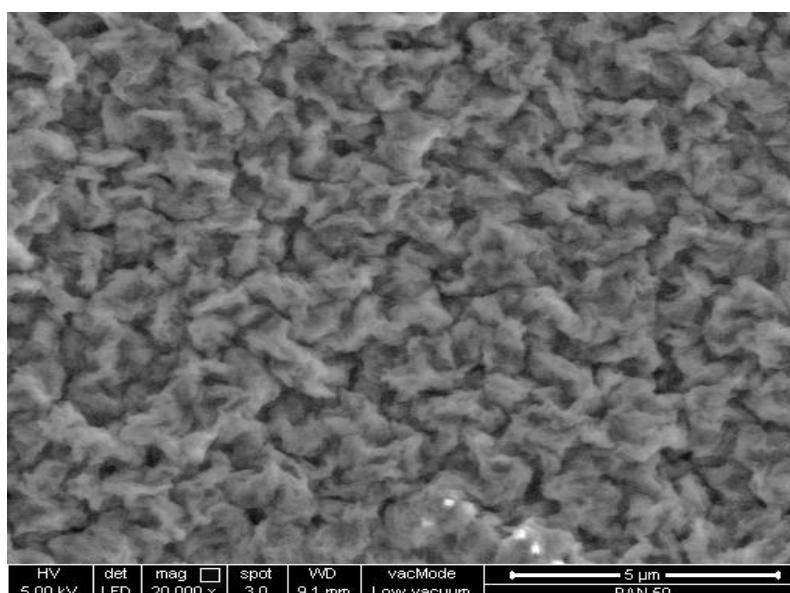


**Figure 4.42(c):** Micrograph of PAN film containing 50 wt.% of  $\text{LiBF}_4$

#### 4.4.5 PAN-EC-DMP- $\text{LiBF}_4$ system

The structural changes in PAN-EC-DMP matrix upon addition of  $\text{LiBF}_4$  with different concentrations was visualised based on the FESEM photographs as shown in Figure 4.43(a-c). The absence of salt crystal and no observable phase separation infers excellent dissolution of  $\text{LiBF}_4$  in the polymer electrolyte and excellent complexation between  $\text{LiBF}_4$  and PAN-EC-DMP. Comparing with PAN-EC-DMP films, some degree

of swelling of the polymer is observed when 10 wt.% of salt is incorporated into the polymer matrix. Besides that, the overlapping layered features are on the verge of forming with the presence of salt. With addition of more salt, the formation of layered structure is clearly observed as shown in Figure 4.43(b). Similar to PAN-LiBF<sub>4</sub> system, the formation of uniform tracks which are represented by the dark region was observed. Figure 4.43(c) depicts the micrograph for the highest conducting sample experienced the greatest structural disorder at which portraying a three-dimensional like structure other than a simple layered structure. This structure suggested that addition of plasticizers and salt into the polymer matrix has increased the total surface area for ion coordination. This strongly discloses the amorphous nature of the SPE which has been confirmed by XRD analysis. The interaction between polymer chains and ions is favoured with the increased coordination sites offered by the structure as a result of addition of plasticizers. This clearly indicates the reduction in the overall crystallinity of the sample with further doping of LiBF<sub>4</sub> that crucial in enhancing the ionic conductivity.

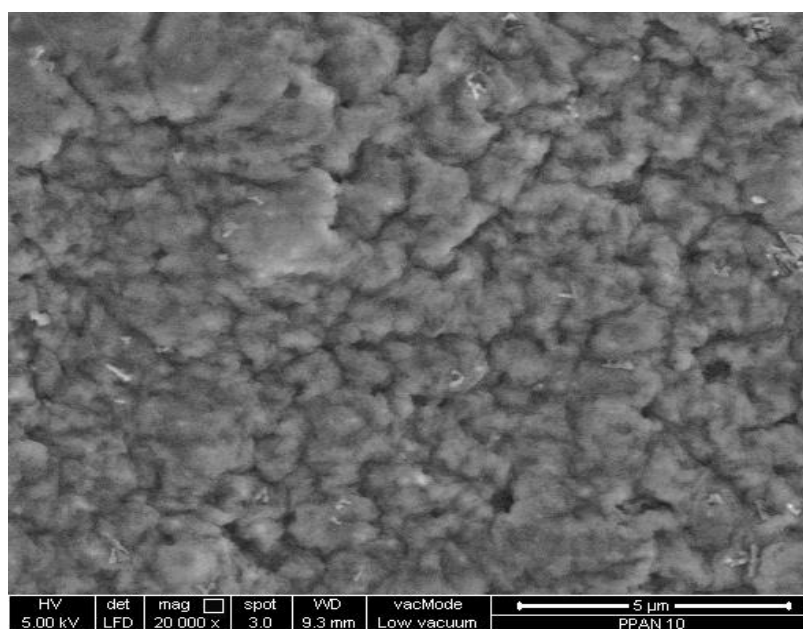


**Figure 4.43(a):** Micrograph of PAN-EC-DMP film containing 10 wt.% of LiBF<sub>4</sub>

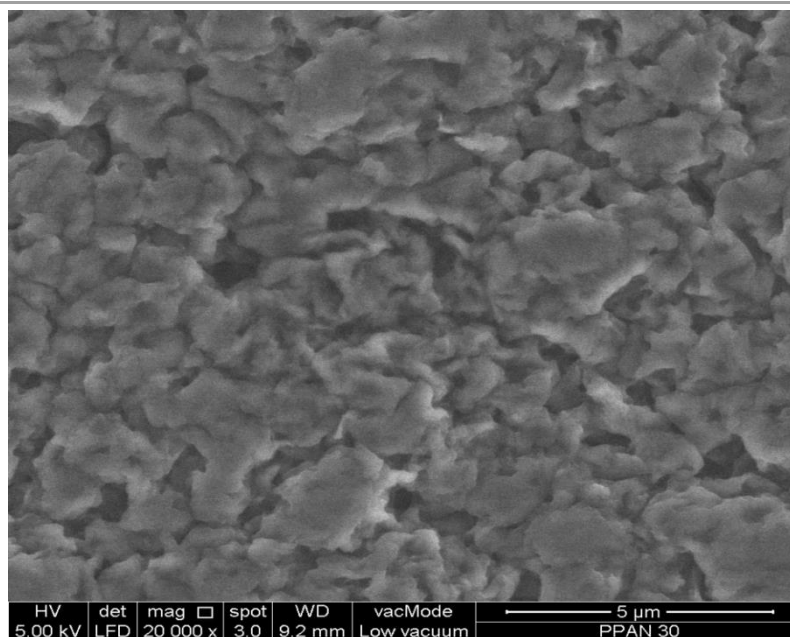


**Figure 4.43(b):** Micrograph of PAN-EC-DMP film containing 30 wt.% of LiBF<sub>4</sub>

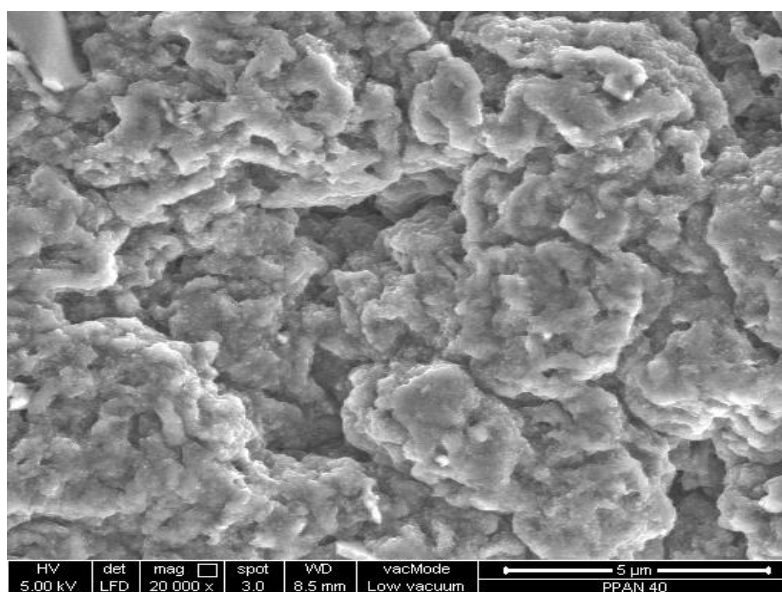


**Figure 4.43(c):** Micrograph of PAN-EC-DMP film containing 40 wt.% of LiBF<sub>4</sub>

## 4.5 Thermal Studies

### 4.5.1 Introduction

Thermal analysis accounts to the thermal properties of polymer electrolytes which includes heat-resistivity and thermal stability. The thermal properties of samples were obtained by referring to the maximum decomposition temperature ( $T_d$ ) and percentage of total weight loss (wt. %) respectively with the aid of Thermogravimetric Analysis (TGA) thermograms. The specific processes correspond to heat treatment such as glass transition, crystallization and melting can be determined by Differential Scanning Calorimetry (DSC). Thermogravimetric (TG) measurement was recorded using TA TGA Q500 at heating rate of  $10\text{ }^{\circ}\text{C min}^{-1}$ . DSC measurements were performed using DSC instrument with TA DSC Q2000 for selected samples with heating rate of  $10\text{ }^{\circ}\text{C/min}$ .

### 4.5.2 Pure PAN

Figure 4.44(a) shows the DSC thermogram of pure PAN film heated up to  $400\text{ }^{\circ}\text{C}$ . It has been reported that an exothermic reaction ranging between  $200$  and  $350\text{ }^{\circ}\text{C}$ , in an inert atmosphere, is typical behaviour of PAN (Sarvaranta, 1995). A single intense exotherm ( $8608\text{ J/g}$ ) observed centred at  $286\text{ }^{\circ}\text{C}$  is attributed to the degradation reactions involving cyclization and cross-linking of the nitrile group (Grassie & McGuchan, 1971; Bashir, 2001). According to Gupta et al. (1970), the melting point of PAN is only detectable at temperature above  $300\text{ }^{\circ}\text{C}$  when heated at a fast heating rate of  $80\text{ }^{\circ}\text{C/min}$  or higher. PAN tends to degrade that is undergoing exothermic cyclization reactions before melting. At slow heating rates, the exothermic cyclization process initiates in the amorphous phase and consequently, the heat is liberated which results the high exothermic maxima (Ko, Lin & Ting, 1989). The melting endotherm may be observable at higher heating rates. The corresponding TG

thermogram of pure PAN is presented in Figure 4.44 (b). The minor weight loss (2%) from room temperature to 150 °C is associated to the evaporation of solvent and absorbed moisture. The second stage decomposition is up to 300 °C with weight loss of ~5%, which is closely related to the exotherm reaction when comparing with DSC result. A rapid weight loss is observed when a sample is further heating at temperature higher than 300 °C. This major weight loss upon heating above 300 °C was due to decomposition of the polymer.

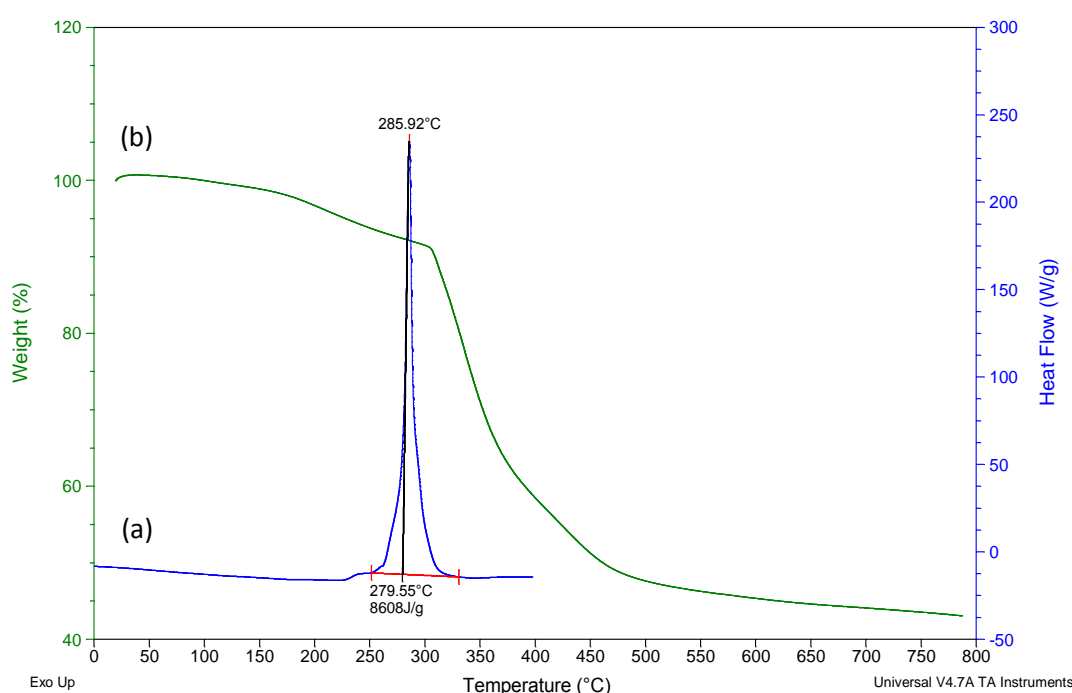


**Figure 4.44:** (a) DSC and (b) TG thermograms of pure PAN film.

### 4.5.3 PAN-EC-DMP system

The effect of plasticization on the thermal properties of PAN was studied. Figure 4.45 (a) shows the DSC thermogram for PAN-EC-DMP film. The glass transition temperature of PAN is dependent on the structural orientation of the polymer. Hence, inconsistent  $T_g$  values are reported in temperature range from 80 to 120 °C in literature reports (Rosenbaum, 1965; Minagawa, Kanoh, Tanno & Nishimoto, 2002).

The glass transition temperature of the plasticized PAN film is observed at 86 °C in this work. This value falls in the lower limit of the range. The low  $T_g$  value is due to the reduced stiffness of the PAN as a result of structural distortion of the polymer chains with the addition of plasticizers as confirmed in XRD analysis. Two exothermic peaks are observed at 278 and 309 °C with smaller amount of heat liberated in PAN-EC-DMP system. The reduced intensity of the exotherm from 8608 J/g of pure PAN film to 4647 J/g of PAN-EC-DMP film is owing to the incorporation of plasticizers. According to Grassie, small amount of impurities can greatly influence the nature of the exotherm. It has been found that with the presence of plasticizers, the initiation temperature of cyclization reaction decreased from 280 °C of pure PAN to 273 °C for plasticized-PAN as shown in Figure 4.45. On the other hand, an endothermic peak is observed at 217 °C with only 91.1 J/g of heat absorbed. This value is far below the melting point of PAN. The endotherm appeared just before the decomposition exotherm is ascribed to the mesophase isotropization of the material (Bashir, 2001). Some of them are liquid crystalline and may give rise to relatively sharp peaks in DSC traces upon mesophase transitions. Thus, the endothermic transition at 217 °C should not be considered as the conventional crystal-melting endotherm of a semi crystalline polymer. The corresponding TG curve is shown in Figure 4.45 (b). A small mass loss (1 %) was observed up to 80 °C is attributed to the removal of the absorbed water content and solvent evaporation. The evaporation of plasticizers is responsible for the abrupt weight loss of 36 % detected from 80 to 120 °C. It was reported that phthalates are not chemically bound in the polymers (Schettler 2006). Thus, the evaporation of the material is likely to occur upon heating. Besides, it should be noted that 60 % of this sample made up of plasticizers. Thus, the major weight loss is reasonable. The endotherm is responsible for the steady weight loss of about 5 % in the temperature range between 120 and 270 °C. The rapid weight loss up to 350 °C is closely related to

the exotherm. The last step of the decomposition above 400 °C is ascribed to decomposition of the sample.

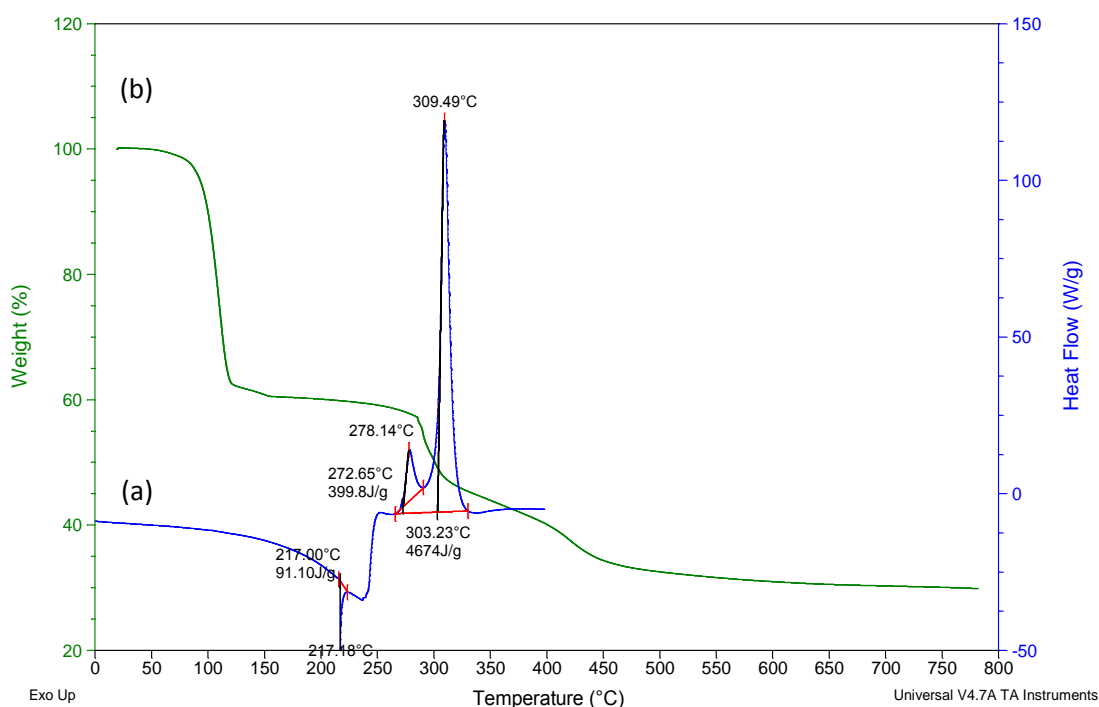


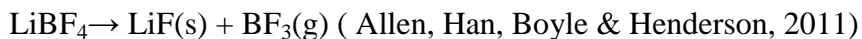
**Figure 4.45:** (a) DSC and (b) TG thermograms of PAN-EC-DMP film.

#### 4.5.4 PAN-LiBF<sub>4</sub> System

Figure 4.46 shows the DSC thermograms of films in PAN-LiBF<sub>4</sub> system. The glass transition temperature of the sample obtained from the thermograms shows a gradual decrease with increasing salt concentration. The endothermic peak which is absent in pure PAN remains undetectable in the samples containing 10 and 20 wt. % of LiBF<sub>4</sub>. However, an endothermic peak appeared around 231 °C are detected for sample containing 30-50 wt.% of LiBF<sub>4</sub>. The glass transition temperature and endothermic peak temperature of heat treated PAN films in PAN-LiBF<sub>4</sub> system are listed in Table 4.13. It can be observed that addition of LiBF<sub>4</sub> salt has decreased the glass transition temperature of the films. It was believed that presence of LiBF<sub>4</sub> contributes a plasticizing effect which in turns helps in lowering the  $T_g$  of the host polymer as



reported by Silva, Barros, Smith and MacCallum (2004). This result agrees with the variation of conductivity with salt concentration as shown in Figure 4.46. The endothermic DSC event can be correlated to the weight loss of the sample. Figure 4.47 shows the TG thermograms of films in PAN-LiBF<sub>4</sub> system. The decomposition of the films is divided into three regions. Region I represents the weight loss from room temperature to 150 °C. The weight loss in this region is attributed to the removal of surface adsorbed moisture and solvent evaporation. Other than that, the weight loss in Region I increase linearly with the salt concentration. This behaviour may ascribe to the hygroscopic nature of LiBF<sub>4</sub>. Besides the sample containing 50 wt.% of LiBF<sub>4</sub>, further heating of the samples from 150 to 300 °C does not cause a major weight loss (2-4 %) for sample containing 10 wt.% to 40 wt.% of LiBF<sub>4</sub> as shown in Region II. The apparent weight loss of ~13 % for the highest salted film may assign to decomposition of LiBF<sub>4</sub>. The thermal decomposition mechanism of LiBF<sub>4</sub> is known as



The occurrence of endothermic peak in DSC thermograms is expected to be associated with LiBF<sub>4</sub> at the higher temperature. Due to decomposition reactions resulting in the Lewis acids BF<sub>3</sub>, which is unstable and easily decompose at lower temperature than the decomposition temperature of LiBF<sub>4</sub> itself (Hong, Okada, Sonoda, Gopukumar & Yamaki, 2004). The loss of BF<sub>3</sub> correlates with the reduction in mass as shown in Region II. The weight loss in Region III is due to the exothermic degradation of the polymer as exhibited in pure PAN accompanied by the decomposition of LiBF<sub>4</sub>.

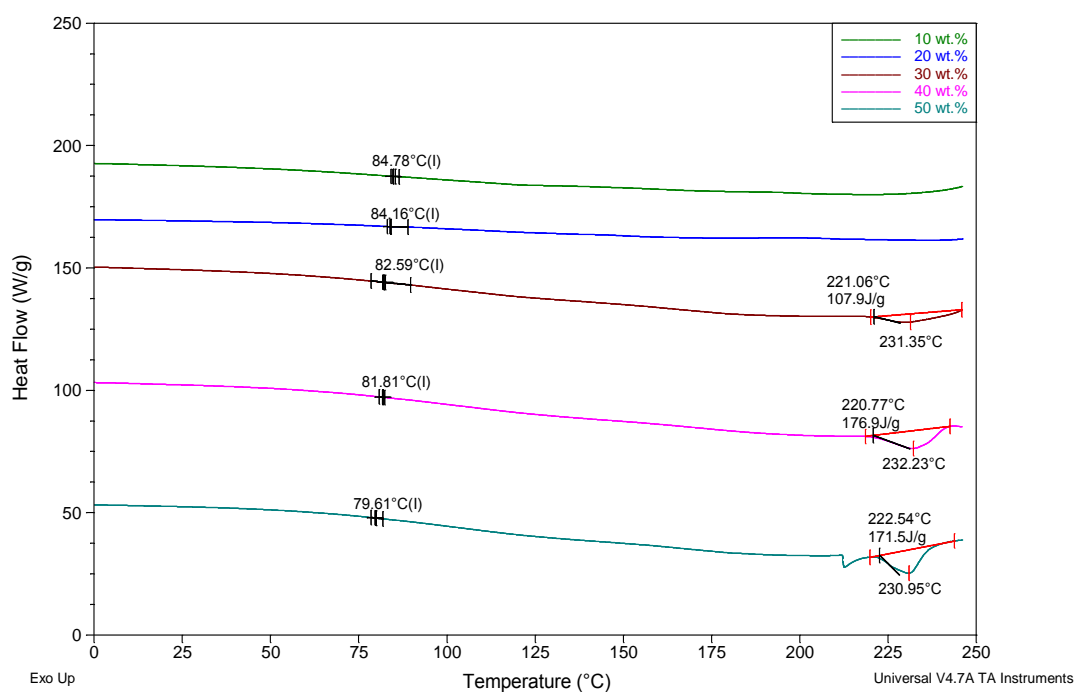


**Figure 4.46:** DSC curves for films in PAN-LiBF<sub>4</sub> system.

**Table 4.14:** Glass transition temperature and endotherm peak temperature of heat treated PAN films in PAN-LiBF<sub>4</sub> system.

Salt content (wt.%)	Glass transition temperature, $T_g$ (°C)	Endotherm peak temperature, $T_p$ (°C)
10	85	-
20	84	-
30	83	231
40	82	232
50	80	231

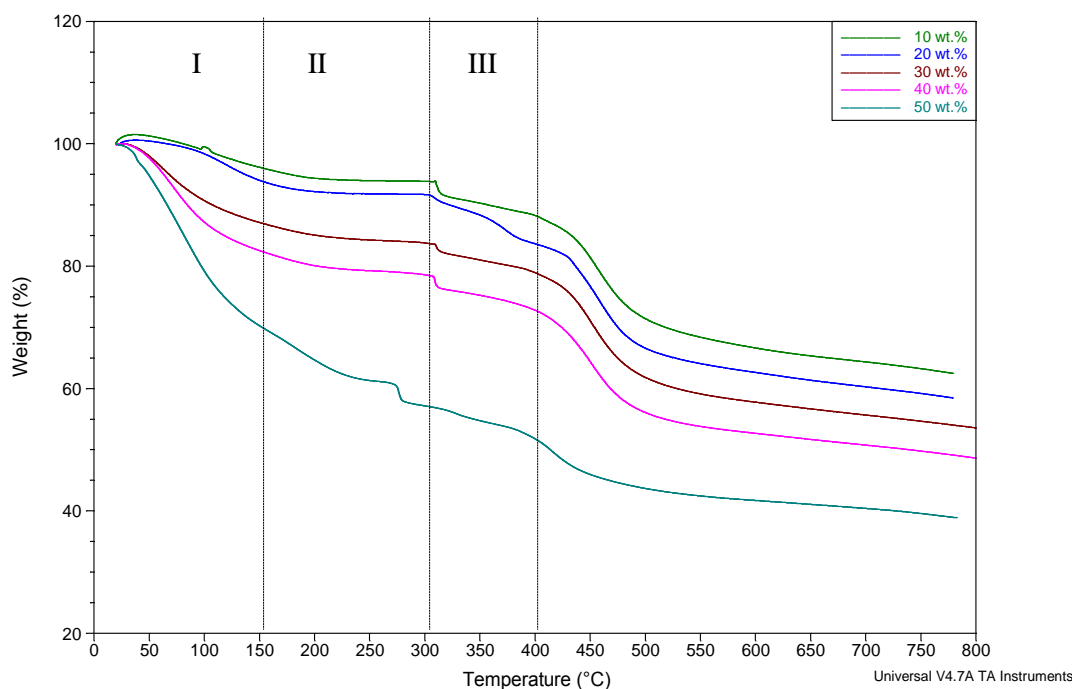


**Figure 4.47:** TGA thermograms for films in PAN-LiBF<sub>4</sub> system.

#### 4.5.5 PAN-EC-PC-LiBF<sub>4</sub> System

Figure 4.48 depicts the DSC thermograms for films containing varied amounts of salt in PAN-EC-PC-LiBF<sub>4</sub> system. The glass transition temperature of the films can be detected in the temperature region around 70 to 80 °C. These  $T_g$  values are found to be lower than the PAN-EC-DMP film, again revealed the plasticizing effect of LiBF<sub>4</sub>. In addition, the  $T_g$  observed in this system is lower than the PAN-LiBF<sub>4</sub> shows that plasticizers play the role in reducing the crystallinity of the polymer. Similar to PAN-EC-DMP film, an endotherm appeared between 215 to 220 °C. The addition of salt does not make a significant effect on the mesophase transition temperature. Figure 4.49 shows the TG thermograms of the samples in this system. The decomposition is divided into four regions. Comparing to the TG curve of PAN-EC-DMP film, the weight loss due to the evaporation of surface adsorbed moisture is more vigorous as shown in Region I. Similar to the PAN-LiBF<sub>4</sub> system; this result is associated with the hygroscopic nature of the LiBF<sub>4</sub>. The evaporation of the plasticizers accounts for the

weight loss in Region II as discussed in Section 4.5.3. The samples in this system exhibited a better thermal stability in Region II which displaying better weight retention than the unsalted PAN-EC-DMP film. The weight loss is about 18 % for the lowest salt content films to 10 % for the highest salt content film. This loss is much lower than the rapid weight loss of 36 % for PAN-EC-DMP film. The reduction in the mass loss may attribute to the interaction between the plasticizers and  $\text{LiBF}_4$  as validated in the FTIR study. The coordination between  $\text{LiBF}_4$  and plasticizers molecules is believed to be responsible to the reduced mass loss in Region II. Unlike the unsalted plasticized film, the endotherm corresponds to the mesophase transition of the polymer is not the only cause for the steep weight loss in Region III. As what can be seen in the DSC thermograms, the enthalpy correspond to the endotherms are much higher than that observed in PAN-EC-DMP films. Thus, the major weight loss in Region III is associated to the endotherm of two combined events which are the mesophase transition of the polymer and the decomposition of  $\text{LiBF}_4$  as discusses in Section 4.5.4. The typical exothermic degradation of polymer and decomposition of the  $\text{LiBF}_4$  are possibly the reasons for the fourth step decomposition as shown in Region IV.

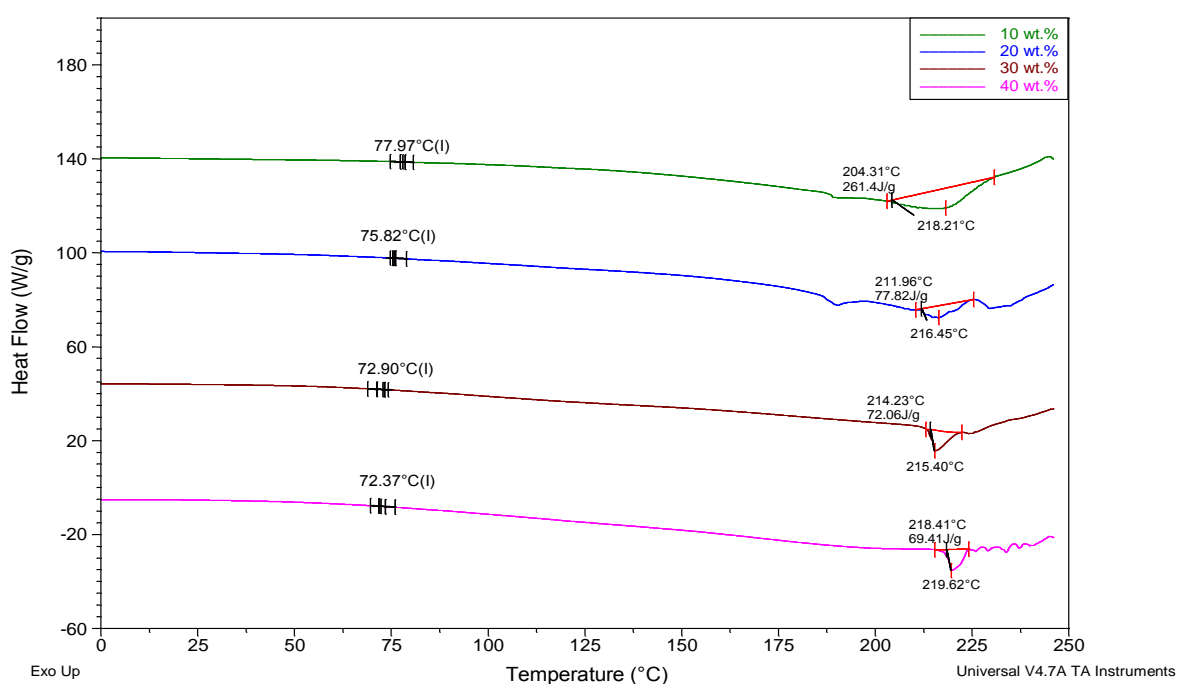


**Figure 4.48:** DSC thermograms for films in PAN-EC-DMP- $\text{LiBF}_4$  system.

**Table 4.15:** Glass transition temperature and endotherm peak temperature of heat treated PAN films in PAN-EC-DMP-LiBF<sub>4</sub> system.

Salt content (wt.%)	Glass transition temperature, $T_g$ (°C)	Endotherm peak temperature, $T_p$ (°C)
10	78	218
20	76	216
30	73	215
40	72	220

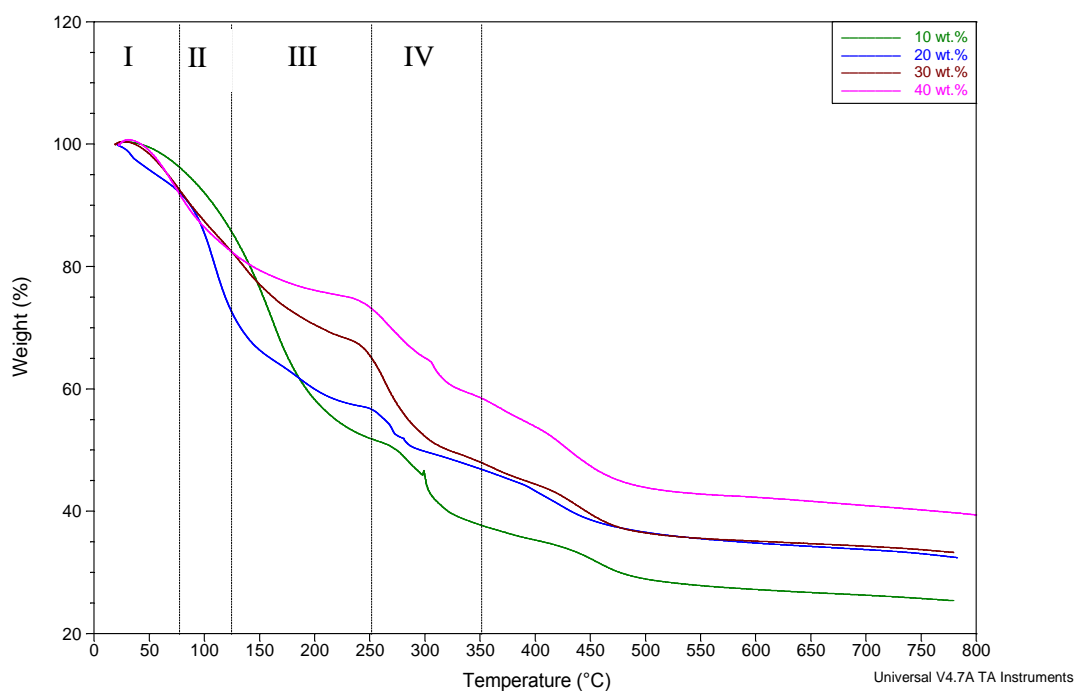


**Figure 4.49:** TGA thermograms for films in PAN-EC-DMP-LiBF<sub>4</sub> system.

## 4.6 Electrochemical Studies

### 4.6.1 Introduction

The successful use of an electrolyte in lithium metal battery requires good electrochemical stability and an excellent compatibility with the lithium metal used as the anode material. Both linear sweep voltammetry (LSV) and cyclic voltammetry (CV) measurements were taken at ambient temperature using electrochemical cells assemblies by sandwich electrolyte membrane between two planar electrodes. LSV and CV were carried out to estimate the electrochemical stability window of the polymer electrolyte and to investigate the electrochemical behaviour at the interface between electrode and electrolyte. In this work, the films of both systems were characterized through LSV techniques by using WPG100e potentiostat/galvanostat system. CV was performed on the most electrochemically stable films obtained from the LSV analysis using the same operating system.

### 4.6.2 Linear Sweep Voltammetry (LSV)

#### 4.6.2.1 PAN-LiBF<sub>4</sub> System

The stability of the electrolyte toward oxidation process is related to the interface with the electrode and is another important issue for the selection of a polymer electrolyte for battery applications. The linear sweep voltammetry was performed on a SS | SPE | Li cell where stainless steel as working electrode, with counter and reference electrode of lithium metal. The reduction or oxidation of a substance at the surface of a working electrode, at the appropriate applied potential, results in the mass transport of new material to the electrode surface and the generation of a current. The voltage was swept from 0 V towards more anodic values until a large current due to electrolyte decomposition at the electrode interface occurred. Figure 4.50 (a-d) shows the current-voltage response for selected sample containing varied amounts of LiBF<sub>4</sub> salt. The

current onsets are detected between 3.6 - 4.4 V which can be assigned to the decomposition voltages of the polymer electrolytes. It is found that the decomposition limit of the films falls within the range as reported (Subramania, Sundaram & Kumar, 2006) As shown in the voltammograms, a small hump before the high current onset is detected which may attributed to the surface reactions or due to the oxidation of some trace species such as water and oxygen. However, the magnitude of the current correspond to the humps decreases with salt concentration and shows a minimum for sample containing 40 wt.% of salt. The sample containing 40 wt.% of the  $\text{LiBF}_4$  was found to be most electrochemically stable electrolyte film with anodic stability limit of  $\sim 4.4\text{V}$ . A further analysis will be discussed in the following section.

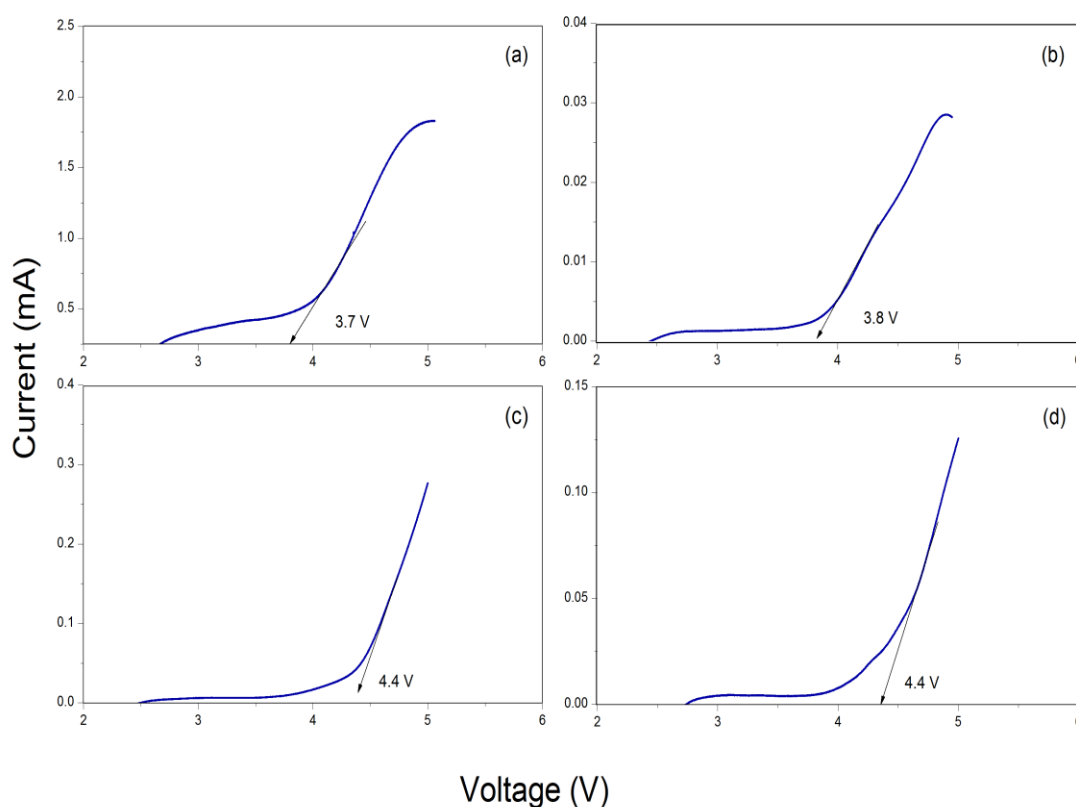


**Figure 4.50 :** Linear sweep voltammograms of the cell prepared with the PAN films containing (a) 20 wt.% (b) 30 wt.% (c) 40 wt.% (d) 50 wt.% in PAN- $\text{LiBF}_4$  system.

#### 4.6.2.2 PAN-EC-DMP-LiBF<sub>4</sub> System

The electrochemical stability of the films in PAN-EC-DMP-LiBF<sub>4</sub> system is evaluated by the same method as mentioned in Section 4.6.2.1. The current-voltage response curve of polymer electrolyte containing different concentrations of LiBF<sub>4</sub> is shown in Figure 4.51 (a)-(d). The small hump before the current onset is obviously reduced with the presence of plasticizers. The decomposition limit of the films in this system falls between 3.8 and 4.4 V and exhibits higher value than the unplasticized system. This behaviour suggested the ions in the electrolyte are stabilized by the solvation of plasticizers. The sample containing 30 wt.% of the LiBF<sub>4</sub> was found to be most electrochemically stable electrolyte film with anodic stability limit of ~4.4 V. A more comprehensive analysis will be discussed using cyclic voltammetry.

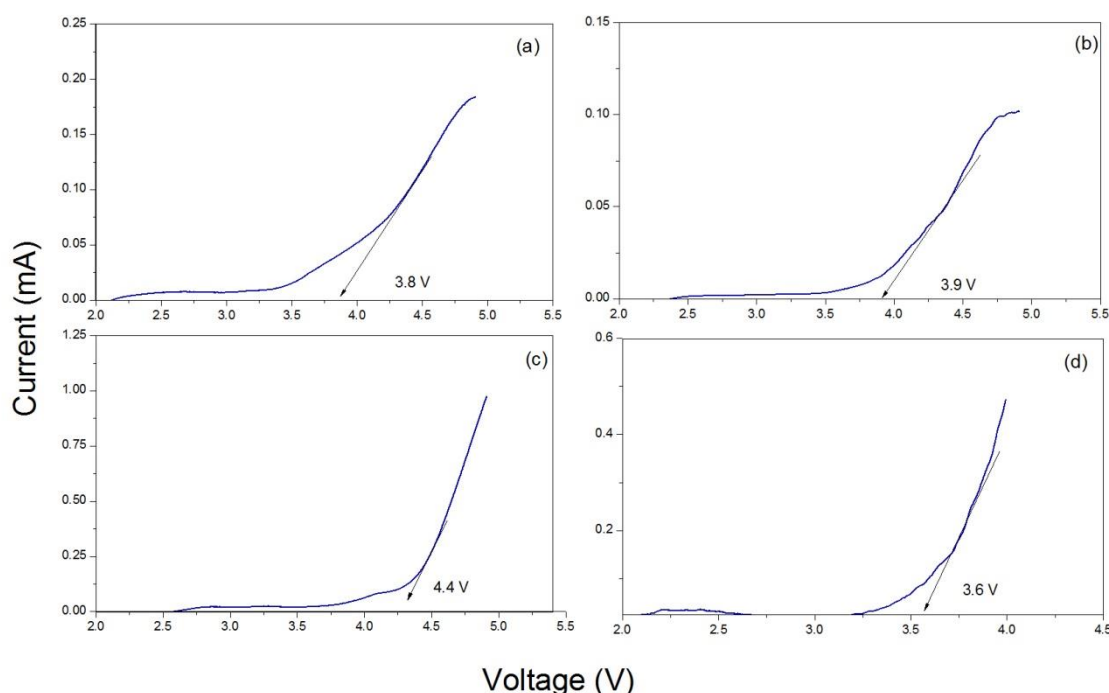


**Figure 4.51 :** Linear sweep voltammograms of the cell prepared with the PAN films containing (a) 10 wt.% (b) 20 wt.% (c) 30 wt.% (d) 40 wt.% of LiBF<sub>4</sub> in PAN-EC-DMP-LiBF<sub>4</sub> system.



### 4.6.3 Cyclic Voltammetry (CV)

#### 4.6.3.1 PAN-LiBF<sub>4</sub> System

CV is a powerful tool to investigate the electrochemical behaviour at the interface between electrode and electrolyte by using a three electrode system to compensate the bulk resistance of electrolytes and exclude the effects of counter electrode polarization. It has been performed on symmetrical cells SS| SPE| SS (Cell-I) and Li| SPE| Li (Cell-II) for the most electrochemically stable film in PAN-LiBF<sub>4</sub> system at room temperature. Figure 4.52 shows a cyclic sweeping between -5 and 5 V of Cell I. The stability of the electrolyte at the interface with the SS electrode is limited by a potential of about 3.0 V in the anodic side and -3.0 V in the cathodic side. The potentials are first scanned in the positive direction and then reversed. The anodic and cathodic peaks of the cells are not observed with small flow of current. This inferred that the electrodeposition of lithium is not facilitated on the SS electrode suggesting the non-intercalation of lithium in the polymer electrolyte with the SS electrode. Figure 4.53 shows the first, fifth and tenth scan of CV for Cell II. There are four main features can be observed from the curve

- i) The anodic current reaching a maximum and maintaining a plateau in the first positive sweep, but showing broader peaks in subsequent sweeps
- ii) The magnitude of the peak current tends to decay with the increase in cycle number
- iii) The current in the reverse sweep being significantly smaller than forward sweep
- iv) All curves cross two zero-current points corresponding to positive and negative sweeps, respectively;

Phenomenon (i) and (ii) may be attributed to the formation of a passive layer on the electrode which hindering the charge transfer. A charge concentration gradient is

developed at the electrode interface during Li stripping in the forward sweep. Thus a reverse sweep is more favourable in order to achieve equilibrium causing the current in the reverse sweep to be smaller than forward sweep. As can be seen in Figure 4.53, there are no more oxidation peaks up to 5.0 V (versus Li/Li<sup>+</sup>). Thus, it can be concluded that PAN-based has sufficient electrochemical stability to allow safe operation in lithium battery system. However, a continuous degradation of the anodic and cathodic current was observed even up to 10 cycles. The result suggests that Cell II may suffer poor cyclability.

#### 4.6.3.2 PAN-EC-DMP-LiBF<sub>4</sub> System

The charge transfer kinetics of the polymer electrolyte in this system was performed on symmetrical cells SS| SPE| SS (Cell-III) and Li| SPE| Li (Cell-IV) for the highest conducting film in PAN-EC-DMP-LiBF<sub>4</sub> system at room temperature. Figure 4.54 shows a cyclic sweeping between -5 and 5 V of Cell III. Similarly to PAN-LiBF<sub>4</sub> system, no distinct peaks observed indicating the ion blocking nature of the SS electrodes. Figure 4.55 presents the CV curves for first, fifth and tenth cycle of Cell IV. There are three main features can be observed from the curve

- (i) The anodic current reaching a maximum and maintaining a plateau in the first positive sweep, but showing broader peaks in further sweeps.
- (ii) The peak current tends to decrease with the increase in cycle number and remains constant after few cycles.
- (iii) The subsequent sweeps nearly overlapping with symmetric anodic and cathodic sweeps.

Comparing to the unplasticized system, the broad nature of the redox peaks and the greater suppression of the magnitude of peak currents can be clearly observed even at

fifth sweep in this system can be explained as the solvation effect of plasticizers. It was reported the addition of organic solvent to PAN based polymer electrolyte appears to influence the oxidation potential (Kuo et al., 2002). The accumulation of free plasticizers aggregates at the interface facilitates ions migration and causes the anodic current to increase faster in the following sweeps than that in the first anodic sweep and gives the CV feature (i) (Cheng & Wen, 1998). The redox peaks corresponding to anodic oxidation at 1.0 V and cathodic reduction at  $-1.0$  V occur versus  $\text{Li}^+/\text{Li}$ . The peak currents tend to decrease markedly during the initial cycles may due to formation of passivation layer on electrode and stabilize afterwards. On cycling, there is no substantial change in the redox peak voltages and the overlapping of the subsequent sweeps indicates that the charge transfer reaction at the interface between the film and lithium metal is reversible and the polymer electrolyte is able to support fully reversible redox process. Thus, it can be concluded that the film containing 30 wt.% of  $\text{LiBF}_4$  in this system has sufficient electrochemical stability and provide better cycle stability for the operation in lithium battery system.

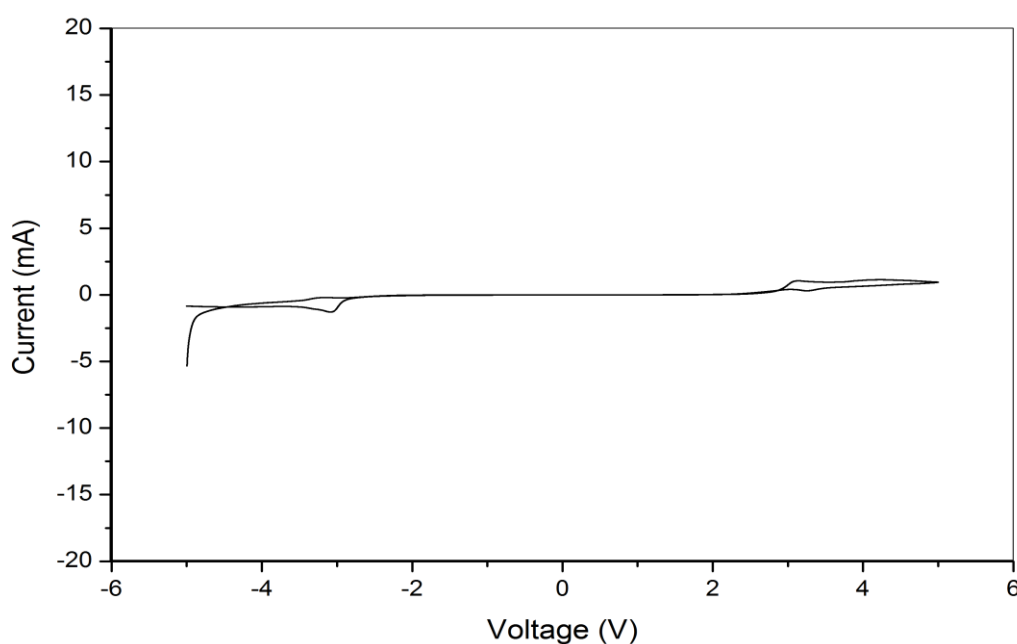


**Figure 4.52:** Cyclic voltammogram of cell-I: SS|SPE|SS with 40 wt.% of  $\text{LiBF}_4$  salt at scan rate of  $5 \text{ mV s}^{-1}$ .

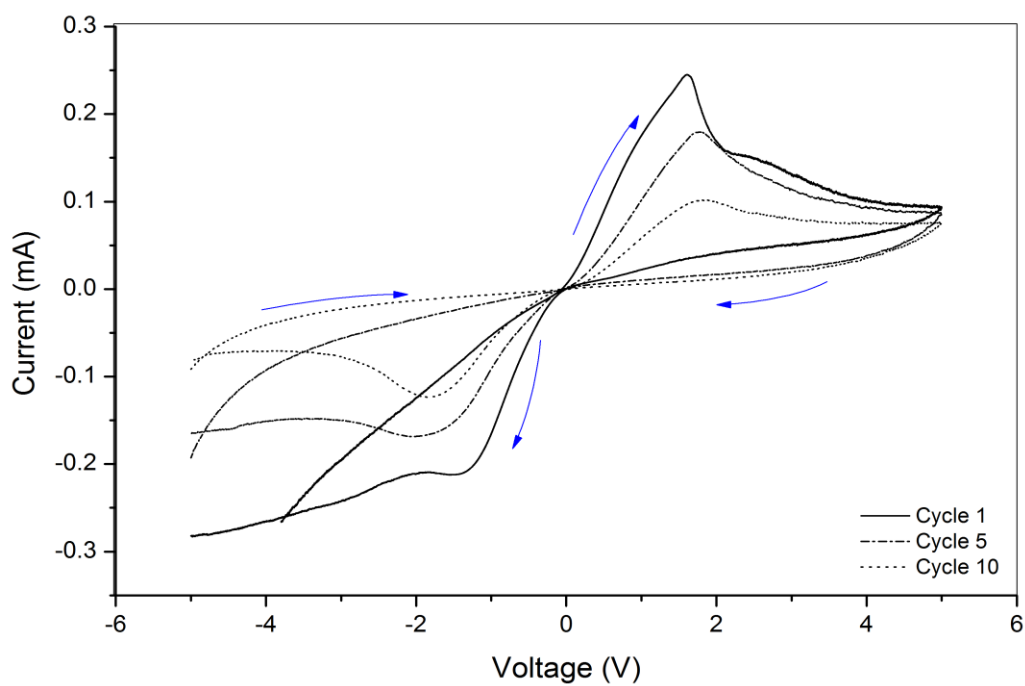


**Figure 4.53:** Cyclic voltammogram of cell-II: Li|SPE|Li with 40 wt.% of LiBF<sub>4</sub> salt at scan rate of 5 mV s<sup>-1</sup>.

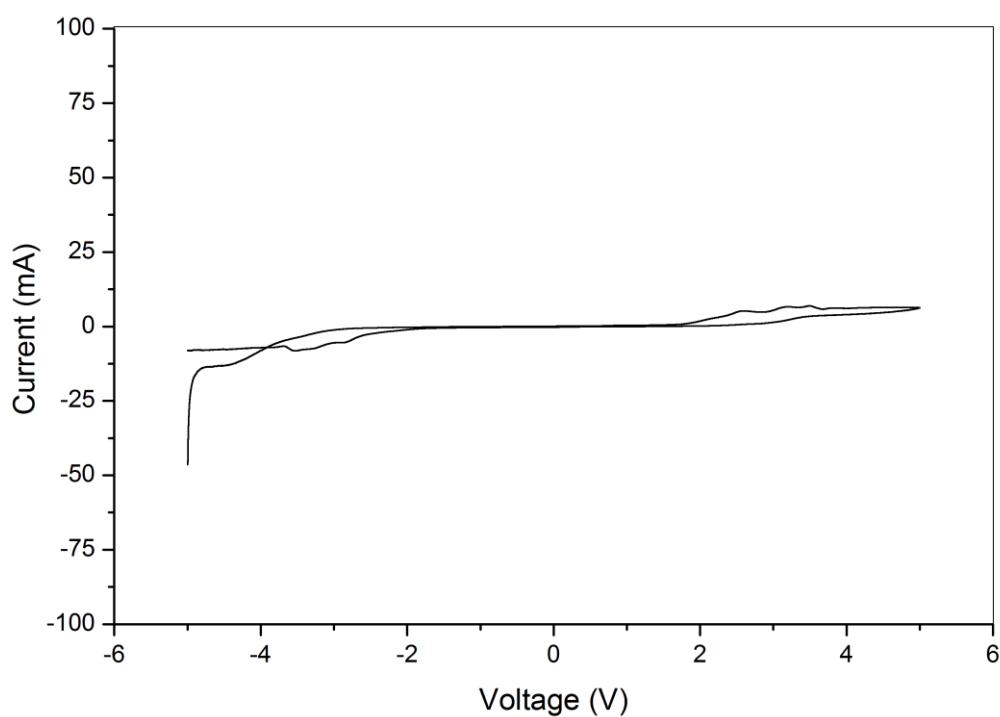


**Figure 4.54:** Cyclic voltammogram of cell-III: SS|SPE|SS with 30 wt.% of LiBF<sub>4</sub> salt at scan rate of 5 mV s<sup>-1</sup>.

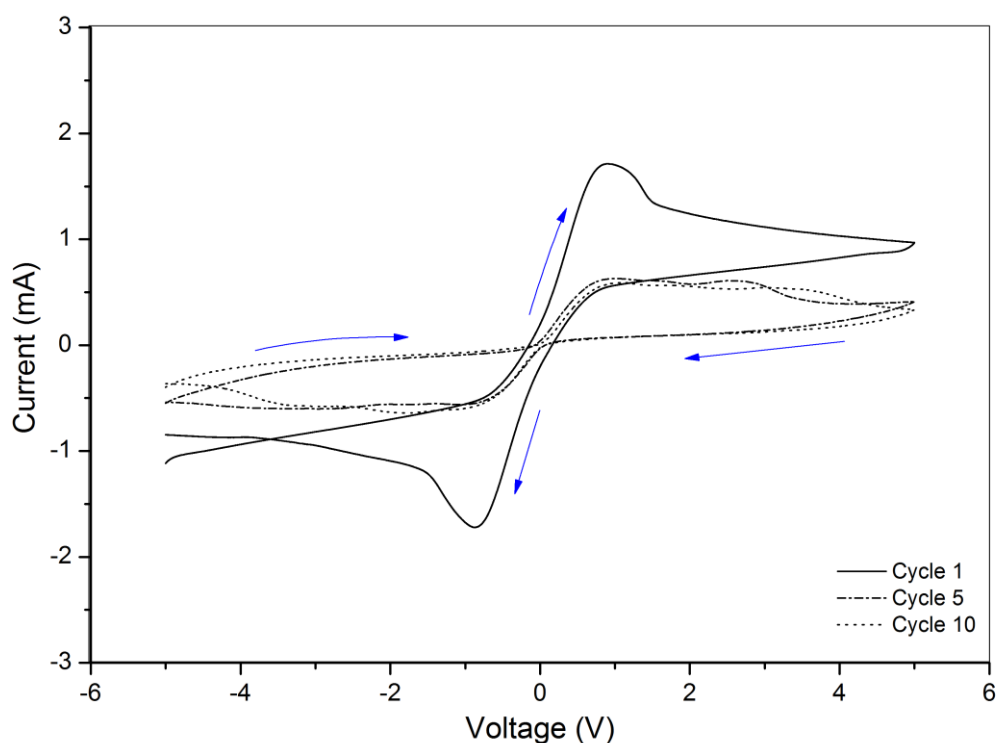


**Figure 4.55:** Cyclic voltammogram of cell-IV: Li| SPE |Li with 30 wt.% of LiBF<sub>4</sub> salt at scan rate of 5 mV s<sup>-1</sup>.

#### 4.7 Cell Performance

The study of cell performance characteristics of the cell fabricated using the prepared polymer electrolyte is done to examine the applicability of the material in battery applications. In this work, the cell was fabricated using a LiCoO<sub>2</sub> cathode, lithium foil anode and the plasticized-PAN film containing 30 wt.% of LiBF<sub>4</sub> salt. The size of the electrodes and electrolyte film was fixed at 4 cm<sup>2</sup>. The chosen SPE film has the most electrochemical stability with high conductivity in this work. As fabricated, the cell with the optimized SPE exhibited an open circuit voltage of 3.8 V. The cell was then charge to 4.3 V with current of 0.05 mA, followed by discharging with at 0.03 mA to 2.5 V. The charge-discharge process was repeated up to 20 cycles at room temperature. Figure 4.56 represents the variation of voltage with the discharge capacity for selected cycles. The highest capacity of 0.6 mAh achieved at the first cycle. This

value is comparable to the discharge capacity of cell consists of poly(acrylonitrile-methylmethacrylate)-based microporous gel electrolyte reported by Zhang, Ervin, Xu and Jow (2005). However, the discharge capacity abruptly decreased after second cycle and approaching constant started from the fifth cycle. This result is consistent with the cyclic voltammogram displayed in Section 4.6.3.2. The initial irreversibility is due to the increase in interfacial impedance resulting from the precipitation of reduce species on the electrode surface or oxidation of the positive electrode, which is known to result in the formation of a necessary solid-electrolyte interface (SEI) (Kanevskii & Dubasova, 2005).

Figure 4.57 shows the discharge capacities of Li | SPE | LiCoO<sub>2</sub> cell for twenty cycles. The reversibility of the cell was fairly high after four cycling although the discharge and recharge capacities of the cell were gradually decreased with the repetition of the cycle. The reason for the capacity decreasing is considered to be some degradation of the interface structure between the oxide electrode and polymeric electrolyte. The SEI thickens upon cycling has consumed large amount of Li<sup>+</sup>. The cationic transference number of this sample determined in Section 4.1.4.2 has the value of 0.16. During discharging, the concentration at the surface drops faster than the bulk concentration as a consequence of the slow time constant for transport. As discharge proceeds, the surface concentration ultimately decreases to zero, resulting in the precipitous drop in the cell voltage. The impact of concentration gradient is unavoidable with such low cationic transport number of the polymer electrolyte which accounts for the declined capacity.

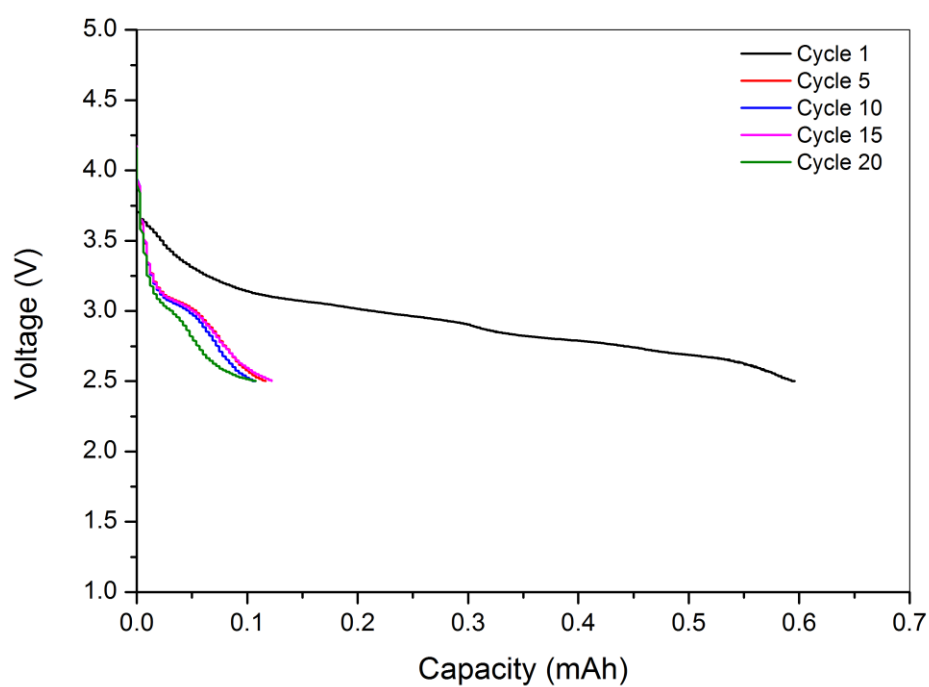


**Figure 4.56 :** Variation of voltage of a Li / SPE / LiCoO<sub>2</sub> cell during discharge with a current of 30  $\mu$ A.

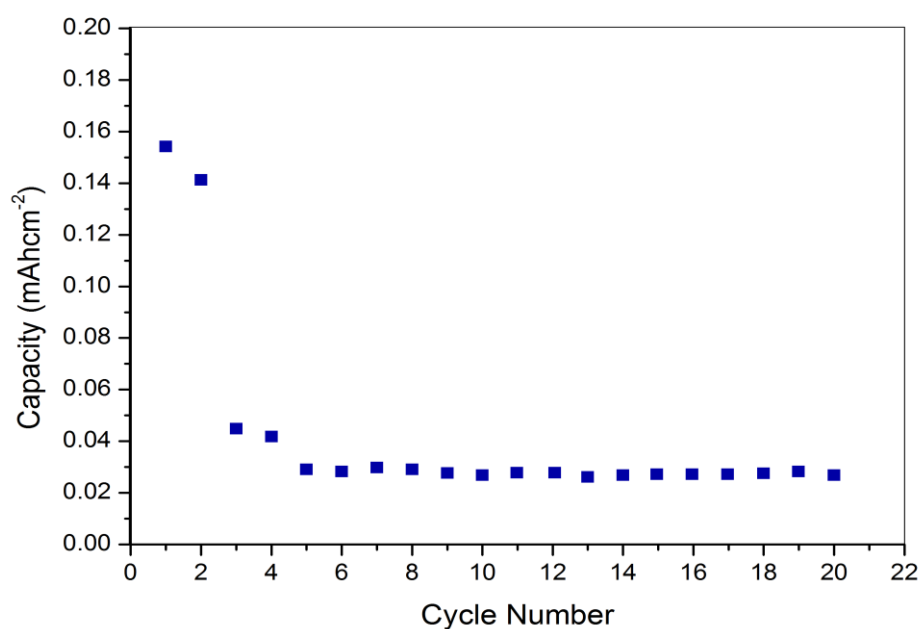


**Figure 4.57:** Discharge capacities of Li / SPE / LiCoO<sub>2</sub> cell as a function of cycle number.

**CHAPTER 5**

**CONCLUSION & SUGGESTIONS FOR  
FUTURE WORK**



---

**CONCLUSIONS AND SUGGESTIONS FOR FURTHER WORK**

Three different systems of PAN-based solid polymer electrolytes films were prepared by solution casting technique. The effect of incorporation of LiBF<sub>4</sub>, EC and DMP in the PAN matrix on the structural, electrical, thermal, morphological and electrochemical properties of the films produced was investigated.

The occurrence of some degree of co-ordination between the chemical constituents was revealed by the FTIR spectra, the resultant structural disorderliness was evident by the XRD and surface morphology analysis by FESEM. The salt-plasticizer interaction has a profound effect on the conductivity of the samples. From the present investigation, it can be concluded that the factors lead to the increase in conductivity are:

(i) Reduced crystallinity of polymers

The enhancement in conductivity is primarily due to the capability of the additives in increasing the amorphous elastomeric phase that crucial in enhancing the ionic transport mechanism. For the PAN-LiBF<sub>4</sub> system, the reduction in crystallinity is clearly revealed by XRD. The suppression of T<sub>g</sub> can be greatly related to the reduction in crystalline phase of the polymer. Based on the observation of DSC, incorporation of LiBF<sub>4</sub> has slightly suppressed the glass transition temperature T<sub>g</sub> of the polymer. Similar result was observed in the PAN-EC-DMP-LiBF<sub>4</sub> system. Plasticizers, EC and DMP have played its role in softening the polymer backbone and accelerating the ion conductions which is responsible to the overall higher conductivity than the unplasticized system. The incorporation of plasticizers helps lowering the T<sub>g</sub> of PAN to 86 °C as shown in DSC curve. The plasticized samples exhibited the most amorphous phase as observed from XRD. The reduced crystallinity of the polymer electrolytes films is consistent with its morphological properties studied from micrographs obtained from FESEM. The addition of salt

and plasticizers causes structural disorder in the polymer chains can be greatly related to the improved conductivity values.

(ii) Increased in mobile ions concentrations

The conductivity of the polymer electrolyte films is facilitated by the diffusion of ions. In this work, the ionic conductivity shows a linear relationship with the salt concentrations. In other words, as the amount of salt increases, the number of ions increases at the same time. The high dielectric constant plasticizers have increased the degree of dissociation of the salt and thereby increase the number of ions in the system resulting higher conductivity. The variation of ions concentrations can be implied from the dielectric studies. From the dielectric studies, the highest conducting sample shows the highest value of dielectric constant,  $\epsilon_r$  and dielectric loss,  $\epsilon_i$ . As frequency decreases, the value of the dielectric constant,  $\epsilon_r$  and dielectric loss,  $\epsilon_i$  decreases. This inferred that the increase in ionic conductivity is due to an increasing of ions diffusion through their free volume. The increased in mobile ions can be observed from FTIR studies by band fitting to resolve the peaks corresponding to free ions and ion pairs. The variation of number of mobile ions with salt concentration was confirmed by this study.

(iii) Temperature

The raise in temperature is believed aiding in dissociation of salt, where ions acquired more energy and the relaxation time of the ions is shortened. The conductivity- temperature plots for both systems obey Arrhenius theory in which the conductivity enhancement is thermal assisted. This study also indicates that the charge carriers were transport via ion hopping mechanism.

Summarizing the factors discussed above, plasticization was proven as an effective way in improving conductivity of polymer.

The activation energy of the highest conducting sample in PAN-LiBF<sub>4</sub> system has reduced from 0.29 eV to 0.22 eV for the highest conducting sample in the PAN-EC-DMP-LiBF<sub>4</sub> system. The low value of  $E_a$  suggests the complete amorphous nature of the electrolytes films which facilitates the fast ionic motion in the polymer network. The ionic transport number ( $t_{ion}$ ) has been evaluated using the D.C. polarization method and the results confirmed that the total conductivity of the polymer electrolytes is predominantly due to ions. The cationic transport number has been evaluated using a combination of A.C. impedance and D.C. polarization techniques and the value is found to be 0.17 for the highest conducting sample.

The thermal stability of PAN-based polymer electrolytes was found to diminish as increase in either LiBF<sub>4</sub> or EC and DMP concentration. However, the films in both systems are stable up to 200 °C which is sufficiently stable for practical use.

The electrolyte films for both PAN-LiBF<sub>4</sub> and PAN-EC-DMP-LiBF<sub>4</sub> system are electrochemically stable up to 4.4 V and 4.5 V, respectively. This value of working voltage range appears to be high enough to be used as an electrolyte in lithium battery system. Based on the cyclic voltammograms for the film containing 30 wt.% in PAN-EC-DMP-LiBF<sub>4</sub> system, the cycling is reproducible up to 10 cycles. This result infers that plasticization helps to enhance the cycle stability of the polymer electrolyte.

A cell of Li|SPE|LiCoO<sub>2</sub> has been assembled and its performance has been characterized. The cell could acquire a voltage of 4.3 V and the discharge voltage of 2.5 V. The cell can be considered as a “working” cell as it can store energy. The reversibility of the cell was fairly high after 4 cycles. The capacity loss is mainly due to the electrochemical irreversibility of Li metal and the growth of the layer at the interface between electrode and the SPE film.

As the suggestions for future work, the conductivity of the SPE films can be enhanced by blending the PAN with other polymer such as PVdF and PEO. Blending

---

polymer has been reported to be a useful method in order to develop new materials with improved mechanical stability. Another suggestion to improve the mechanical stability of the SPE films is by dispersing nano-sized ceramic fillers such as  $\text{SiO}_2$  or  $\text{TiO}_2$ . Furthermore, we can also study the performance of the lithium polymer battery by using the different type of cathode materials such as  $\text{LiFePO}_4$  and metal oxides. Both of these materials are expected to give high discharge capacity with high stability of the battery.

## **REFERENCES**

- Andrade, C., Oliveira, M.D., Faulin, T., Hering, V., Abdalla, D.S.P. (2011). *Biosensors for detection of Low-Density Lipoprotein and its modified forms*. Retrieved from <http://www.intechopen.com/books/biosensors-for-health-environment-and-biosecurity/biosensors-for-detection-of-low-density-lipoprotein-and-its-modified-forms>
- Abouimrane, A., Belharouak, I., & Amine, K. (2009). Sulfone-based electrolytes for high-voltage Li-ion batteries. *Electrochemistry Communications*, 11(5), 1073-1076.
- Abraham, K. M., & Alamgir, M. (1990). Li<sup>+</sup>-Conductive Solid Polymer Electrolytes with Liquid-Like Conductivity. *Journal of The Electrochemical Society*, 137(5), 1657-1658.
- Abraham, K. M., & Alamgir, M. (1994). Room temperature polymer electrolytes and batteries based on them. *Solid State Ionics*, 70-71, Part 1(0), 20-26.
- Abraham, K. M., Jiang, Z., & Carroll, B. (1997). Highly Conductive PEO-like Polymer Electrolytes. *Chemistry of Materials*, 9(9), 1978-1988.
- Acma etrainig (2013) FESEM Equipment Status. Retrieved from [http://electronmicroscopy.org/FE\\_Form\\_Function.htm](http://electronmicroscopy.org/FE_Form_Function.htm)
- Agrawal, R C, & Pandey, G P. (2008). Solid polymer electrolytes: materials designing and all-solid-state battery applications: an overview. *Journal of Physics D: Applied Physics*, 41(22), 223001.
- Akashi, H., Tanaka, K., & Sekai, K. (2002). A flexible Li polymer primary cell with a novel gel electrolyte based on poly(acrylonitrile). *Journal of Power Sources*, 104(2), 241-247.
- Allen, J.L., Han, S.D., Boyle, P.D., Henderson, W.A. (2011). Crystal structure and physical properties of lithium difluoro(oxalato)borate (LiDFOB or LiBF<sub>2</sub>Ox). *Journal of Power Sources*, 196, 9737-9742.
- Amaral, F. A., Dalmolin, C., Canobre, S.C., Bocchi, N., Rocha-Filho, R.C. & Biaggio, S.R. (2007). Electrochemical and physical properties of poly(acrylonitrile)/poly(vinyl acetate)-based gel electrolytes for lithium ion batteries. *Journal of Power Sources*, 164(1), 379-385.
- Angell, C.L. (1956). The infrared spectra and structure of ethylene carbonate. *Trans. Faraday Soc.*, 52, 211-219.
- Angell, C. A., Liu, C., & Sanchez, E. (1993). Rubbery solid electrolytes with dominant cationic transport and high ambient conductivity. *Nature*, 362(6416), 137-139.
- Aono, H., Imanaka, N. & Adachi, G.. (1994). High Li<sup>+</sup> Conducting Ceramics. *Accounts of Chemical Research*, 27(9), 265-270.
- Bange, K. & Gambke, T. (1990). Electrochromic Materials for optical switching devices. *Advanced Materials*, 2(1), 10-16.
- Bard, A.J., & Faulkner, L.R. (2000). *Electrochemical Methods: Fundamentals and Applications*. New York: Wiley.

- Bard, A.J. & Reichman, B. (1980). Electrochromism at Niobium Pentoxide Electrodes in Aqueous and Acetonitrile Solutions. *Journal of the Electrochemical Society*, 127(1), 241-242.
- Bashir, Z. (2001). The hexagonal mesophase in atactic polyacrylonitrile: A new interpretation of the phase transitions in the polymer. *Journal of Macromolecular Science, Part B*, 40(1), 41-67.
- Bellis, M.(n.d.). How a Battery Works. Retrieved from <http://inventors.about.com/od/bstartinventions/ss/How-A-Battery-Works.htm>
- Bellon-Maurel, V., Calmon-Decriaud A., Chandrasekhar V., Hadjichristidis N., Mays J.W., Pispas S., Pitsikalis M., Silvestre F. (Eds.). (1998). *Blockcopolymers/ Polyelectrolytes/ Biodegradation*. Berlin Heidelberg : Springer.
- Benedict, T. Jose, Banumathi, S., Veluchamy, A., Gangadharan, R., Ahamad, A. Zulfihar, & Rajendran, S. (1998). Characterization of plasticized solid polymer electrolyte by XRD and AC impedance methods. *Journal of Power Sources*, 75(1), 171-174.
- Bockris, J.O.M., & Khan, S.U.M. (1993). *Surface Electrochemistry: A Molecular Level Approache*. Heidelberg: Springer Verlag GmbH.
- Bonino, F., Ottaviani, M., Scrosati, B., & Pistoia, G. (1988). A Polymeric Electrolyte Rechargeable Lithium Battery. *Journal of The Electrochemical Society*, 135(1), 12-15.
- Brett, C.M.A. & Brett, A.M.O. (1993). *Electrochemistry: Principles, Methods, and Applications*. New York: Oxford University Press, Incorporated.
- Brown, E. (2001). *Introduction to Thermal Analysis: Techniques and Applications*. New York: Springer.
- Bruce, P.G. (Eds.). (1995). *Solid State Electrochemistry* (P. G. Bruce Ed.). United Kingdom: Cambridge University Press.
- Buraidah, M. H., Teo, L. P., Majid, S. R., & Arof, A. K. (2009). Ionic conductivity by correlated barrier hopping in NH4I doped chitosan solid electrolyte. *Physica B: Condensed Matter*, 404(8–11), 1373-1379.
- Büttiker, R, Ebert, J., Hinderling, C., Adlhart, C. (2011). Membranes for Specific Adsorption: Immobilizing Molecularly Imprinted Polymer Microspheres using Electrospun Nanofibers. *CHIMIA International Journal for Chemistry*, 65(3), 182-186.
- Chang, H.C., Huang, K.H., Yeh, Y.L. & Lin, S.H. (2000). A high-pressure FT-IR study of the isotope effects on water and high-pressure ices. *Chemical Physics Letters*, 326(1–2), 93-100.
- Chen-Yang, Y. W., Chen, H. C., Lin, F. J., & Chen, C. C. (2002). Polyacrylonitrile electrolytes: 1. A novel high-conductivity composite polymer electrolyte based on PAN, LiClO<sub>4</sub> and  $\alpha$ -Al<sub>2</sub>O<sub>3</sub>. *Solid State Ionics*, 150(3–4), 327-335.

- Chen, Y. T., Chuang, Y. C., Su, J. H., Yu, H. C., & Chen-Yang, Y. W. (2011). High discharge capacity solid composite polymer electrolyte lithium battery. *Journal of Power Sources*, 196(5), 2802-2809.
- Cheng, Y.T. & Wen, T.C. (1998). Novel waterborne polyurethane based electrolytes for lithium batteries – (II) the effect of adding LiCF<sub>3</sub>SO<sub>3</sub>-PC. *Solid State Ionics*, 107(1-2), 161-171.
- Chintapalli, S., & Frech, R. (1996). Effect of plasticizers on high molecular weight PEO-LiCF<sub>3</sub>SO<sub>3</sub> complexes. *Solid State Ionics*, 86-88, Part 1(0), 341-346.
- Choe, H. S., Carroll, B. G., Pasquariello, D. M., & Abraham, K. M. (1997). Characterization of Some Polyacrylonitrile-Based Electrolytes. *Chemistry of Materials*, 9(1), 369-379.
- Chowdari, B.V.R., Chandra, S., Singh, S., Srivastava, P.C. (Eds.). (1992). *Solid state ionics: Materials and Applications* Singapore: World Scientific.
- Croce, F., & Scrosati, B. (1993). Interfacial phenomena in polymer-electrolyte cells: lithium passivation and cycleability. *Journal of Power Sources*, 43(1-3), 9-19.
- Dawy, M. (2000). Electrical Properties and Infrared Studies of Heated Mica Sheets. *Egyptian Journal of Solids*, 25(1), 137-152.
- Dimethyl phthalate. (2013) Retrieved from [http://commons.wikimedia.org/wiki/File:Dimethyl\\_phthalate\\_V.1.svg](http://commons.wikimedia.org/wiki/File:Dimethyl_phthalate_V.1.svg)
- Di Noto, V., Lavina, S., Giffin, Guinevere A., Negro, E., & Scrosati, B. (2011). Polymer electrolytes: Present, past and future. *Electrochimica Acta*, 57(0), 4-13.
- Duclot, Michel, Alloin, Fannie, Brylev, Oleg, Sanchez, Jean Yves, & Souquet, Jean Louis. (2000). New alkali ionomers: transport mechanism from temperature and pressure conductivity measurements. *Solid State Ionics*, 136-137(0), 1153-1160.
- Evans, J., Vincent, C.A. & Bruce, P.G. (1987). Electrochemical measurement of transference numbers in polymer electrolytes. *Polymer*, 28(13), 2324-2328.
- Ethylene carbonate. (n.d.) Retrieved from [http://commons.wikimedia.org/wiki/File:Ethylene\\_carbonate.png](http://commons.wikimedia.org/wiki/File:Ethylene_carbonate.png)
- FEI (2009). Product Data. Retrieved from [http://www.fei.com/uploadedfiles/documentsprivate/content/2009\\_03\\_quanta450feg\\_ds.pdf](http://www.fei.com/uploadedfiles/documentsprivate/content/2009_03_quanta450feg_ds.pdf)
- Fenton, D. E., Parker, J. M., & Wright, P. V. (1973). Complexes of alkali metal ions with poly(ethylene oxide). *Polymer*, 14(11), 589.
- Fini, G., Mirone, P., Fortunato, B. (1973). Evidence for short-range orientation effects in dipolar aprotic liquids from vibrational spectroscopy. Part 1.-Ethylene and propylene carbonates. *Journal of the Chemical Society, Faraday Transactions 2: Molecular and Chemical Physics*, 69(0), 1243-1248.



- Frech, R., & Chintapalli, S. (1996). Effect of propylene carbonate as a plasticizer in high molecular weight PEO LiCF<sub>3</sub>SO<sub>3</sub> electrolytes. *Solid State Ionics*, 85(1–4), 61–66.
- Gabano, J.P. (Eds.). (1983). *Lithium Batteries*. London: Academic Press.
- Geochemical Instrumentation and Analysis (2013), X-ray Powder Diffraction (XRD). Retrieved from [http://serc.carleton.edu/research\\_education/geochemsheets/techniques/XRD.html](http://serc.carleton.edu/research_education/geochemsheets/techniques/XRD.html)
- Gileadi, E., Kirowa-Eisner, E., & Penciner, J. (1975). *Interfacial electrochemistry: an experimental approach*. United States: Addison-Wesley Pub. Co., Advanced Book Program.
- Grassie, N., & McGuchan, R. (1971). Pyrolysis of polyacrylonitrile and related polymers—II: The effect of sample preparation on the thermal behaviour of polyacrylonitrile. *European Polymer Journal*, 7(8), 1091–1104.
- Gray, F.M. (1991). *Solid Polymer Electrolytes: Fundamentals and Technological Applications*. Germany: Wiley VCH.
- Hagenmuller, P., Van Gool, W. (1978). *Solid Electrolytes General Principle: Characterization, Materials, Applications, Material Science and Technology*. New York: Academic Press.
- Helmenstin, A.M. (n.d.). Polyacrylonitrile Chemical Structure. Retrieved from <http://chemistry.about.com/od/factsstructures/ig/Chemical-Structures---P/Polyacrylonitrile.htm>
- Hong, E.S., Okada, S., Sonoda, T., Gopukumar, S., & Yamaki, J. (2004). Thermal Stability of Electrolytes with Mixtures of LiPF<sub>6</sub> and LiBF<sub>4</sub> Used in Lithium-Ion Cells. *Journal of The Electrochemical Society*, 151(11), A1836–A1840.
- Howell, F. S., Bose, R. A., Macedo, P. B., & Moynihan, C. T. (1974). Electrical relaxation in a glass-forming molten salt. *The Journal of Physical Chemistry*, 78(6), 639–648.
- Huang, B.Y., Wang, Z.X., Li, G.B., Huang, H., Xue, R.J., Chen, L.Q. & Wang, F.S. (1996). Lithium ion conduction in polymer electrolytes based on PAN. *Solid State Ionics*, 85(1–4), 79–84.
- Jacob, M. M. E., & Arof, A. K. (2000). FTIR studies of DMF plasticized polyvinylidene fluoride based polymer electrolytes. *Electrochimica Acta*, 45(10), 1701–1706.
- Jacob, M. M. E., Prabakaran, S. R. S., & Radhakrishna, S. (1997). Effect of PEO addition on the electrolytic and thermal properties of PVDF–LiClO<sub>4</sub> polymer electrolytes. *Solid State Ionics*, 104(3–4), 267–276.
- Kanevskii, L. S., & Dubasova, V. S. (2005). Degradation of Lithium-Ion batteries and how to fight it: A review. *Russian Journal of Electrochemistry*, 41(1), 1–16.
- Kazuo Nakamoto. (1922). *Infrared and Raman Spectra of Inorganic and Coordination Compounds* (3 ed.). New York: John Wiley & Sons, Inc.

- Kim, H. S., Paik, C. H., Cho, B. W., Kim, J. T., Yun, K. S., & Chun, H. S. (1997). Discharge characteristics of an Li/LiCoO<sub>2</sub> cell with poly(acrylonitrile)-based polymer electrolyte. *Journal of Power Sources*, 68(2), 361-363.
- Klassen, B., Aroca, R., Nazri, M., & Nazri, G. A. (1998). Raman Spectra and Transport Properties of Lithium Perchlorate in Ethylene Carbonate Based Binary Solvent Systems for Lithium Batteries. *The Journal of Physical Chemistry B*, 102(24), 4795-4801.
- Ko, T.H., Lin, C.H. & Ting, H.Y. (1989). Structural changes and molecular motion of polyacrylonitrile fibers during pyrolysis. *Journal of Applied Polymer Science*, 37(2), 553-566.
- Kumar D. & Hashmi S. A. (2010). Ionic liquid based sodium ion conducting gel polymer electrolytes. *Solid State Ionics*, 181(8–10), 416-423.
- Kuo, H.H., Chen, W.C., Wen, T.C. & Gopalan, A. (2002). A novel composite gel polymer electrolyte for rechargeable lithium batteries. *Journal of Power Sources*, 110(1), 27-33.
- Lasia, Andrzej. (2002). Electrochemical Impedance Spectroscopy and its Applications. In B. E. Conway, J. O. M. Bockris & R. White (Eds.), *Modern Aspects of Electrochemistry*. United States: Springer.
- Lee, C. C., & Wright, P. V. (1978). Order-disorder transformations in ionic complexes of poly (ethylene oxide). *Polymer*, 19(2), 234-235.
- Lewandowski, A., Stępnia, I. & Grzybkowski, W. (2001). Copper transport properties in polymer electrolytes based on poly(ethylene oxide) and poly(acrylonitrile). *Solid State Ionics*, 143(3–4), 425-432.
- Li, Jianlin, Daniel, Claus, & Wood, David. (2011). Materials processing for lithium-ion batteries. *Journal of Power Sources*, 196(5), 2452-2460.
- Lithium tetrafluoroborate. (2013) Retrieved from [http://en.wikipedia.org/wiki/Lithium\\_tetrafluoroborate](http://en.wikipedia.org/wiki/Lithium_tetrafluoroborate)
- MacCallum, J.R., & Vincent, C.A. (1987). *Polymer Electrolyte Reviews*. London: Springer.
- MacCallum, J.R., & Vincent, C.A. (1989). *Polymer Electrolyte Reviews*. London: Springer.
- Matsuda, Yoshiharu, Morita, Masayuki, & Tsutsumi, Hiromori. (1993). Polarization behavior of lithium electrode in polymeric solid electrolytes. *Journal of Power Sources*, 44(1–3), 439-443.
- McQuarrie, D.A., Rock, P.A., & Gallogly, E.B. (2011). *General Chemistry*. United States: University Science Books.
- Michael, M. S., Jacob, M. M. E., Prabakaran, S. R. S., & Radhakrishna, S. (1997). Enhanced lithium ion transport in PEO-based solid polymer electrolytes employing a novel class of plasticizers. *Solid State Ionics*, 98(3–4), 167-174.

- Minagawa, M., Kanoh, H., Tanno, S. & Nishimoto, Y. (2002). Glass-Transition Temperature (T<sub>g</sub>) of Free-Radically Prepared Polyacrylonitrile by Inverse Gas Chromatography, 1. A Study on T<sub>g</sub> of Atactic Monodisperse Polystyrenes. *Macromolecular Chemistry and Physics*, 203(17), 2475-2480.
- Moreno, M., Ana, M. A. S., Gonzalez, G. & Benavente, E. (2010). Poly(acrylonitrile)-montmorillonite nanocomposites: Effects of the intercalation of the filler on the conductivity of composite polymer electrolytes. *Electrochimica Acta*, 55(4), 1323-1327.
- Nicholson, P.S., Whittingham, M.S., Farrington, G.C., Smeltzer, W.W., Thomas, J. (Eds.). (1992). Solid State Ionics-9. In *Proceeding of the International Conference on Solid State Ionics*. North-Holland, Amsterdam.
- Osman, Z., Ibrahim, Z. A., & Arof, A. K. (2001). Conductivity enhancement due to ion dissociation in plasticized chitosan based polymer electrolytes. *Carbohydrate Polymers*, 44(2), 167-173.
- Ouyang, Q., Cheng, L., Wang, H.J. & Li, K.X. (2008). Mechanism and kinetics of the stabilization reactions of itaconic acid-modified polyacrylonitrile. *Polymer Degradation and Stability*, 93(8), 1415-1421.
- Papke, B.L., Ratner, M.A. & Shriver, D.F. (1982). Vibrational Spectroscopic Determination of Structure and Ion Pairing in Complexes of Poly(ethylene oxide) with Lithium Salts. *Journal of The Electrochemical Society*, 129(7), 1434-1438.
- Park, J.K. (2012). *Principles and Applications of Lithium Secondary Batteries*. Weinheim: Wiley.
- Pistoia, G., Antonini, A., & Wang, G. (1996). Impedance study on the reactivity of gel polymer electrolytes towards a lithium electrode. *Journal of Power Sources*, 58(2), 139-144.
- Pistoia, G., Rossi, M.D., & Scrosati, B. (1970). Study of the Behavior of Ethylene Carbonate as a Nonaqueous Battery Solvent. *Journal of The Electrochemical Society*, 117(4), 500-502.
- Plieth, W. (1995). C. Julien and G. A. Nazri. Solid State Batteries Materials Design and Optimization. Kluwer Academic Publishers, Boston/Dordrecht/London 1994, 629 Seiten, ISBN 0-7923-9460-7. *Crystal Research and Technology*, 30(3), 396-396.
- polyacrylonitrile (PAN). (2013). In *Encyclopædia Britannica*. Retrieved from <http://www.britannica.com/EBchecked/topic/468259/polyacrylonitrile>
- Prasanth R., Aravindan, V. & Srinivasan M.. (2012). Novel polymer electrolyte based on cob-web electrospun multi component polymer blend of polyacrylonitrile/poly(methyl methacrylate)/polystyrene for lithium ion batteries—Preparation and electrochemical characterization. *Journal of Power Sources*, 202(0), 299-307.
- Qiao, H.W., Fang, X.P., Luan, H.L., Zhou, Z.M., Wu, Y.K., Yao, W., Wang, X., Li, J.M., Chen, C. (2008). Vibrational spectroscopic and density functional studies on ion solvation and ion association of lithium tetrafluoroborate in 4-

- methoxymethyl-ethylene carbonate. *Journal of Molecular Liquids*, 138(1–3), 69-75.
- Rajendran, S., Kannan, R., & Mahendran, O. (2001a). Ionic conductivity studies in poly(methylmethacrylate)–polyethylene oxide hybrid polymer electrolytes with lithium salts. *Journal of Power Sources*, 96(2), 406-410.
- Rajendran, S., Kannan, R., & Mahendran, O. (2001b). Study on Li ion conduction behaviour of the plasticized polymer electrolytes based on poly acrylonitrile. *Materials Letter*(48), 331-335.
- Rajendran, S., Mahendran, O., & Kannan, R. (2002). Investigations on poly(methyl methacrylate)-poly(ethylene oxide) hybrid polymer electrolytes with dioctyl phthalate, dimethyl phthalate and diethyl phthalate as plasticizers. *Journal of Solid State Electrochemistry*, 6(8), 560-564.
- Rajendran, S., Mahendran, O., Krishnaveni, K. (2003). Effect of CeO<sub>2</sub> on Conductivity of PMMA/PEO Polymer Blend Electrolytes. *Journal of New Materials for Electrochemical Systems*, 6, 25-28.
- Rajendran, S., Sivakumar, M., & Subadevi, R. (2003). Effect of salt concentration in poly(vinyl alcohol)-based solid polymer electrolytes. *Journal of Power Sources*, 124(1), 225-230.
- Ramesh, S., & Arof, A. K. (2001). Ionic conductivity studies of plasticized poly(vinyl chloride) polymer electrolytes. *Materials Science and Engineering: B*, 85(1), 11-15.
- Ramya, C. S., Selvasekarapandian, S., Savitha, T., Hirankumar, G., & Angelo, P. C. (2007). Vibrational and impedance spectroscopic study on PVP–NH<sub>4</sub>SCN based polymer electrolytes. *Physica B: Condensed Matter*, 393(1–2), 11-17.
- Randles, J. E. B. (1948). A cathode ray polarograph. Part II.-The current-voltage curves. *Transactions of the Faraday Society*, 44(0), 327-338.
- Retter, U. and Lohse, H. (2002). *Electrochemical Impedance Spectroscopy in Electroanalytical Methods* (F. Scholz Ed.). Berlin: Springer.
- Rhoo, H.J., Kim, H.T., Park, J.K., & Hwang, T.S. (1997). Ionic conduction in plasticized PVC/PMMA blend polymer electrolytes. *Electrochimica Acta*, 42(10), 1571-1579.
- Rickert, Hans. (1978). Solid Ionic Conductors: Principles and Applications. *Angewandte Chemie International Edition in English*, 17(1), 37-46.
- Rosenbaum, S. (1965). Polyacrylonitrile fiber behavior. II. Dependence on structure and environment. *Journal of Applied Polymer Science*, 9(6), 2085-2099.
- Sarvaranta, L. (1995). Shrinkage of short PP and PAN fibers under hot-stage microscope. *Journal of Applied Polymer Science*, 56(9), 1085-1091.
- Schettler, T. E. D. (2006). Human exposure to phthalates via consumer products. *International Journal of Andrology*, 29(1), 134-139.

- Scrosati, B. (Eds.). (1993). *Applications of Electroactive Polymers*. London: Chapman & Hall.
- Selvasekarapandian, S., Baskaran, R., & Hema, M. (2005). Complex AC impedance, transference number and vibrational spectroscopy studies of proton conducting PVAc–NH<sub>4</sub>SCN polymer electrolytes. *Physica B: Condensed Matter*, 357(3–4), 412-419.
- Shanthi, M., Mathew, Chithra M., Ulaganathan, M., & Rajendran, S. (2013). FT-IR and DSC studies of poly(vinylidene chloride-co-acrylonitrile) complexed with LiBF<sub>4</sub>. *Spectrochimica Acta Part A: Molecular and Biomolecular Spectroscopy*, 109(0), 105-109.
- Silva M.M, Barros S. C., Smith M.J. & MacCallum J. R. (2004). Characterization of solid polymer electrolytes based on poly(trimethylenecarbonate) and lithium tetrafluoroborate. *Electrochimica Acta*, 49(12), 1887-1891.
- Silverstein, R.R.M., Bassler, G.C., & Morrill, T.C. (1981). *Spectrometric identification of organic compounds*. Australia: John Wiley & Sons, Limited.
- Smith, B. (1998). *Infrared Spectral Interpretation: A Systematic Approach*. Boca Raton: CRC Press.
- Song, S.W., Richardson, T.J., Zhuang, G.R.V., Devine, T.M. & Evans, J.W. (2004). Effect on aluminum corrosion of LiBF<sub>4</sub> addition into lithium imide electrolyte; a study using the EQCM. *Electrochimica Acta*, 49(9–10), 1483-1490.
- Sony. (n.d.). Lithium Ion Rechargeable Batteries Technical Handbook. Retrieved from <http://www.sony.com.cn/products/ed/battery/download.pdf>
- Subramania, A., Sundaram, N. T. Kalyana, & Kumar, G. Vijaya. (2006). Structural and electrochemical properties of micro-porous polymer blend electrolytes based on PVdF-co-HFP-PAN for Li-ion battery applications. *Journal of Power Sources*, 153(1), 177-182.
- Takata, K., Morita, M., Matsuda, Y. & Matsui, K. (1985). Cycling Characteristics of Secondary Li Electrode in LiBF<sub>4</sub>/Mixed Ether Electrolytes. *Journal of The Electrochemical Society*, 132(1), 126-128.
- Tao, H.S., Feng, Z.Z., Liu, H., Kan, X.W. & Chen, P. (2011). Reality and Future of Rechargeable Lithium Batteries. *The Open Materials Science Journal*, 5, 204-214.
- Thermal Gravimetric Analysis. (n.d.). Analytical Techniques. Retrieved from [http://www.lpdlabservices.co.uk/analytical\\_techniques/chemical\\_analysis/thermal\\_gravim\\_analysis.php](http://www.lpdlabservices.co.uk/analytical_techniques/chemical_analysis/thermal_gravim_analysis.php)
- Thermo Nicole. (n.d.), Introduction to Fourier Transform Infrared Spectroscopy. Retrieved from <http://mmrc.caltech.edu/FTIR/FTIRintro.pdf>
- Tsutsumi, H. & Kitagawa, T. (2006). High ionic conductive behavior of cyanoethylated polyvinylalcohol- and polyacrylonitrile-based electrolytes. *Solid State Ionics*, 177, 2683-2686.

- Ue, M.. (1994). Mobility and Ionic Association of Lithium and Quaternary Ammonium Salts in Propylene Carbonate and  $\gamma$ -Butyrolactone. *Journal of The Electrochemical Society*, 141(12), 3336-3342.
- Ue, M. & Mori, S. (1995). Mobility and Ionic Association of Lithium Salts in a Propylene Carbonate-Ethyl Methyl Carbonate Mixed Solvent. *Journal of The Electrochemical Society*, 142(8), 2577-2581.
- Ue, M., Murakami, A., & Nakamura, S. (2002). Anodic Stability of Several Anions Examined by Ab Initio Molecular Orbital and Density Functional Theories. *Journal of The Electrochemical Society*, 149(12), A1572-A1577.
- Ue, M., Takeda, M., Takehara, M., & Mori, S. (1997). Electrochemical Properties of Quaternary Ammonium Salts for Electrochemical Capacitors. *Journal of The Electrochemical Society*, 144(8), 2684-2688.
- Ulaganathan, M., Nithya, R., & Rajendran, S. (2012). Surface Analysis Studies on Polymer Electrolyte Membranes Using Scanning Electron Microscope and Atomic Force Microscope.
- Uma, T. & Rajendran S. (2000). Characterization of plasticized PMMA–LiBF<sub>4</sub> based solid polymer electrolytes. *Bulletin of Materials Science*, 23(1), 27-29.
- Velasco, J.G.. (1997). Determination of standard rate constants for electrochemical irreversible processes from linear sweep voltammograms. *Electroanalysis*, 9(11), 880-882.
- Visco, S.J., Liu, M.L., Doeff, M.M., Ma, Y.P., Lampert, C., & De Jonghe, L.C. (1993). Polyorganodisulfide electrodes for solid-state batteries and electrochromic devices. *Solid State Ionics*, 60(1–3), 175-187.
- Voigt, N, & van Wüllen, L. (2012). The mechanism of ionic transport in PAN-based solid polymer electrolytes. *Solid State Ionics*, 208(0), 8-16.
- Wakihara, M., & Yamamoto, O. (1998). *Lithium ion batteries: fundamentals and performance*. Tokyo: Kodansha.
- Wang, Z.X., Huang, B.Y., Huang, H., Chen, L.Q., Xue, R.J., & Wang, F.S. (1996). Infrared spectroscopic study of the interaction between lithium salt LiClO<sub>4</sub> and the plasticizer ethylene carbonate in the polyacrylonitrile-based electrolyte. *Solid State Ionics*, 85(1–4), 143-148.
- Wang, Z.X., Huang, B.Y., Xue, R.J., Huang, X.J., & Chen, L.Q. (1999). Spectroscopic investigation of interactions among components and ion transport mechanism in polyacrylonitrile based electrolytes. *Solid State Ionics*, 121(1–4), 141-156.
- Watanabe, M., Kanba, M., Nagaoka, K., & Shinohara, I. (1983). Ionic conductivity of hybrid films composed of polyacrylonitrile, ethylene carbonate, and LiClO<sub>4</sub>. *Journal of Polymer Science: Polymer Physics Edition*, 21(6), 939-948.
- Watanabe, M., Nagano, S., Sanui, K., & Ogata, N. (1988). Estimation of Li<sup>+</sup> transport number in polymer electrolytes by the combination of complex impedance and potentiostatic polarization measurements. *Solid State Ionics*, 28–30, Part 2(0), 911-917.

- 
- Wright, P.V. (1975). Electrical conductivity in ionic complexes of poly(ethylene oxide). *British Polymer Journal*, 7(5), 319-327.
- Wypych, G. (2004). *Handbook of Plasticizers*. Toronto, New York: ChemTec Publishing.
- X-Rays. (n.d.) Retrieved from <http://nothingnerdy.wikispaces.com/X-RAYS>
- Xu, K. (2004). Nonaqueous Liquid Electrolytes for Lithium-Based Rechargeable Batteries. *Chemical Reviews*, 104(10), 4303-4418.
- Xuan, X.P., Zhang, H.C., Wang, J.J. & Wang, H.qing. (2004). Vibrational Spectroscopic and Density Functional Studies on Ion Solvation and Association of Lithium Tetrafluoroborate in Acetonitrile. *The Journal of Physical Chemistry A*, 108(37), 7513-7521.
- Yuan, F., Chen, H.Z., Yang, H.Y., Li, H.Y., & Wang, M. (2005). PAN-PEO solid polymer electrolytes with high ionic conductivity. *Materials Chemistry and Physics*, 89(2-3), 390-394.
- Zhang, S. S., Ervin, M. H., Xu, K., & Jow, T. R. (2005). Li-ion battery with poly(acrylonitrile-methyl methacrylate)-based microporous gel electrolyte. *Solid State Ionics*, 176(1-2), 41-46.

# **APPENDIX**



## **Ionic Conductivity and Dielectric Properties of Plasticized Polyacrylonitrile Based Solid Polymer Electrolyte Films**

W.G. Chong<sup>1, a</sup>, Z. Osman<sup>1, b</sup>, L. Othman<sup>1, c</sup> and K. B. Md. Isa<sup>1, d</sup>

Physics Department, University of Malaya, 50603 Kuala Lumpur, Malaysia

woongie@siswa.um.edu.my<sup>a</sup>, zurinaosman@um.edu.my<sup>b</sup>, amoda78@yahoo.com<sup>c</sup>,  
 wippynie@yahoo.com<sup>d</sup>

**Keywords:** Polymer electrolytes, conductivity, dielectric, plasticizer, PAN, LiCF<sub>3</sub>SO<sub>3</sub>, NaCF<sub>3</sub>SO<sub>3</sub>

**Abstract.** The conducting polymer electrolyte films composed of polyacrylonitrile (PAN) as the host polymer, LiCF<sub>3</sub>SO<sub>3</sub> and NaCF<sub>3</sub>SO<sub>3</sub> as inorganic salts and ethylene carbonate (EC) as plasticizer were prepared by the solution cast technique. The conductivities of the films were characterized by impedance spectroscopy. On addition of more than 14 wt% of salt, the NaCF<sub>3</sub>SO<sub>3</sub>-containing PAN films exhibited higher ionic conductivity than the LiCF<sub>3</sub>SO<sub>3</sub>-containing PAN films. The values of the dielectric constant,  $\epsilon_r$  and dielectric loss,  $\epsilon_i$  increase as frequency decreases at room temperature. The temperature dependence of the conductivity obeys Arrhenius relation in the temperature range of 303 K to 353 K.

### **Introduction**

Solid polymer electrolytes (SPEs) formed by the dissolution of alkali metal salts in a polymer matrix, have been widely explored because of their prospects for achieving high ionic conductivities. The development of SPEs has drawn the attention of many researchers due to their potential applications in solid-state batteries, electrochromic devices, and sensors [1–3].

Extensive research has been conducted on lithium salts complexed polymer electrolytes. The most commonly studied lithium salts are LiCF<sub>3</sub>SO<sub>3</sub>, LiBF<sub>4</sub>, and LiClO<sub>4</sub> [4–6]. Studies on sodium ion complexed polymer electrolytes were relatively lesser [7–8]. Sodium ion carries the advantages in its availability in abundance at a cheaper cost than lithium. It is feasible to achieve sufficiently high conductivity because sodium does not form any alloy with the electrode materials, such as aluminum and nickel. Furthermore, the softness of these materials makes it easier to achieve and maintain good contact with other components in the battery.

One method of improving the conductivity of SPEs, is the incorporation of a low molecular weight plasticizer such as propylene carbonate (PC) and ethylene carbonate (EC) to polymer electrolytes [9–10]. The addition of plasticizer helps in improving the ionic conductivity by increasing flexibility in the polymeric segments and dissociating ion aggregates present in polymer electrolytes.

We have reported the preparation of Li and Na conducting polymer electrolytes based on PAN with room temperature conductivity of 10<sup>−4</sup> S cm<sup>−1</sup> and having great potential to be employed practically [11]. In this paper, we present a comparative study of plasticized PAN films doped with lithium and sodium salt. The effects of these salts and plasticizer EC on the ionic conductivity and the dielectric behaviour of the PAN polymer electrolytes were investigated.

### **Experimental Methods**

All electrolytes were prepared by the solution cast technique as reported earlier [11]. The plasticizer, EC (Fluka) and the salts LiCF<sub>3</sub>SO<sub>3</sub> and NaCF<sub>3</sub>SO<sub>3</sub> (Aldrich) were added accordingly. The amount of plasticizer was fixed at 24 wt%. Impedance spectroscopy measurements were used to determine the ionic conductivity of the films. The prepared films were sandwiched between the two stainless steel blocking electrodes with a diameter of 2 cm. A HIOKI 3532 LCR bridge that has been interfaced with a computer was used to perform the impedance measurement for each polymer electrolyte film in the frequency range of 50 Hz to 1 MHz. The temperature conductivity dependence studies were carried out in the range of temperature from 303 K to 353 K.

*Int. J. Electrochem. Sci.*, 8 (2013) 3602 - 3614

---

**International Journal of  
ELECTROCHEMICAL  
SCIENCE**  
[www.electrochemsci.org](http://www.electrochemsci.org)

---

## Magnesium Ion-Based Gel Polymer Electrolytes: Ionic Conduction and Infrared Spectroscopy Studies

*N. H. Zainol, S.M. Samin, L. Othman, K.B. Md Isa, W.G. Chong and Z. Osman\**

Department of Physics, University of Malaya, 50603, Kuala Lumpur, Malaysia

\*E-mail: [zurinaosman@um.edu.my](mailto:zurinaosman@um.edu.my)

*Received:* 12 January 2013 / *Accepted:* 6 February 2013 / *Published:* 1 March 2013

---

The gel polymer electrolyte (GPE) films based on polymethylmethacrylate (PMMA) containing the mixture of ethylene carbonate (EC) and propylene carbonate (PC) as a plasticizing solvent and various concentrations of magnesium triflate or  $\text{Mg}(\text{CF}_3\text{SO}_3)_2$  salt have been prepared using the solution casting technique. The maximum room temperature ionic conductivity of  $1.27 \times 10^{-3} \text{ S cm}^{-1}$  was obtained from the GPE film containing 20 wt.% of  $\text{Mg}(\text{CF}_3\text{SO}_3)_2$  salt. The conductivity-temperature studies of the GPE films follow the Arrhenius behavior with activation energy for ionic conduction are determined to be 0.18 - 0.26 eV. The transport number of magnesium ions in the GPEs was evaluated using the combination of a.c. impedance spectroscopy and d.c. polarization techniques. Fourier Transform Infrared Spectroscopy (FTIR) studies confirmed the increased in conductivity is due to increase of free ions and decrease in ion aggregates.

---

**Keywords:** Gel polymer electrolytes; magnesium ion; ionic conductivity; transport number; FTIR spectroscopy

### 1. INTRODUCTION

Electrochemical energy storage systems have a tremendous role in technical applications such as supercapacitors, electrochemical devices, sensors, fuel cells, etc. [1-2]. In the midst of technologies emerging today, an even higher demand for rechargeable batteries with high specific energy, high power which provides good metal surface stability and high electrochemical stability are expected [2-4]. Although lithium batteries are widely been used in high power application due to its highest electrode potential with an average voltage of 3.8 V, the lithium itself has brought out serious environmental issues due to its reactive nature and safety concern to the device and even the users [5-6]. At the same time, the accessibility of the raw material for the conventional battery is a great challenge that is likely to impact its sustainability in the future. Therefore, an alternative energy